CONTRACT NO. N62269-85-C-0245
REPORT NO. NADC-89061-60

A STUDY OF FORMULATIONS AND THERMOPHYSICS OF INTUMESCENT SYSTEMS

Charles E. Anderson, Jr., Jerome Dziuk, Jr., and Donald E. Ketchum
SOUTHWEST RESEARCH INSTITUTE
P.O. Drawer 28510
6220 Culebra Road
San Antonio, TX 78284

30 SEPTEMBER 1988

FINAL REPORT
Task No. WR10943
Work Unit No. SH850

Approved for Public Release; Distribution is Unlimited

Prepared for
Air Vehicle and Crew Systems Technology Department (Code 6062)
NAVAL AIR DEVELOPMENT CENTER
Warminster, PA 18974-5000

NOTICES

REPORT NUMBERING SYSTEM - The numbering of technical project reports issued by the Naval Air Development Center is arranged for specific identification purposes. Each number consists of the Center acronym, the calendar year in which the number was assigned, the sequence number of the report within the specific calandar year, and the official 2-digit correspondence code of the Command Officer or the Functional Department responsible for the report. For example: Report No. NADC 88020-60 indicates the twentieth Center report for the year 1988 and prepared by the Air Vehicle and Crew Systems Technology Department. The numerical codes are as follows:

CODE	OFFICE OR DEPARTMENT
00	Commander, Naval Air Development Center
01	Technical Director, Naval Air Development Center
05	Computer Department
10	AntiSubmarine Warfare Systems Department
20	Tactical Air Systems Department
30	Warfare Systems Analysis Department
40	Communication Navigation Technology Department
50	Mission Avionics Technology Department
60	Air Vehicle & Crew Systems Technology Department
70	Systems & Software Technology Department
80	Engineering Support Group
90	Test & Evaluation Group

PRODUCT ENDORSEMENT - The discussion or instructions concerning commercial products herein do not constitute an endorsement by the Government nor do they convey or imply the license or right to use such products.

UNCLASSIFIED

SECURITY CLASSIFICATION OF THIS PAGE

REPORT DOCUMENTATION PAGE

Form Approved
OMB No 0704-0188

1a REPORT SECURITY CLASSIFICATION UNCLASSIFIED	1b RESTRICTIVE MARKINGS
2a SECURITY CLASSIFICATION AUTHORITY	3 DISTRIBUTION AVAILABILITY OF REPORT Approved for Public Release Distribution is Unlimited
2b DECLASSIFICATION DOWNGRADING SCHEDULE	
4 PERFORMING ORGANIZATION REPORT NUMBER(S) SwRI 8766/01	5 MONITORING ORGANIZATION REPORT NUMBER(S) NADC-89061-60
6a NAME OF PERFORMING ORGANIZATION SOUTHWEST RESEARCH INSTITUTE 6b OFFICE SYMBOL (If applicable)	7a NAME OF MONITORING ORGANIZATION Air Vehicle and Crew Systems Technology Department (Code 6062)
6c ADDRESS (City, State, and ZIP Code) P.O. Drawer 28510 6220 Culebra Road San Antonio, TX 78284	7b ADDRESS (City, State, and ZIP Code) NAVAL AIR DEVELOPMENT CENTER Warminster, PA 18974-5000
8a NAME OF FUNDING/SPONSORING ORGANIZATION 8b OFFICE SYMBOL (If applicable)	9 PROCUREMENT INSTRUMENT IDENTIFICATION NUMBER N62269-85-C-0245
8c ADDRESS (City, State and ZIP Code)	10 SOURCE OF FUNDING NUMBERS PROGRAM ELEMENT NO: PROJECT NO: TASK NO: WR10943: WORK UNIT ACCESSION NO: SH850

11 TITLE (Include Security Classification)

(U) A Study of Formulations and Thermophysics of Intumescent Systems

12 PERSONAL AUTHOR(S)

Charles E. Anderson, Jr.; Jerome Dziuk, Jr.; Donald E. Ketchum

13a TYPE OF REPORT	13b TIME COVERED	14 DATE OF REPORT (Year, Month Day)	15 PAGE COUNT
Final	FROM 9/85 TO 9/88	1988 Sept. 30	140

16 SUPPLEMENTARY NOTATION

17 COSATI CODES			18 SUBJECT TERMS (Continue on reverse if necessary and identify by block number)
FIELD	GROUP	SUB-GROUP	intumescence; thermal protection; insulation; intumescent systems; intumescent paint; thermal conductivity; char; cook-off; weapons cook-off improvement

19 ABSTRACT (Continue on reverse if necessary and identify by block number)

A variety of intumescent systems were formulated. After screening, six formulations were evaluated further by application of the coatings to metal substrates and exposure to a heat source typical of an aviation fuel fire. The thermal responses are compared to a baseline formulation. Additionally, the self-limiting affect of pressure on intumescence was inferred from differential scanning calorimetry; and models were developed for estimating the effective thermal conductivity of the char from either the temperature-time response of coated coupons, or from theoretical considerations.

20 DISTRIBUTION AVAILABILITY OF ABSTRACT	21 ABSTRACT SECURITY CLASSIFICATION
☒ UNCLASSIFIED/UNLIMITED ☒ SAME AS RPT ☐ DTIC USERS	UNCLASSIFIED
22a NAME OF RESPONSIBLE INDIVIDUAL Dave Pulley	22b TELEPHONE (Include Area Code) 215-441-1904 / 22c OFFICE SYMBOL 6062

DD Form 1473, JUN 86 — Previous editions are obsolete — SECURITY CLASSIFICATION OF THIS PAGE

S/N 0102-LF-014-6603 — UNCLASSIFIED

Contract No. N62269-85-C-0245
NADC-89061-60

TABLE OF CONTENTS

Contract No. N62269-85-C-0245
NADC-89061-60

LIST OF FIGURES

LIST OF FIGURES (CONT'D)

LIST OF TABLES

LIST OF TABLES (CONT'D)

ACKNOWLEDGEMENT

Many people contribute to research projects of the size and scope of this effort. The authors would like to thank Mr. William A. Mallow for providing his expertise and genius to formulating the intumescent systems. We would also like to thank Mr. Joe Fey for his painstaking efforts and care in mixing and screening the many formulations examined. Additionally, Mr. William Mountain provided valuable assistance in the reduction and tabulation of data. Finally, we would like to thank Mr. Dave Pulley at NADC for his continued support in this project, as well as the other personnel at NADC who assisted in the furnace testing of the coated sample coupons.

1.0 INTRODUCTION

Intumescent systems provide thermal protection to an underlying substrate by several mechanisms [1-5]. As demonstrated in References 3 or 5, the formation of an intumescent front, with a well-defined temperature, necessarily limits the heat flux to the substrate. It was also shown that tumescence itself carries heat away from the substrate. The formation of a multicellular char also contributes to the insulation of the substrate.

Intumescent coating systems are formulated such that there is a large volume release of gases which acts as a blowing agent to the solid material. If the blowing agent action occurs too early, the intumescent action is reduced because the "solid" material is too viscous. If the action occurs too late, solidification of the "char" inhibits intumescence. If the molten material becomes too fluid, i.e., the viscosity becomes very low, large cells are formed during the blowing process and gel in the char. These large cells are relatively ineffective as insulators and the char can become quite frangible. Thus, the insulation efficiency of the char depends on the cell structure, which in turn, depends on the staging of the blowing agent relative to the viscosity in the semi-molten layers formed by the active filler and the binder system.

In a previous study [5], Southwest Research Institute (SwRI) developed several candidate intumescent systems which showed some promise as alternate formulations to the current formulation used by the Navy for extending the protection time of ordnance from aviation-type fuel fires. This study has focused on further development and assessment of the more promising formulations developed in the previous program. Additionally, several new formulations were developed and examined. The Naval Air Development Center (NADC), who supervised the current research effort, performed the instrumented coupon tests which give a temperature-time response of coated metallic substrates. The results of these coupon tests provide a quantitative evaluation of the thermal protection performance of the intumescent system.

2.0 DEVELOPMENT OF INTUMESCENT SYSTEMS

2.1 Introduction

The objective of this task was to develop alternate intumescent systems for the NASA formulation EX-1C-82 [4,5]. From the data derived during previous research [2,5], seven formulations were identified as possible alternates to the NASA formulation. These formulations are designated 523, 526, 546, 571, 736, 746, and 753; the constituents of these intumescent systems are given in Table 1. The intumescent systems in Table 1, which consisted of the original formulations given in Reference 5, and variations of these formulations, were evaluated in the current study. Several new formulations were also evaluated during this study. These formulations and their variations are designated as Series 1, 2, 3, and 4; the constituents to these formulations are also given in Table 1. It should be noted that the constituents of the coating systems given in Table 1 are for the base formulation only--variations of the base formulations were investigated where other materials were substituted for a base constituent.

2.2 Initial Evaluation of Coatings

The first step in determining the efficiacy of alternate intumescent formulations to NASA EX-1C-82, was to examine and evaluate the most promising coating systems developed in the previous study [5]. Comments concerning this initial evaluation are given below.

Coating 523 was rejected due to poor adhesion during the coupon test in the NASA T-3 furnace testing performed at the NADC [5]. Coating 571 was rejected because of inconsistent thermal performance during the coupon fire tests [5]. After two years of storage, Coating 546 had completely debonded from the steel coupon retained at SwRI. This coupon was identical to the coupon used for fire testing. The metal coupon was also badly corroded at the interface between the plate and the intumescent coating. Thus, Coating 546 was eliminated from further study.

Table 1. Constituents of Intumescent Formulations (Base Formulations)

Designation	Constituents (Base Formulations)		
	Binder	Intumescing Agent	Fiber
513	NASA formulation EX-1C-82 Polysulfide/Epoxy	Borax	Glass
523	Polysulfide/Epoxy	SMS	Glass
526	Neoprene	SMS	Glass
546	Neoprene	Aluminum Sulfate	Glass
571		NASA Salt	
736	Foundrez/Epoxy	SMS	Glass
746	Flexible Epoxy	SMS	Glass
753	Polyurethane Resin	Borax	Glass
Series 1	Foundrez & Neoprene	Aluminum Sulfate Hydrate	Glass
Series 2	Uralite urethane	Borax	Glass Flake
Series 3		Fire Barrier 303 (3M)	
Series 4	Flexible Epoxy (R-10)	SMS	

The other four coatings, 526, 736, 746, and 753, survived this initial screening process. Samples of these coatings were prepared and applied to an aluminum coupon and a steel coupon. During the preparation and casting of these coatings, they were evaluated for uniformity of mixture, workability, pot life, ease of application, and slump. After the coatings were cured, their adhesion to two types of metal substrates (steel and aluminum) was qualitatively determined by trying to pry them off the metal coupon.

These coatings were then fire tested by mounting them over a flame from a bunsen burner. By using a screen, the flame from the burner was spread sufficiently to impinge uniformly upon the central half of the coated area. The coating was evaluated for degree of intumescence, flammability, char adhesion and integrity.

Once these qualitative tests were completed, variations were made to the four formulations to investigate their physical and thermal properties. These changes included variations in the fiber, filler, and binder content. Samples of the modified coatings were then applied to aluminum coupons and steel coupons for quantitative fire testing at SwRI, conducted during the second phase evaluation of the coatings.

Another coating series, designated Series 1, also was evaluated during this initial screening period. This coating series was evaluated in a fashion similar to Coatings 526, 736, 746, and 753. The Series 1 coating was considered to warrant further study, and was included with the other four coating systems for the second phase of evaluation.

2.3 Second Phase of Coating Evaluation

Coupon samples were made from each of the five intumescent coating systems surviving the initial investigation. The coatings were made by spreading the intumescent mixtures on aluminum and mild steel coupons that had been thoroughly cleaned with acetone. The coatings were spread and leveled by the use of a spatula to a nominal thickness of 2.5 mm (0.10 inches). The coatings were qualitatively evaluated for ease of handling, working time, coating integrity, and adhesion to the two types of metal substrates after

curing. The coatings were then subjected to the flame from a bunsen burner; the coatings were qualitatively evaluated for flammability, intumescence, char integrity and adhesion of the char to the two types of metal substrates. For each of the coating types, the basic formulation was used initially, with variations to the intumescing agent or glass fiber being made subsequently for comparison with the base formulation. The materials, with a brief description of each material, used to make the various coatings are listed in Table 2.

The coating designated 526 was of particular interest since it exhibited excellent thermal performance in the prior study [2,5]. This coating contains a neoprene binder with sodium metasilicate (SMS) as the intumescing agent, and glass flake as a bridging material to aid in char integrity. Using the neoprene binder, additional intumescing agents were substituted for SMS: borax, sodium perborate hydrate, aluminum sulfate hydrate, Expantrol 4, and Wamtrol I. Owen Corning 1/32-inch milled fiber, and HSA fiber were tested in place of glass flake. Table 3 lists the various formulations. The neoprene binder provided for a coating that was easy to handle and apply, and had good adhesion to metal. The coatings performed well during the qualitative burn tests, with the rigid char adhering well to the metal substrate. The coatings designated 526, 526-6, and 526-18 were deemed to be superior to other 526 series coatings in handling and intumescent quality, and were selected as candidates for thermal performance testing using the NASA T-3 furnace [2,5]. To simplify marking of the coupons for identification purposes, the coupon designations were changed. Formulation 526 remained as Formulation 526. Formulation 526-18 was changed to Formulation 5. Formulation 526-6 was changed to Formulation 6.

The coating depicted as Formulation 736 was also investigated. This coating used a Foundrez/Epon 828 copolymer catalyzed with the epoxy hardener "U". The base intumescing agent for this coating is SMS. Additional intumescing agents such as Expantrol 4, sodium perborate hydrate, aluminum sulfate hydrate, and Wamtrol I were also tested. Glass flake was used as the bridging agent; 1/32-inch milled glass fiber, and HSA fiber also were evaluated. Solvents were used in many of the formulations to facilitate mixing and handling, Table 4. The material exhibited good handling properties and cured to a hard, durable coating. Upon flame testing, the coating

Table 2. **Materials Used in Formulations**

1.0 Binder	
Neoprene AD-10	Supplied by Jones Chemical. Polychloroprene elastomer in toluene solvent. Flexible.
EPON 828	Supplied by Shell Chemical Co. A bisphenol-A-polyepichlorhydrin epoxy resin having excellent adhesion, strength, and chemical resistance.
Foundrez	Supplied by Reichold Chemical Co. A phenol-formaldehyde and urea-formaldehyde resin.
DER 736	Supplied by Dow Chemical Co. A flexible epoxy resin having a low viscosity.
Adiprene L-100	Supplied by E.I. DuPont de Nemours and Co. A polyurethane elastomer.
Chemglaze M-200	Supplied by Hughson Chemical Co. A moisture cured polyurethane elastomer.
Hardening Agent "U"	Supplied by Shell Chemical. Used to harden epoxy resins.
DEH 58	Supplied by Dow Chemical Co. Used to harden epoxy resins.
Uralite 3148	Polyurethane resin supplied by HEXCEL Corp. Includes Uralite "A" and the hardener "B".
TC-10	A flexible epoxy supplied by Thermal Chem.
Fire Barrier 303	A commercially available intumescent coating supplied by 3M Company
Polysulfide LP-3	An organic polymer used as a flexibilizer for Epon 828 epoxy resin.
DMP-30	Organic amine-based hardener for Epon 828/LP3 copolymer
2.0 Intumescing Agent	
DS SMS Pentahydrate	Sodium Metasilicate Pentahydrate. Supplied by Diamond Shamrock. A hydrated sodium silicate that releases its water of hydration as the blowing agent.

Table 2. Materials Used in Formulations (Cont'd)

PQ SMS Pentahydrate (fine)	Sodium metasilicate pentahydrate. Supplied by Philadelphia Quartz Co. More finely divided than the DS SMS. Called Metsopentabead 20. Releases its water of hydration as the blowing agent.
Borax	Sodium pentaborate decahydrate. An ideal blowing agent. Loses its abundant water when heated to 75 - 320°C.
Iron Oxide	Ferric oxide. Does not intumesce itself but is sometimes used with SMS to facilitate intumescence.
Sodium Perborate	Sodium perborate tetrahydrate. Loses its water of hydration at 120 - 150°C.
Aluminum Sulfate	Aluminum sulfate hexadecahydrate ($16H_2O$) and octadecahydrate ($18H_2O$) has an abundance of water and a low melting point of 87°C.
Expantrol 4	Made by 3M Company. Proprietary formula.
Wamtrol I	Mixture of sodium metasilicate and zinc borate
Sodium Phosphate	Sodium phosphate heptahydrate. Dibasic. Loses H_2O at 48°C and 93°C
Calcium Chloride	Calcium chloride hydrate loses water from 35-200°C
Calcium Sulfate	Calcium sulfate hemihydrate. Plastic of paris. Sets to a hard material.
Potassium Borate	Potassium pentaborate tetrahydrate loses its water at around 180°C
Sodium Phyrophosphate	Sodium pyrophosphate hexahydrate. Loses its water at around 220°C
Potassium tetrafluoroborate	Decomposes at 350°C.
Hydrated Lime	Calcium hydroxide. Loses water at 600°C.
Britesil	Sodium silicate. Spray dried.

Table 2. Materials Used in Formulations (Cont'd)

3.0 Fibers

Glass Flake	A bridging agent. Glass.
1/32 inch Glass Fiber	Supplied by Owens-Corning. A milled fiber having a nominal length of 1/32 inch. An excellent bridging material to hold the coating and char together. Too high a concentration of glass fiber would make for application problems.
ASA Fiber	A ceramic aluminum silicate fiber.

Table 3. Formulations Evaluated: 526 Series

Series ID	Neoprene AD-10	SMS	Borax	Iron Oxide	Sodium Perborate	Aluminum Sulfate $\cdot 4H_2O$	Expantrol 4 $\cdot 16H_2O$	Wamtrol I	HSA Fiber	Glass Flake	Glass Fiber	Solvent Type
526-	31.1	68.3									0.6	
1X	31.1	68.3										0.6
2X	30.9	67.9									1.2	
3X	31.1	68.3									0.6	Toluene
4X	29.0	64.0		6.4							0.6	Toluene
5X	30.9	67.9								1.2		
6X	33.3	33.3			33.3							
7X	45.5								54.5			
8X	45.5									54.5		
9X	33.3	40.0			26.7							
10X	33.3	26.7			40.0							
11X	33.3	33.3	33.3									
12X	66.7			33.3								
13X	33.3	33.3	33.3									
14X	33.3					33.3	33.3					
15X	33.3					66.7						
16X	71.4										28.6	
17X	33.3	53.4								13.3		
18X	33.3	33.3								33.3		
19X	71.4										28.6	
20X	55.6										44.4	
21X	45.5										54.2	
22X	33.3										66.7	
23X	33.3										66.7	
24X	45.4	27.3								27.3		
25X	29.4	35.3								35.3		
26X	33.3	40.0								26.7		
27X	33.3	26.7								40.0		
28X	33.3	13.3								53.3		
29X	33.3				33.3						33.3	
30X	33.3				40.0						26.7	
31X	33.3				26.7						40.0	
32X	35.8	21.4		21.4						21.4		
33X	33.3	33.3								33.3		
34X	33.3	33.3		33.3								
35X	35.7	42.9								21.4		Methylene Chloride
36X	38.5	15.4	46.2									

Contract No. N62269-85-C-0245
NADC-89061-60

Table 4. Formulations Evaluated: 736 Series

Series	Foundrez	Epon 828	"U"	SMS	Glass Flake	Glass Fiber	HSA Fiber	Iron Oxide	Expantrol 4	Sodium Perborate $\cdot 4\ H_2O$	Aluminum Sulfate $\cdot 16\ H_2O$	HS 240	Wamtrol I	Solvent Type
736-	15.8	31.6	4.3	47.5	.8									
- 1	15.8	31.6	4.3	47.5		0.8								
- 2	15.7	31.4	4.3	47.0	1.6									
- 3	14.8	29.6	10.4	44.4	.7									Methylene Chloride
4	30.5	15.3	7.6	45.8	.8									Methylene Chloride
- 5	15.3	30.5	7.6	45.8	.8									Isopropyl Alcohol
- 6	30.5	15.3	7.6	45.8	.8									Isopropyl Alcohol
- 7	30.5	15.3	7.6	45.8		.8								Isopropyl Alcohol
- 8	15.3	30.5	7.6	45.8		.8								Isopropyl Alcohol
- 9	15.2	30.3	7.6	45.5		1.5								Isopropyl Alcohol
-10	30.3	15.2	7.6	45.5		1.5								Isopropyl Alcohol
-11	30.3	15.2	7.6	45.5			1.5							Isopropyl Alcohol
-12	29.0	14.5	7.2	43.5			1.4	4.3						Isopropyl Alcohol
-13	30.8	15.4	7.7	46.2										Isopropyl Alcohol
-14	30.8	15.4	7.7	30.8					15.4					Isopropyl Alcohol
-15	30.8	15.4	7.7	23.1					23.1					Isopropyl Alcohol
-16	30.8	15.4	7.7	15.4					15.4	15.4				Isopropyl Alcohol
-17	30.8	15.4	7.7						15.4	15.4	15.6			Isopropyl Alcohol
-18	30.8	15.4	7.7						15.4	15.4		15.4		Isopropyl Alcohol
-20	30.8	15.4	7.7						23.1			23.1		
-21	30.8	15.4	7.7	30.8									15.4	

Contract No. N62269-85-C-0245
NADC-89061-60

intumesced fairly well, but the char was more "crumbly" and friable than the char made from the neoprene binder in the 526 series of coatings. Also, the char did not have as good adhesion to the plate as the char for the 526 series. Thus, the 736 coating series was not considered to be one of the better coating formulations; thus, further evaluation was not warranted.

The 746 formulation series contains DCR736 epoxy resin hardened with DEH58 and "U" catalysts. The intumescing agent is SMS with glass flake or glass fiber used as the bridging agent, Table 5. This mixture would not adhere very well to either of the metal substrates during application, and was somewhat difficult to trowel. After curing, the material exhibited good adhesion to the metal substrate. During flame testing, the material softened and tended to drip off the metal sheet. The resultant char was crumbly but had good adhesion to metal. Because of the mentioned detriments, this material was also not considered to be one of the better coatings, and received no further consideration.

The 753 coating series contains the urethane Adiprene L-100, hardened with Chemglaze M-200 catalyst. This system uses borax as an intumescing agent, with glass flake as the bridging material. Alternate bridging agents are glass fiber and HSA fiber. Table 6 contains the detailed information concerning the formulations. When cured, this coating exhibited fair adhesion to the aluminum and steel coupons although some separation was noted. Upon burn testing, the char exhibited fair to poor adhesion. A number of the trial coupons had partial or total separation of the char from the substrate. Because of the poor adhesion of the char, this coating series was not investigated further.

Another coating system evaluated during this study was designated Series 1. This coating contains Foundrez and neoprene as the binder. SMS is the primary intumescing agent, but numerous other intumescing agents were tested within this coating series. The formulations are listed in Table 7. The Series 1 coating system exhibited good workability and easy handling. The cured coating was flexible and bonded well to both steel and aluminum. Formulation 1-13, containing aluminum sulfate hydrates as the intumescing agent, performed well during the qualitative burn test. This coating

Table 5. Formulations Evaluated: 746 Series

Series ID	DER	DGH 736	"U" 58	SMS	Glass Flake	Glass Fiber	Solvent Type
746-	22.1	4.1	4.1	69.0	.7		
- 1	22.1	4.1	4.1	69.0		.7	
- 2	21.9	4.1	4.1	68.5	1.4		
- 3	22.6	2.8	2.8	70.9	.7		Methylene Chloride

Table 6. Formulations Evaluated: 753 Series

Series ID	Adiprene L-100	Chemglaze M-220	Borax	Glass Flake	Glass Fiber	HSA Fiber	Solvent Type
753-	12.4	12.4	74.5	.6			
-1	12.4	12.4	74.5		.6		
-2	12.3	12.3	74.1	1.2			
-3	12.4	12.4	74.5	.6			Toluene
-4	12.3	12.3	74.1			1.2	Toluene
-5	12.5	12.5	75.0				Toluene
-6	12.5	12.5	75.0				Methylene Chloride

Table 7A. Formulations Evaluated: Series 1

ID	Foundrez	Neoprene AD-10	SMS	Expantrol II	Sodium Bicarbonate	Glass Flake	Glass Fiber	HSA Fiber	Iron Oxide	Solvent Type
1-1	6.2	24.8	68.3	.1		.5				Toluene
-2	6.2	24.8	68.1	.5		.5				Toluene
-3	6.2	24.8	68.1	.5			.5			Toluene
-4	6.1	24.6	67.6	.5			1.2			Toluene
-5	6.1	24.6	67.6	.5		1.2				Toluene
-6	6.1	24.4	67.0	1.2		1.2				Toluene
-7	5.8	23.1	63.6			1.2			6.4	Toluene
-8	6.6	26.3	32.9		32.9	1.3				Toluene
-9	6.1	24.4	67.1	1.2				1.2		Toluene
-10	6.1	24.4	67.1	1.2				1.2		Isopropyl Alcohol
-11	6.1	24.4	67.1	1.2				1.2		Methylene Chloride

Contract No. N62269-85-C-0245
NADC-89061-60

Table 7B. Formulations Evaluated: Series 1

ID	Foundrez	Neoprene AD-10	Glass Flake	Sodium Phosphate $\cdot 7\ H_2O$	Aluminum Sulfate $\cdot 16\ H_2O$	Calcium Chloride $\cdot 2\ H_2O$	Calcium Sulfate $\cdot \frac{1}{2}\ H_2O$	Potassium Borate $\cdot 4\ H_2O$	Sodium Pyrophosphate $\cdot 6\ H_2O$	Solvent Type
1-12	6.2	24.7	1.2	67.9						Toluene
13	6.2	24.7	1.2		67.9					Toluene
14	6.2	24.7	1.2			67.9				Toluene
15	6.2	24.7	1.2				67.9			Toluene
16	6.2	24.7	1.2					67.9		Toluene
17	6.2	24.7	1.2						67.9	Toluene

Contract No. N62269-85-C-0245
NADC-89061-60

Table 7C. Formulations Evaluated: Series 1

ID	Foundrez	Neoprene AD-10	SMS	Glass Flake	Potassium Tetra-fluoroborate	Hydrated Lime	Sodium Perborate $\cdot 4H_2O$	Borax	Aluminum Sulfate $\cdot 18\ H_2O$	Expantrol 4	HS 200	HS 240	Britesil	Solvent Type
1 18	6.2	24.7		1.2	67.9									
-19	7.7	30.8				61.5								Toluene
-20	6.2	24.7		1.2			67.9							Toluene
-21	6.3	25.0	68.7											Toluene
-22	6.2	24.7	67.9	1.2										
-23	6.3	25.0						68.7						
-24	6.3	25.0							68.7					Toluene
-25	6.3	25.0									68.7			Toluene
-26	6.3	25.0										68.7		Toluene
-27	6.3	25.0											68.7	
-28	6.3	25.0								68.7A				Toluene
-29	6.3	25.0								68.7B				Toluene
-30	6.7	26.6	33.3							33.3B				Toluene
-31	6.7	26.6	33.3							33.3A				Toluene
-32	6.7	26.6	33.3				33.3							Toluene

Contract No. N62269-85-C-0245
NADC-89061-60

exnibited good intumescence, and the rigid char had good integrity and adhesion to metal. The coating designated 1-20 was difficult to apply, but it exhibited excellent intumescence when burned. The char was somewhat friable but had good adhesion to metal. Both coatings warranted further study. Coating 1-13 was designated as coating 5, while coating 1-20 was renamed coating 7.

Additional coatings designated 2, 3, and 4 were also evaluated. Coating 2 contains Uralite 3148 urethane as a binder with borax as the intumescing agent, Table 8. This coating performed poorly during burn tests. The char was crumbly and would not adhere to metal. No further evaluation was warranted. Coating 3 is a commercially available product called Fire Barrier 303 from 3M, Table 9. This coating has excellent intumescence but the char is extremely friable and would probably slough away during a large fire. Coating 4 consists of a flexible epoxy TC-10, and SMS as an intumescing agent, Table 10. This coating was difficult to apply and tended to bubble and separate during flame testing. No further evaluations were planned for coating series 3 and 4.

2.4 Coupon Preparation for Thermal Performance Testing

Six coating formulations were selected during the evaluation trials as warranting further study. These formulations are summarized in Table 11. The coating systems were cast onto steel coupons for shipment to NADC for thermal performance testing in the NASA T-3 furnace [2,5]. Specimens were also cast for the NASA EX-1C-82 formulation (Table 11). The NASA coating was cast to provide current comparative data with the new, alternate formulations.

The steel coupons, 7.6 cm by 7.6 cm (3.0 in x 3.0 in) have a 2.54 cm (1.0 in) diameter disc cut from the center of the coupon, which is then epoxied back into position using a high-temperature epoxy. This mechanical arrangement serves to insulate the disc from edge effects, thus providing a one-dimensional heat path through the coating system to the metal disc substrate. The metal coupons and the NASA T-3 furnace are described more fully in Reference 2 or 5.

Table 8. Formulations Evaluated: Series 2

ID	Uralite 3148 "A"	Uralite 3148 "B"	Glass Flake	Borax
2-1	45.5	18.2	2.3	34.1
2-2	41.7	16.7		41.7

Table 9. Formulations Evaluated: Series 3

ID	Fire Barrier	SMS	Glass	Water Flake	Solvent Glass
3-1	100				
3-2	100				Acetone
3-3	100				Isopropyl Alcohol
3-4	100				Toluene
3-5	66.7	33.3			Toluene
3-6	98.4		1.6		Toluene
3-7	100				MEK
3-8	70.6			29.4	

Table 10. Formulations Evaluated: Series 4

ID	TC-10 A	TC-10 B	SMS	Wamtrol I	Borax
4	32.8	1.6	65.6		
4-1	32.8	1.6	32.8	32.8	
4-2	44.5	2.1			53.4

Table 11. Formulations

SPECIMENS CAST FOR THERMAL PERFORMANCE TESTING

Formulation 513 (EX-1C-82)	% by Mass
Epon 828	21.7
Polysulfide LP-3	21.3
DMP-30	3.2
Borax	52.9
Glass Flake	0.9

Formulation 526	
Neoprene AD-10	31.1
SMS DS	68.3
Glass Flake	0.6

Formulation 1 (Designated 1-13 in Table 7)	
Foundrez	6.2
Neoprene AD-10	24.7
Aluminum Sulfate·$16H_2O$	67.9
Glass Flake	1.2
Toluene Solvent	6.2 g Toluene/100 g coating

Formulation 5 (Designated 526-18 in Table 3)	
Neoprene AD-10	33.3
SMS (PQ)	33.3
Wamtrol I	33.3

Formulation 6 (Designated 526-6 in Table 3)	
Neoprene AD-10	33.3
SMS (PQ)	33.3
Sodium Perborate·$4H_2O$	33.3

Formulation 7 (Designated 1-20 in Table 7)	
Foundrez	6.2
Neoprene AD-10	24.7
Sodium Perborate·$4H_2O$	67.9
Glass Flake	1.2
Toluene Solvent	18.5 g Toluene/100 g coating

The materials used in each formulation were weighed to the nearest 0.1 gram into a polyethylene beaker on a Mettler platform balance. These ingredients were then thoroughly mixed. To cast the coating, the mixture was poured into the respective molds and the excess material removed by the use of a screed.

To better characterize the thermal performance of the coatings sent to the NADC, specimens of each type were cast with three different thicknesses. Each coating was cast by placing two clean, bare steel coupons side-by-side on an aluminum plate. The steel coupons were stamped with an "ID", then were cleaned with acetone. The coupons were surrounded by a thicker plate conforming exactly to the sides of the coupons to form the mold.

To make the three different coating thicknesses, the plates used were either 3.18 mm (1/8 in), 4.76 mm (3/16 in), or 6.35 mm (1/4 in). The coating thickness would then be equal to the thickness of the surrounding plates (mold) minus the thickness of the steel coupon, which has a nominal thickness of 1.57 mm (0.062 in). A sufficient number of molds were constructed to permit casting of all the coupons for each coating system from one batch of material; thus, differences due to batch variation were eliminated. The coatings, upon curing, had nominal thicknesses of 1.78 mm (0.07 in), 3.30 mm (0.13 in), or 4.83 mm (0.19 in). The actual coating thicknesses varied due to differences in workability of the coatings and different degrees of expansion or contraction as the coatings cured, Table 12.

Interpretation of the thermal performance data during the previous study [5] was made more difficult by the differences in coating thicknesses of the test specimens. In that study, a recommendation was made to mill the coatings to the same initial thicknesses prior to testing. The specimens in Table 12 were milled to a thickness of 1.52 mm (0.060 in), 3.05 mm (0.120 in) and 4.57 mm (0.180 in). The coatings were milled to a tolerance of ± 0.05 mm (± 0.002 in) on a Bridgeport milling machine.

After milling, the coupons were weighed to the nearest 0.1 mg on a Mettler analytical balance, Table 12. The coating thickness was determined to the nearest 0.025 mm (0.001 in) by a micrometer caliper, Table 12. Two

Table 12. Coupon Mass and Coating Thickness (Pretest)

Specimen ID	Cured Coating Thickness (in.)	Milled Coating Thickness (in.)	Coating Mass (g)
513-1BB	.0780	0.060	11.21
513-1AA	.0840	0.061	10.85
513-2A	.1340	0.119	21.59
513-3A	.1811	0.180	33.04
526-1A	.0936	0.059	6.36
526-1AA	.0876	0.060	7.58
526-2A	.1513	0.122	14.86
526-3A	.1975	0.180	22.43
1-1A	.0781	0.059	8.34
1-1AA	.0789	0.060	7.86
1-2A	.1459	0.121	16.90
1-3A	.1926	0.181	26.16
*5-1A	.0864	0.062	7.86
5-1AA	.0864	0.061	7.44
5-2A	.1460	0.121	16.59
5-3A	.2089	0.180	25.09
6-1A	.0741	0.062	8.20
6-1AA	.0768	0.062	7.93
6-2A	.1406	0.119	16.73
6-3A	.1870	0.180	25.21
7-1A	.0831	0.060	7.26
7-1AA	.1039	0.058	7.29
7-2B	.1289	0.120	15.60
7-3A	.1838	0.178	22.89

* Misaligned disc in coupon affects coating thickness measurements.

coupons were provided for the 1.52 mm thick coating samples to demonstrate repeatability in the tests.

The specimens were sent to the NADC for thermal performance testing in the NASA T-3 furnace.

2.5 Summary

All of the formulations were qualitatively evaluated and five formulations were considered to be possible alternates to the NASA formulation. These five candidate formulations are designated 526, 1, 5, 6, and 7, and were cast upon coupons and sent to the Navy for thermal performance testing. Formulation 526 is unchanged from the previous program, so it retained its original designation. Coatings 5 and 6 are variations to the 526 formulation and have received new identification numbers to prevent confusion. Coatings 1 and 7 are variations of coating Series 1 and received the single digit identification number. Coupons coated with the NASA formulation EX-1C-82, designated 513, were also prepared for thermal performance testing with the alternate coatings, to serve as the baseline coating system. Thermal performance is presented in Section 5.0, and conclusions concerning thermal performance are discussed in Section 6.0.

3.0 SOME THERMODYNAMIC PROPERTIES OF INTUMESCENT FORMULATIONS

3.1 Introduction

Concurrent with the work to develop alternate intumescent systems, tests designed to obtain thermodynamic properties of intumescent formulations were performed: thermogravimetric analysis and differential scanning calorimetry. The analyses measure, respectively, mass loss and heat absorption as a function of temperature. Enthalpy changes and specific heats are determined from these data. Also, the effect of pressure on intumescence was investigated. Since this phase of the project was concurrent with the work described in the last section, not all the formulations ultimately chosen for fire tests were analyzed for their thermodynamic characteristics. However, the work performed here should be representative of a range of intumescent formulations, particularly those which use bound water as the blowing agent. The formulations tested were 523, 526, 546, 736, 743, 746, and 753. The specific formulations are listed in various tables in the previous section; the components of the formulations are given in Table 1.

3.2 Thermogravimetric Analysis

Thermogravimetric analysis (TGA) determines the change in weight of a small sample of material as a function of the temperature of that material. The instrument used for the analysis was a Perkin-Elmer TGS-2. The analysis was performed at a heating rate of 20°C/minute over a range of 25°C to 950°C. A nitrogen atmosphere was used to blanket the specimens during heating. The mass of the sample is normalized to 1.0; therefore, as the mass of the sample changes due to pyrolyzation of components within the sample, the output directly gives the ratio of the remaining mass m/m_o as a function of temperature. The rate of mass loss is also obtained by use of the Perkin-Elmer FDC-1, a first derivative computer. Figures 1-7 depict the TGA results for this series of tests. The remaining mass fraction (m/m_o) is plotted as the solid line, and the dashed line indicates the rate of mass loss; both are plotted as a function of temperature. These formulations lose between 40 to 60 percent of their mass during intumescence and subsequent formation of the char material.

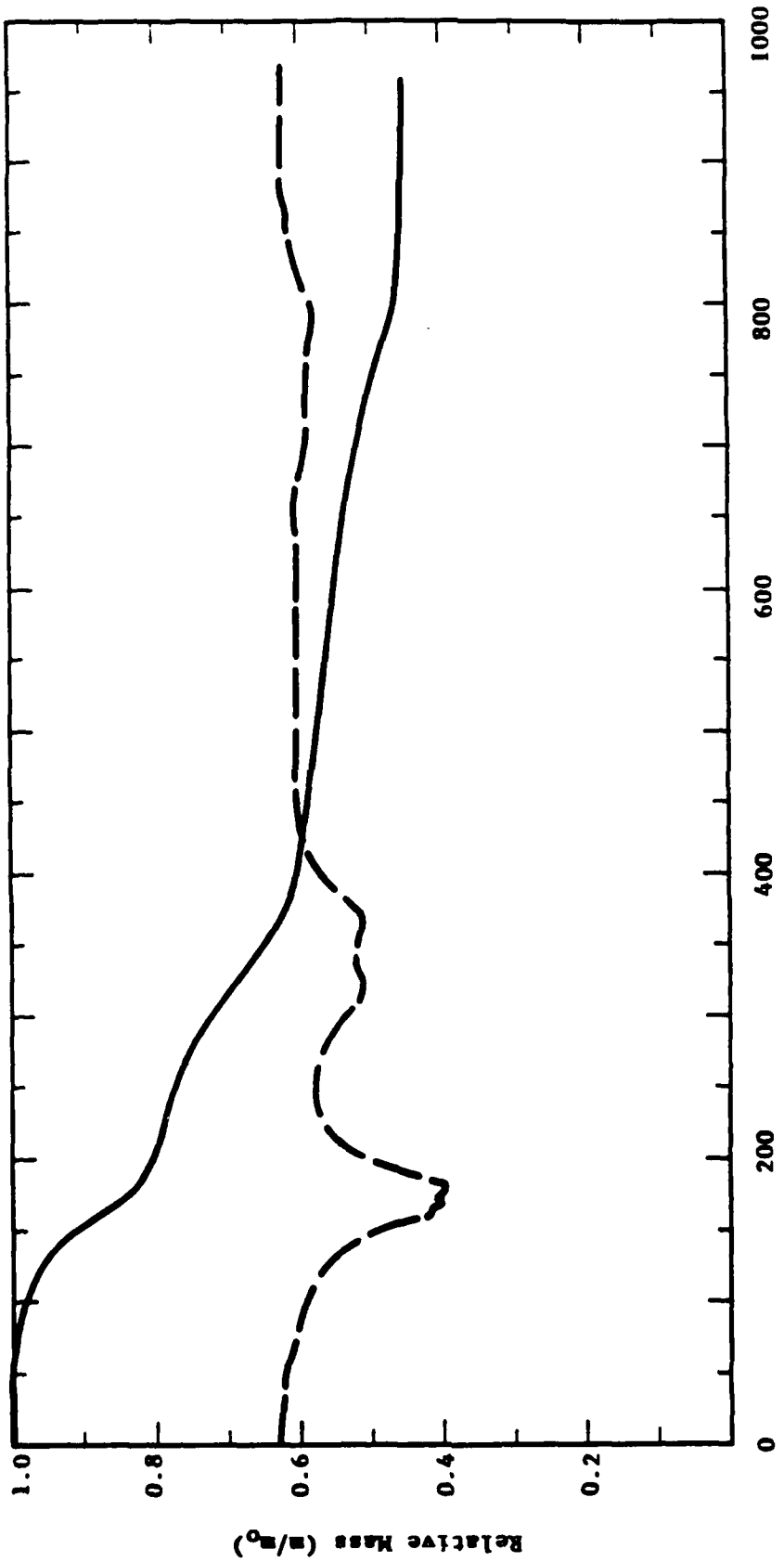

Figure 1. TGA Data for Formulation 523

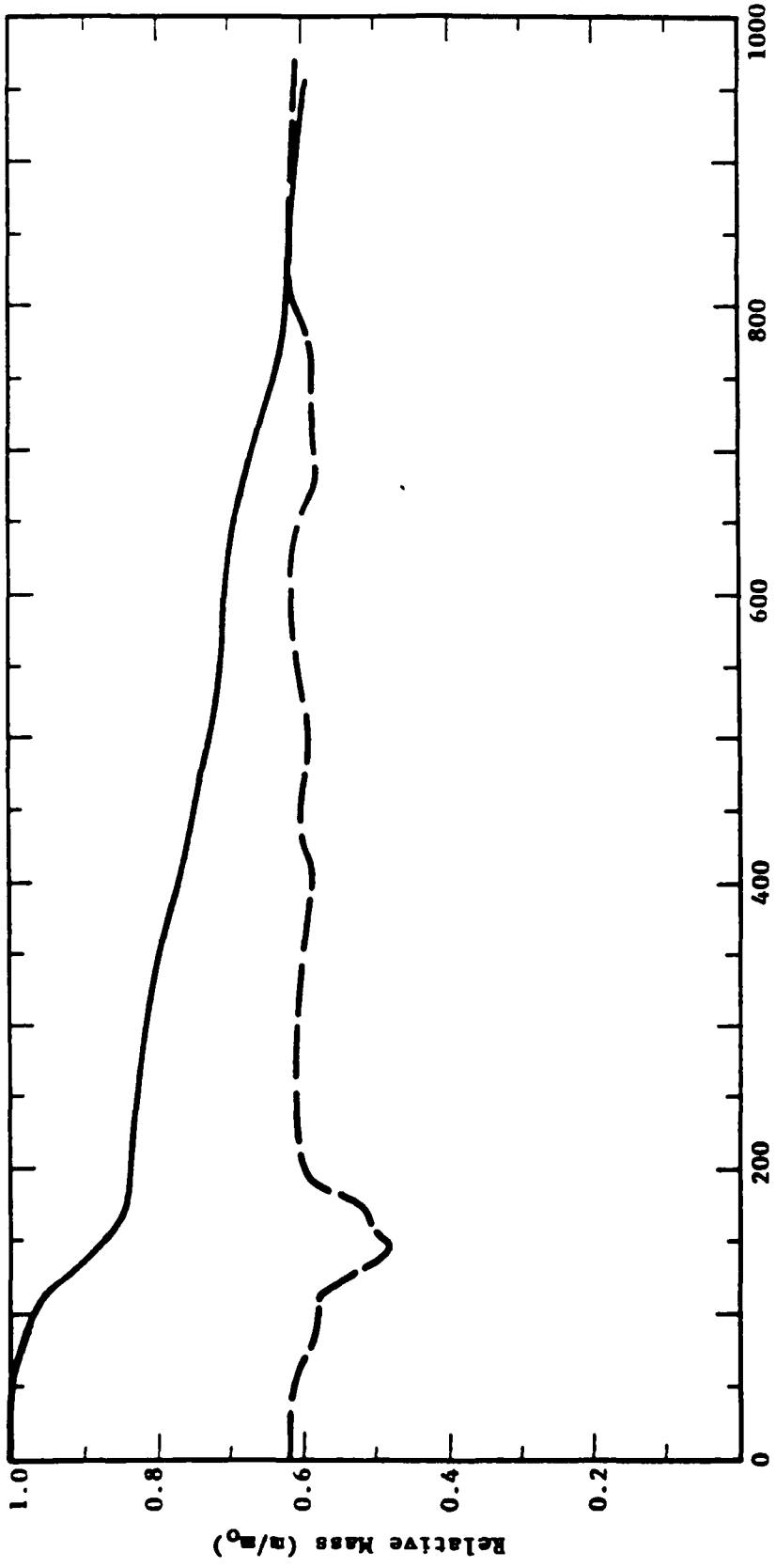

Figure 2. TGA Data for Formulation 526

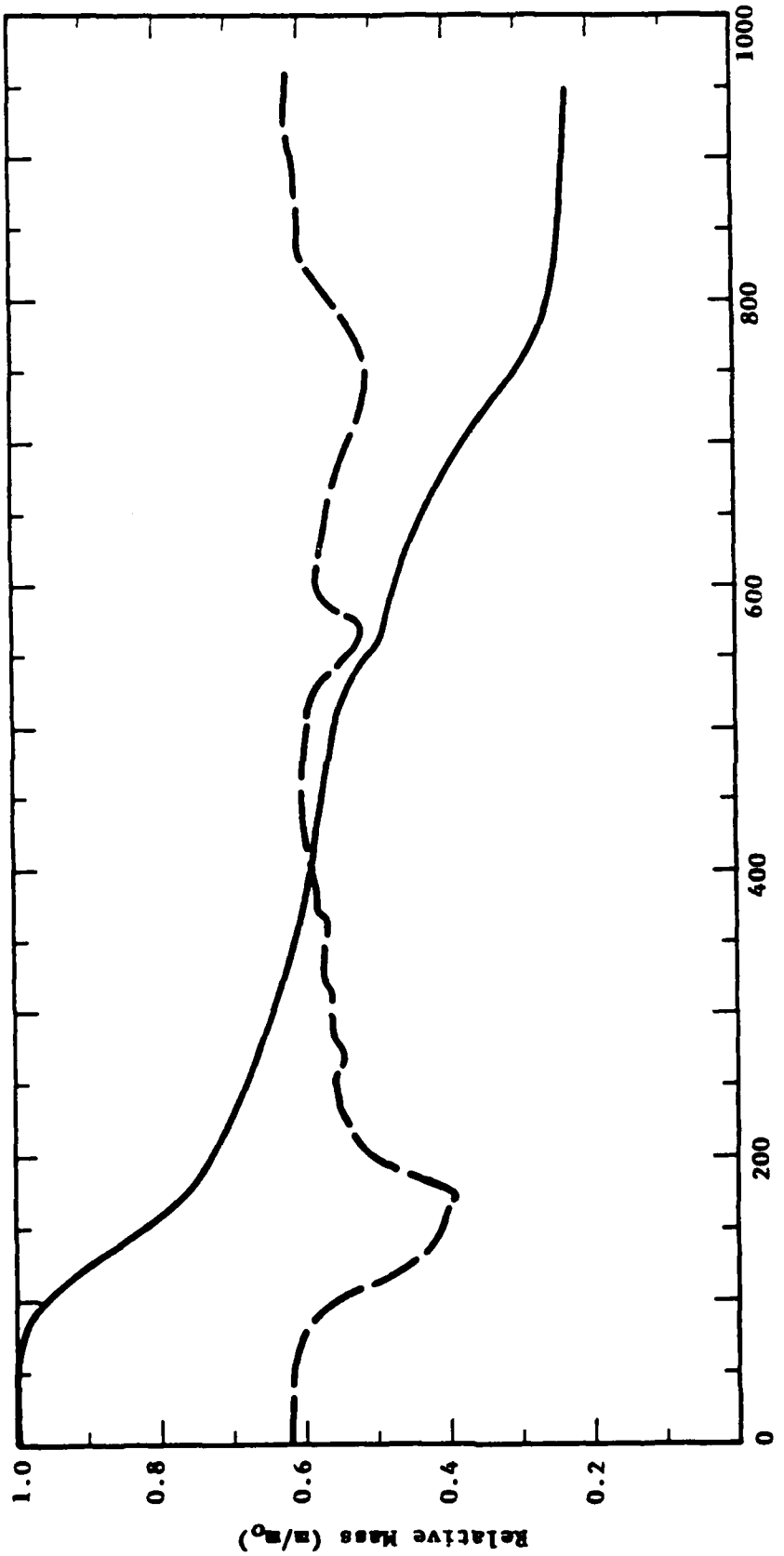

Figure 3. TGA Data for Formulation 546

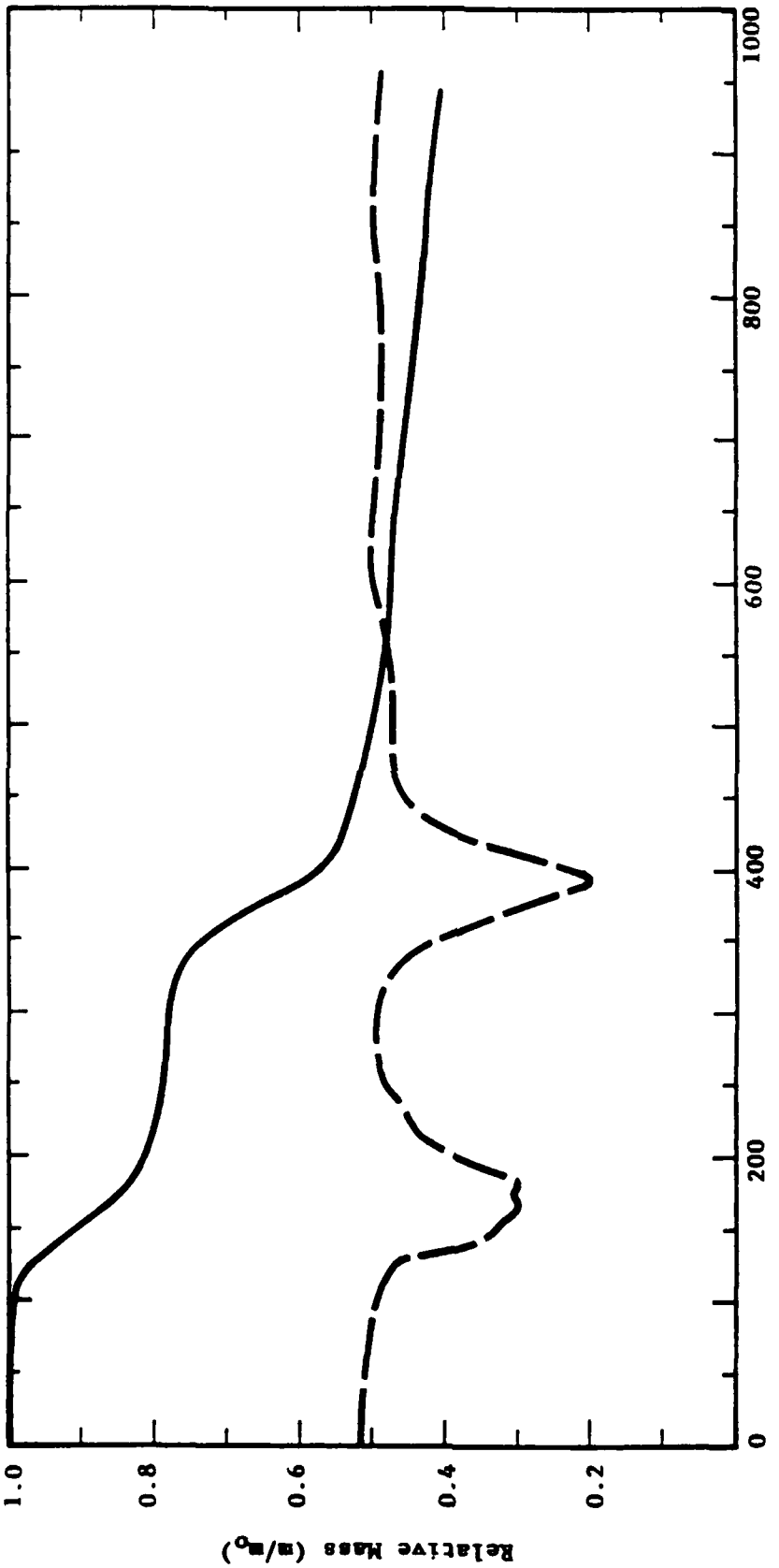

Figure 4. TGA Data for Formulation 736

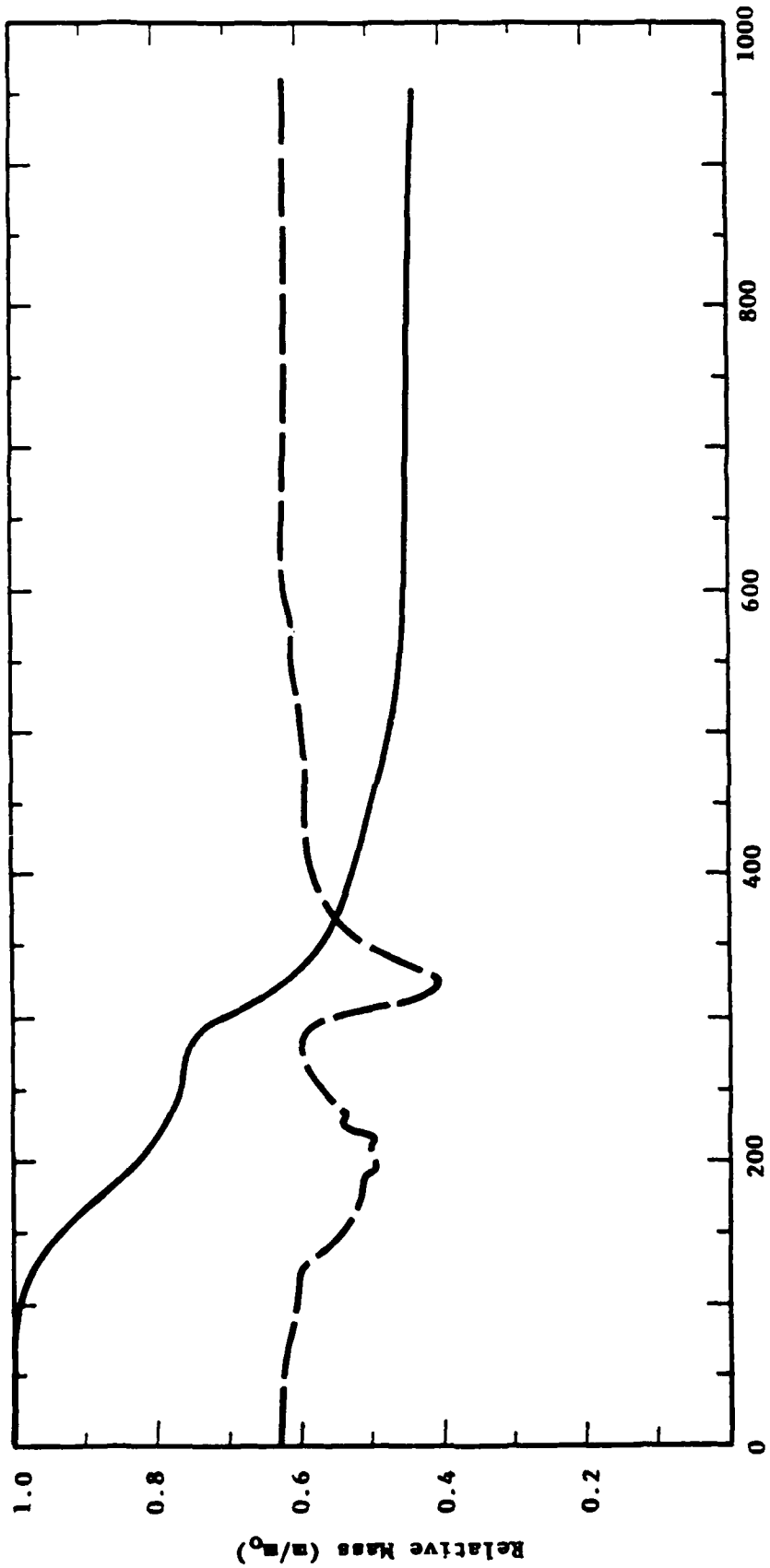

Figure 5. TGA Data for Formulation 743

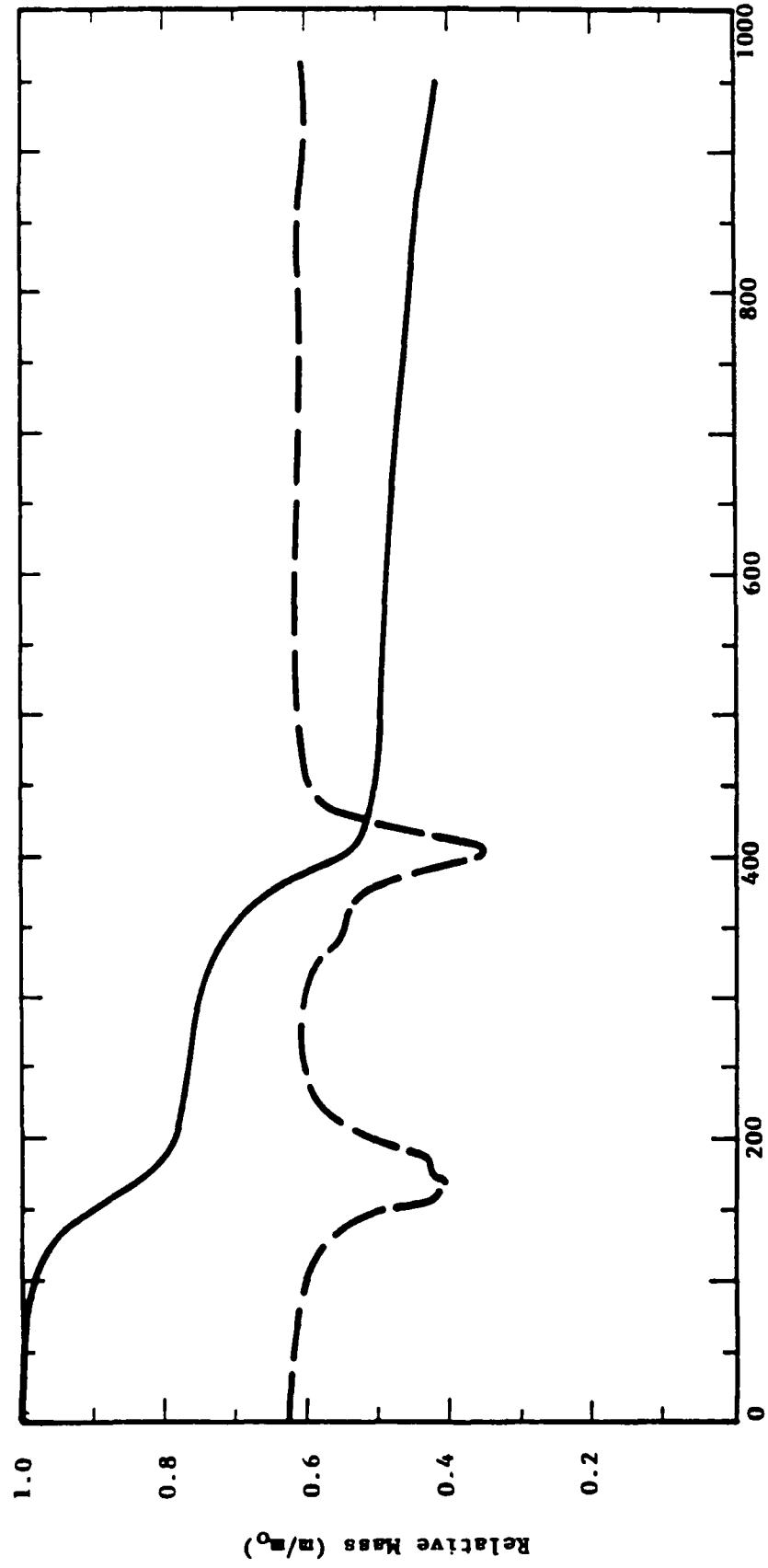

Figure 6. TGA Data for Formulation 746

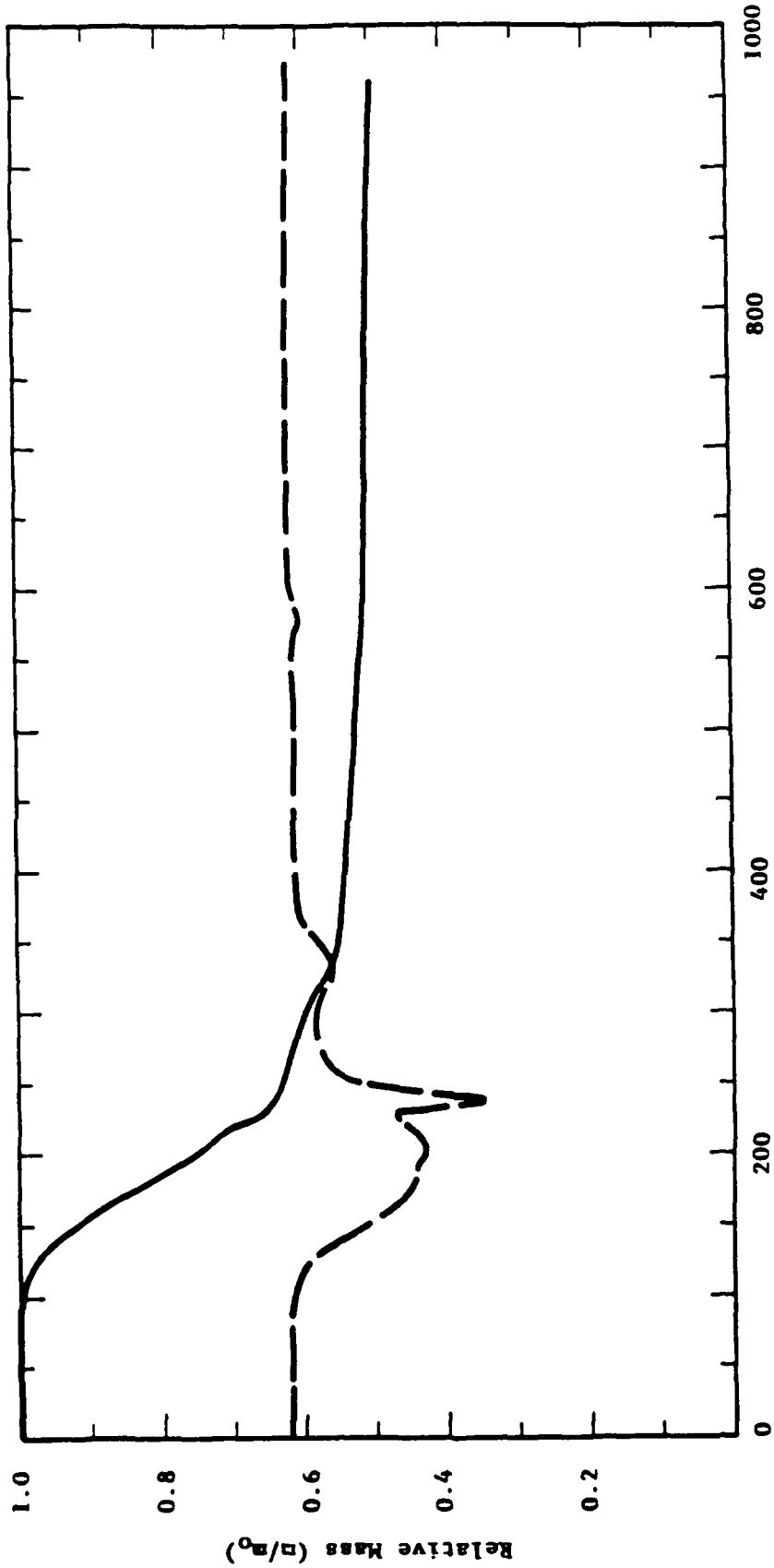

Figure 7. TGA Data for Formulation 753

TGA's were also conducted on the formulations finally selected for fire testing at NADC (Table 1'). The mass fractions as a function of temperature are shown in Figures 8-13; the rate of mass loss was not plotted on these graphs as on the previous graphs. It is curious to note that formulation 1 has a very large mass loss between 600 and 800°C. Since both formulations 1 and 7 have a foundrey/neoprene binder, it would imply that the aluminum sulfate decomposes and releases considerably more violatiles than the sodium perborate.

3.3 Differential Scanning Calorimetry

Differential scanning calorimetry (DSC) measures and records the energy necessary to maintain thermal equilibrium between a test sample and a chosen reference. The sample of known mass is heated at a prescribed rate (typically 20°C/min) while the rate at which energy is absorbed (endothermic) or emitted (exothermic) is recorded versus temperature. Specific heats are proportional to the deviation of the sample thermogram from the baseline, while a phase change is represented by a peak. The area of the peak is proportional to the heat absorbed in the phase change. The DSC experiments were performed on a Perkin-Elmer DSC-4.

Figure 14 illustrates the DSC output. The test is run under three conditions. First, a baseline is established, curve A; i.e., the heat absorbed by the pans and lids, without a sample, is measured. Curve B results are for a DSC run with a paint sample in place. The peaked regions correspond to the intumescent outgassing of the material. Following the testing of the sample to 600°C, the remaining carbonized char was cooled and the DSC repeated as shown for curve C. The enthalpy changes from intumescent outgassing observed in curve B are absent on curve C. An interpretation of the results is described in the next subsection.

The latest group of DSC runs show some distinct differences to those reported in "Intumescent Reaction Mechanisms: An Analytic Model" by Anderson and Wauters [4]. Figure 15 is typical of the results from data obtained on an old Dupont DSC. The curve is inverted, having been conducted on an instrument measuring the heat absorbed relative to the sample rather than the heat

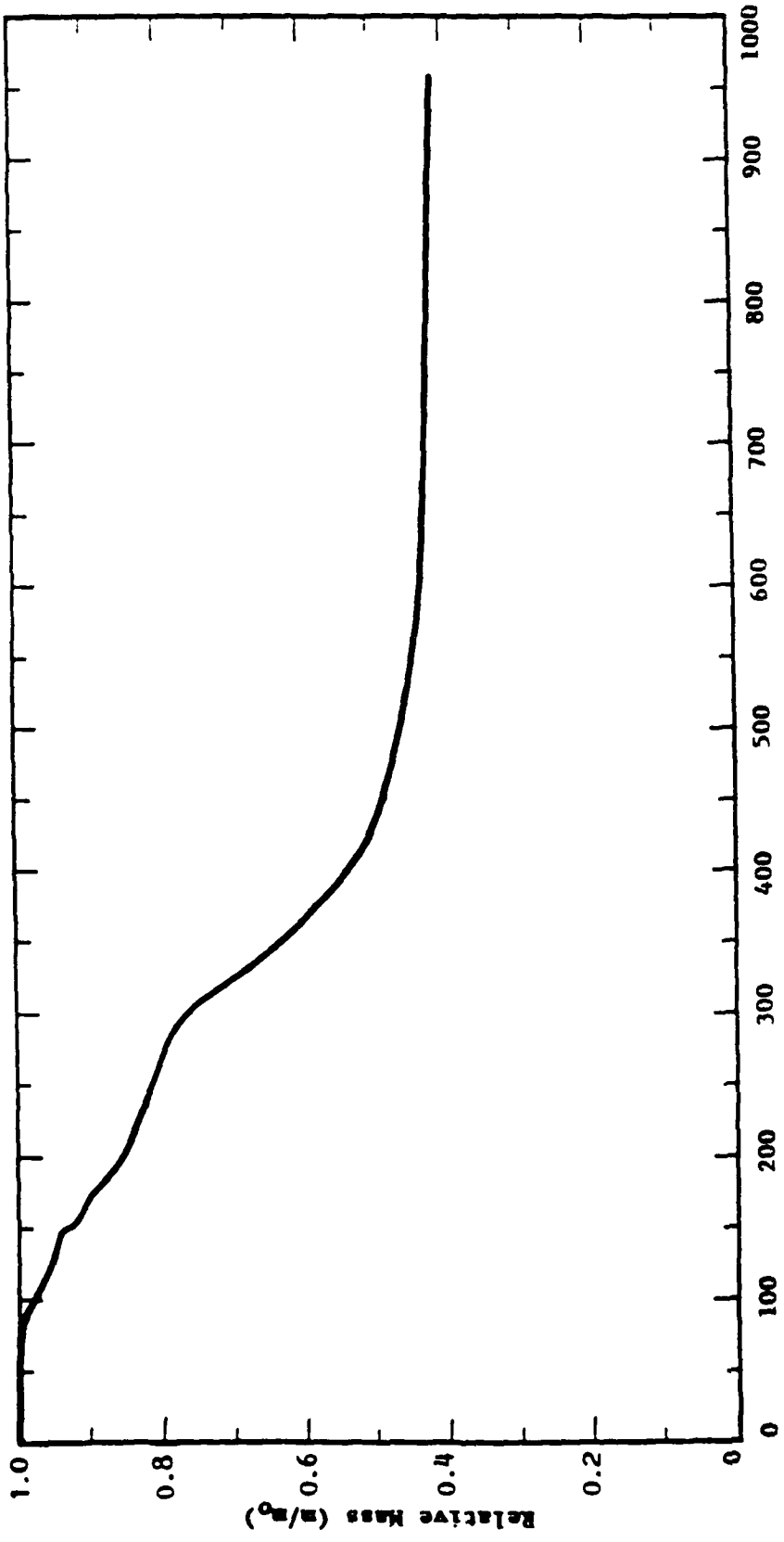

Figure 8. TGA Data for Formulation 513

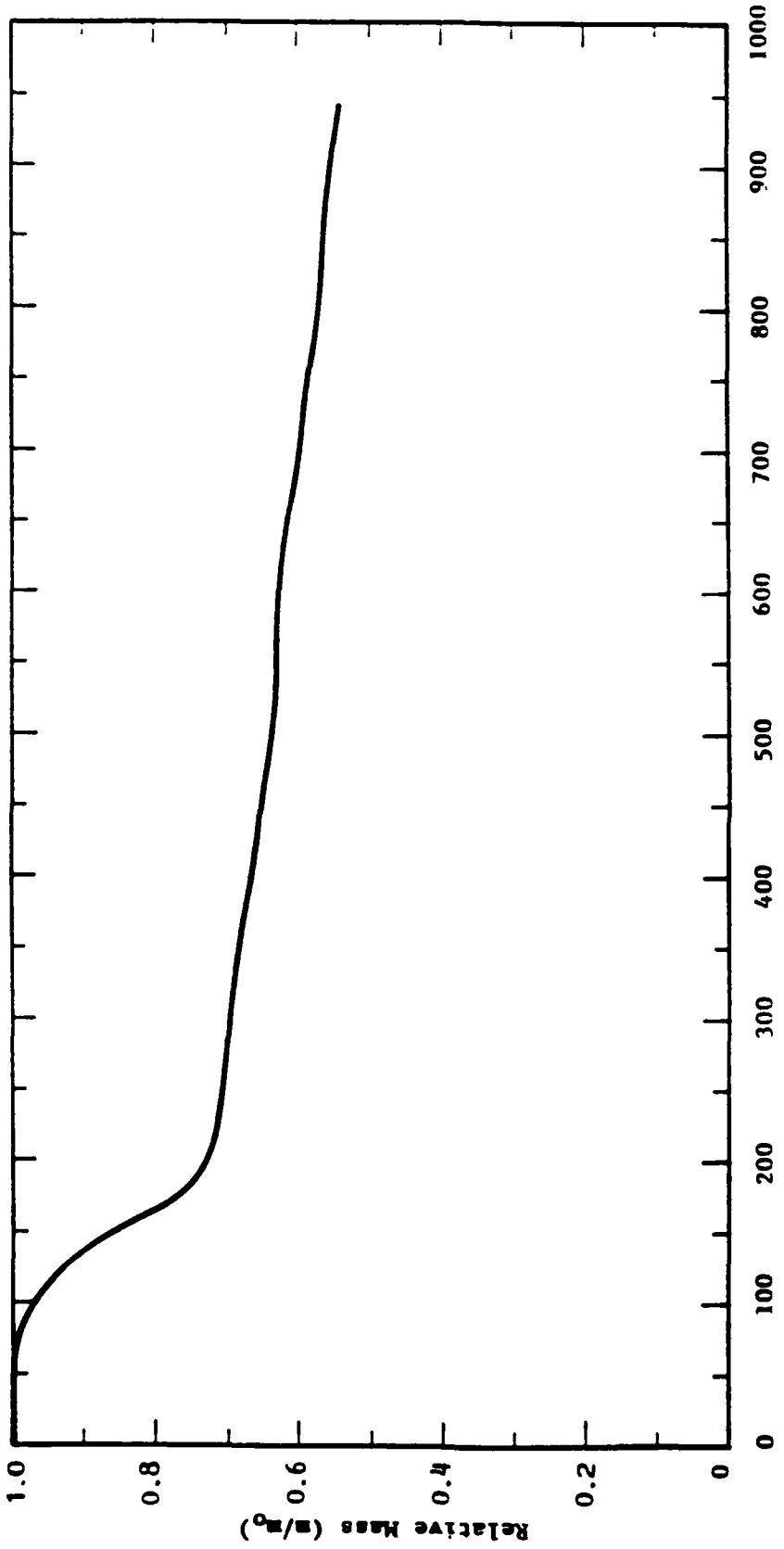

Figure 9. TGA Data for Formulation 526

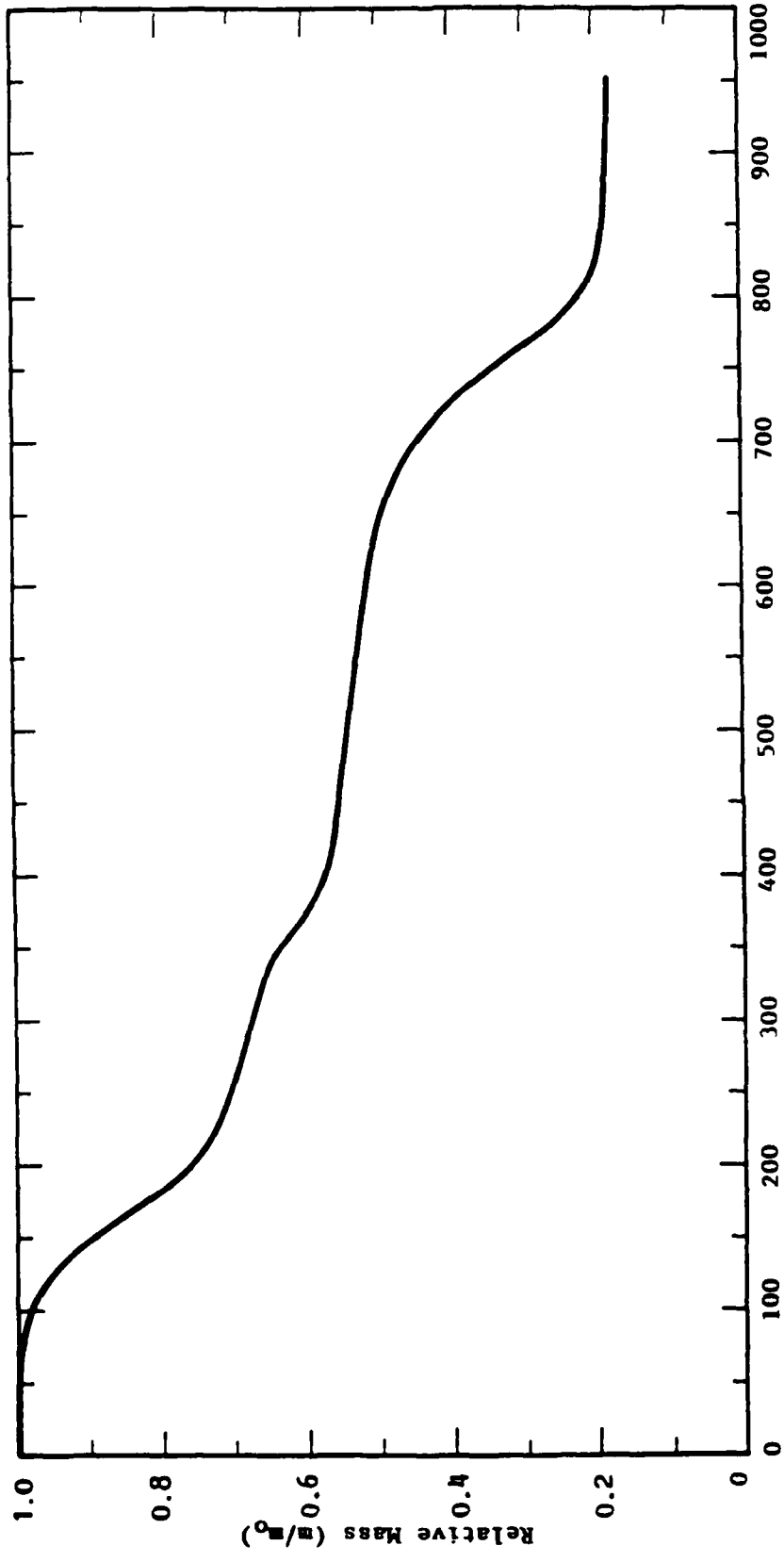

Figure 10. TGA Data for Formulation 1

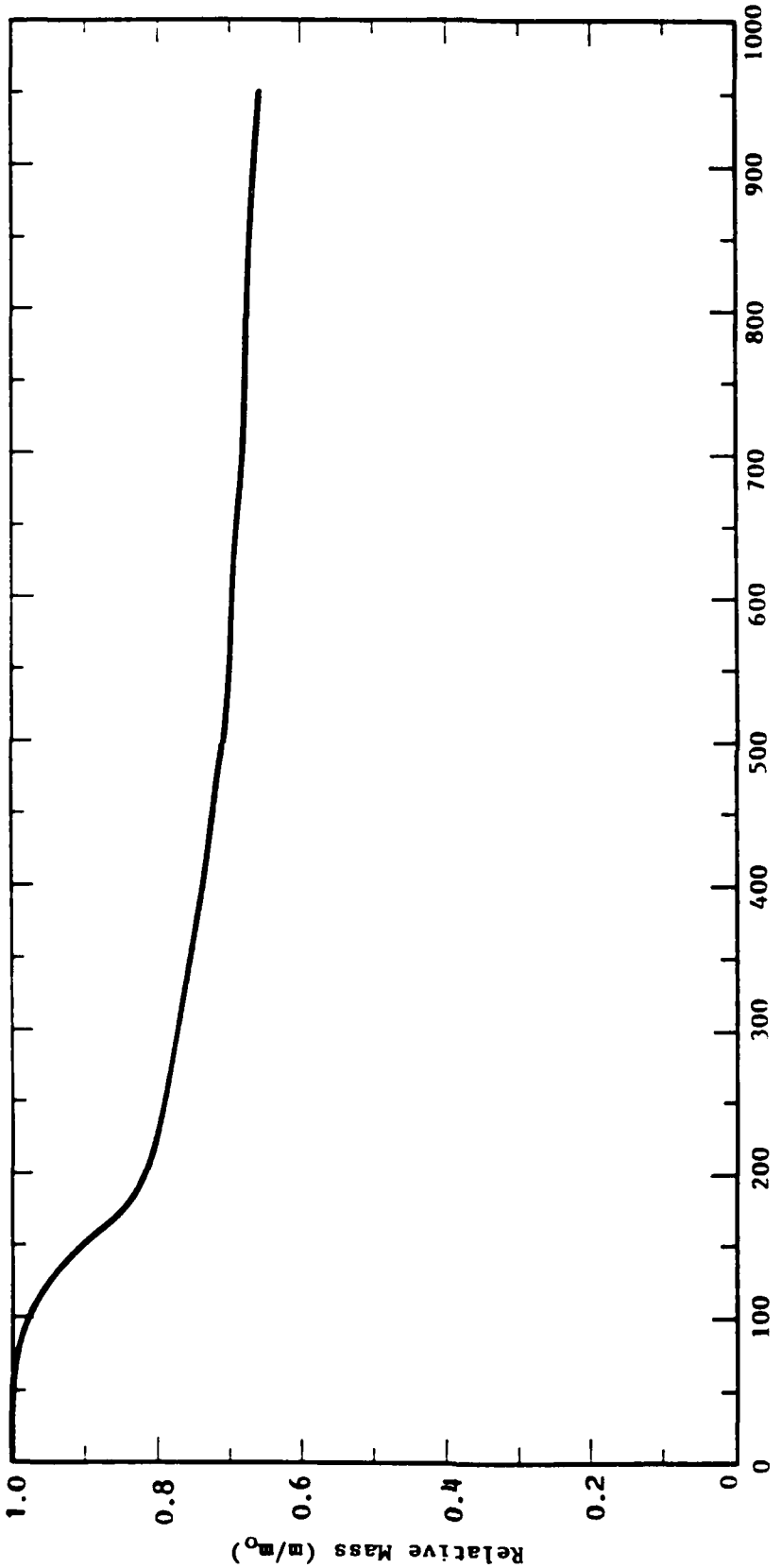

Figure 11. TGA Data for Formulation 5

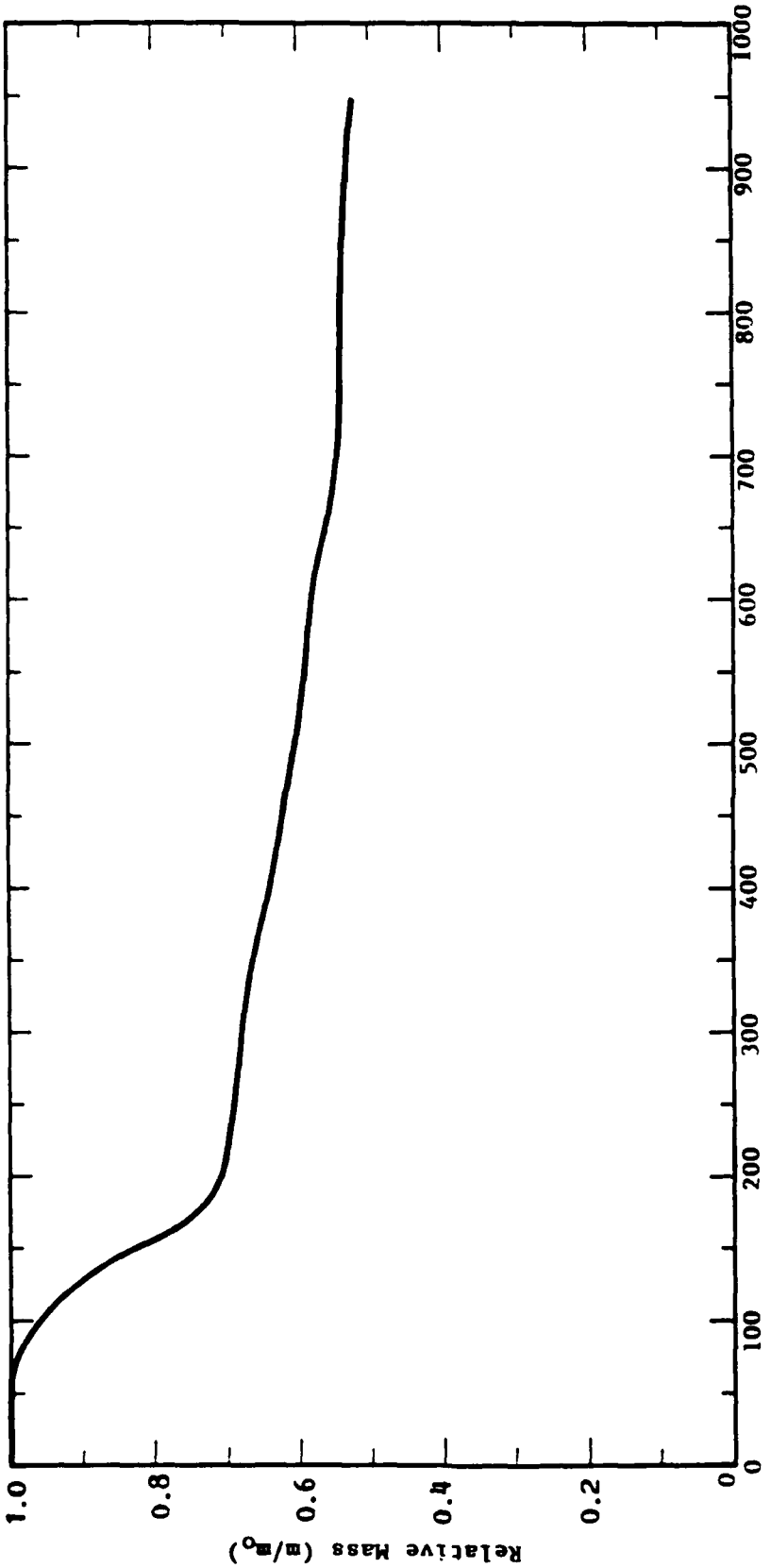

Figure 12. TGA Data for Formulation 6

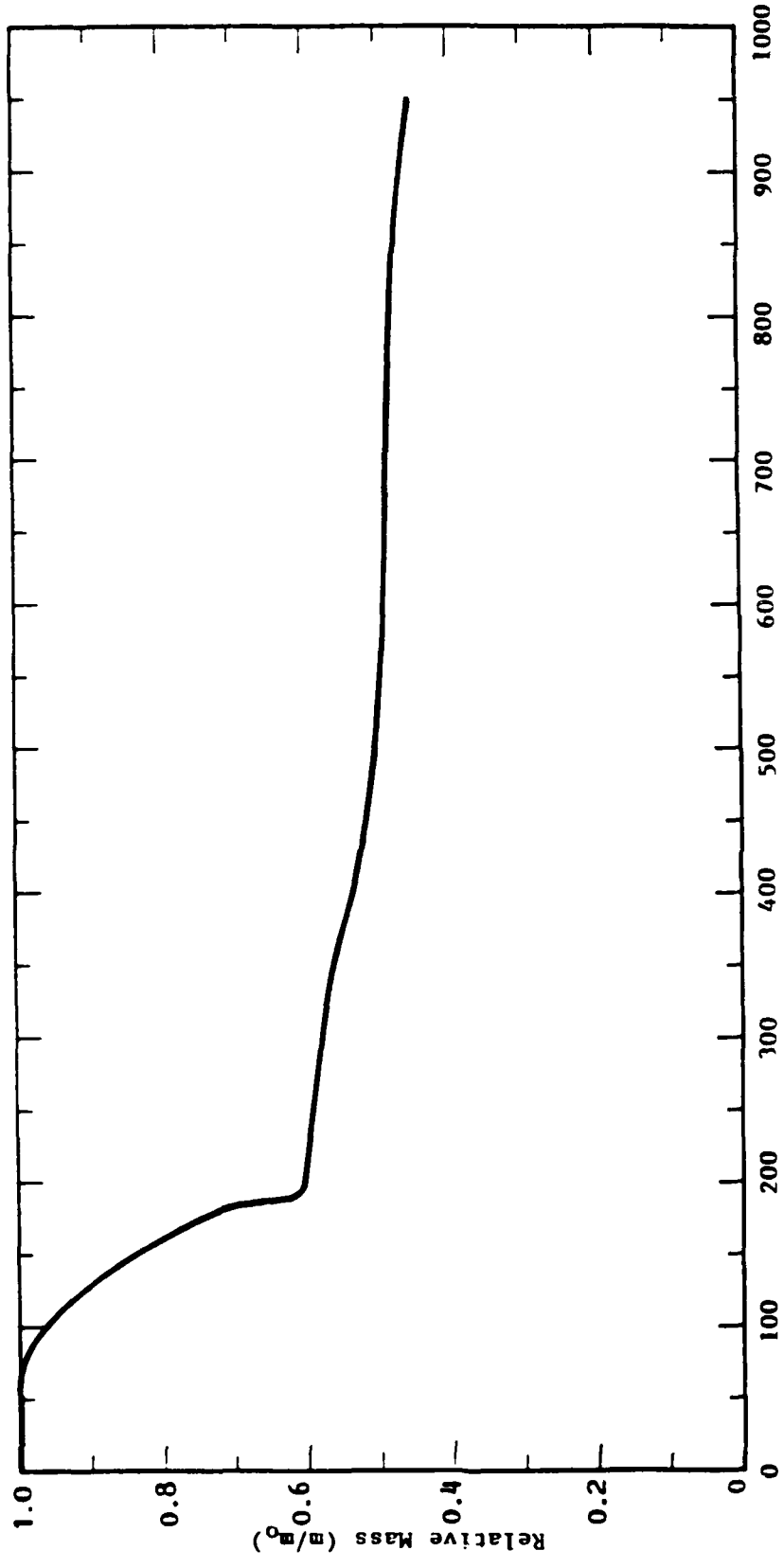

Figure 13. TGA Data for Formulation 7

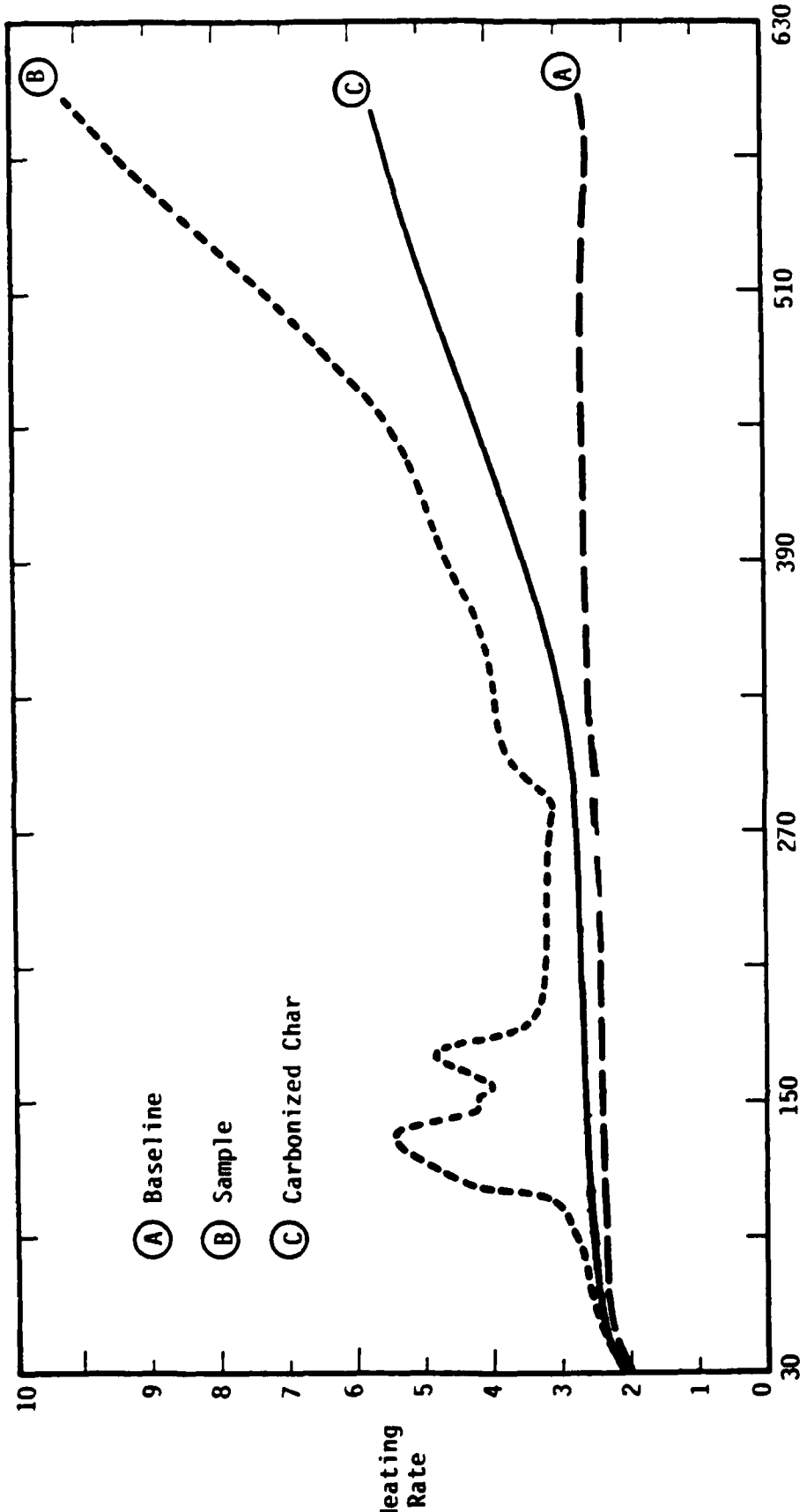

Figure 14. Example of DSC Thermograph

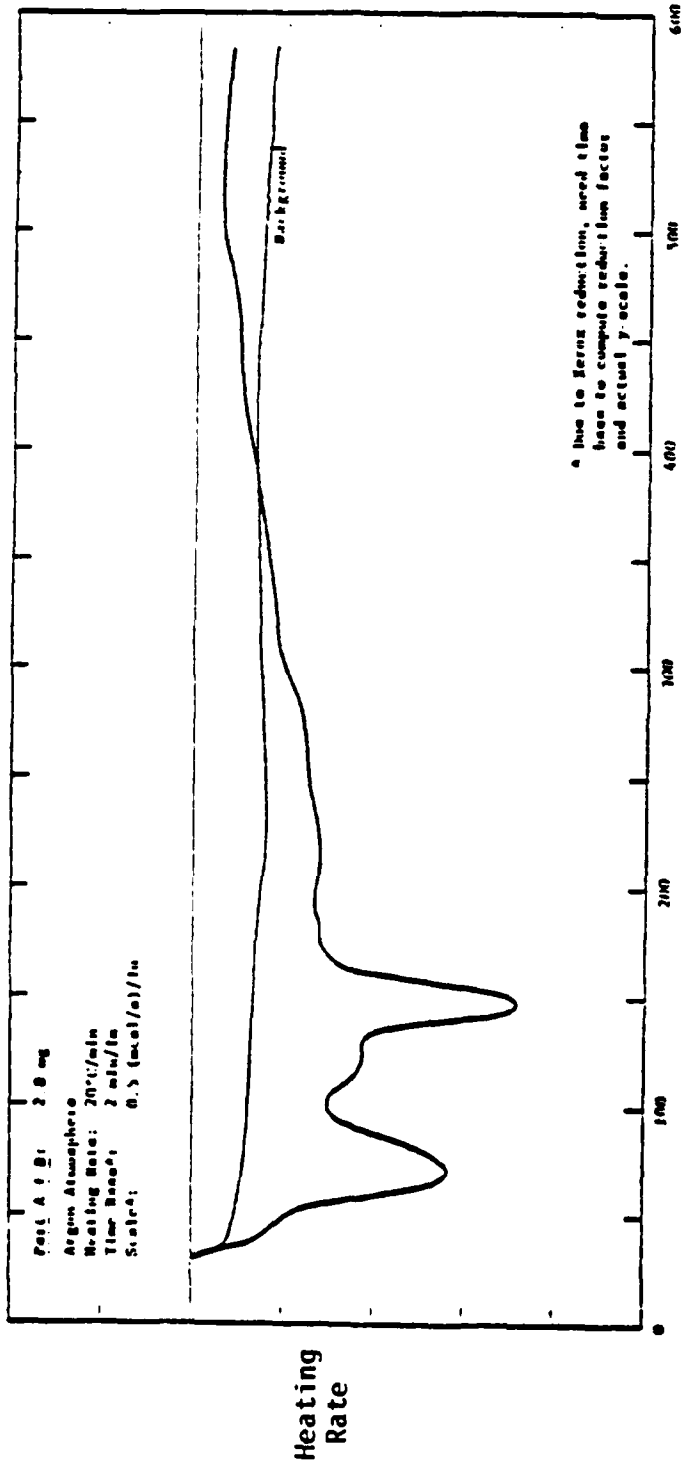

Figure 15. DSC Thermograph from Previous Study [4]

supplied by the machine. The endothermic reactions at elevated temperatures (Fig. 14), attributed to bond breaking, were not observed in those earlier tests. Two phenomena are postulated which can explain the differences. In Figure 15, the sample may not have been completely cured before the DSC test was performed. Heat absorbed in bond breaking was obscured by heat released from the endothermic curing process. A second contributing factor for the difference is an inadequate purging in the early test. Oxygen may have contacted the sample surface and pyrolytically reacted with the carbonized char. The pyrolysis produced heat that was absorbed by the chemical bond breaking and so created a DSC curve that showed heat release at high temperatures. The current procedure used a nitrogen purge.

Specific Heats and Energy Absorbed

The effective heat capacity, C_p^*, was determined at several temperatures for each sample by:

$$C_p^* = \frac{(\Delta X_1)(HS)}{m_o(\frac{m}{m_o})\ (HR)}$$

where ΔX_1 is the vertical distance between baseline and sample curve; HS is the heating scale [(0.5 mcal/s)/cm]; m_o is the initial mass, m/m_o is the remaining mass fraction at temperature (from the TGA); and HR is the fixed rate of temperature increase (20°C/min).

Similarly, the specific heat of the carbonized char was found by:

$$C_p = \frac{(\Delta X_2)(HS)}{m_o(\frac{m}{m_o})_{min}(HR)}$$

where ΔX_2 is the vertical distance between the baseline and carbonized char curve, and $(m/m_o)_{min}$ is the remaining mass fraction at the maximum DSC temperature.

Enthalpy Changes

Enthalpy changes were found for the samples by measuring the areas under the peaked regions of the curve. The enthalpy changes were computed by

$$\Delta H = \frac{A\ (HS)\ (TS)}{m_o \left[\left(\frac{m}{m_o}\right)_1 - \left(\frac{m}{m_o}\right)_2 \right] (HR)}$$

where A is the area under the peak; TS is the temperature scale (15°C/cm); $(m/m_o)_1$ and $(m/m_o)_2$ are the mass fractures at the beginning and end of the peaked region.

3.4 Summary of Thermodynamic Properties

The first major sign of thermal activity occurs in the range of 110°C, e.g., Curve B of Figure 14. Though the following discussion is specific to systems where the active component is sodium borate decahydrate (borax), the discussion is representative of the other active components examined.

The large double-peak endotherm between 110-180°C is due to the loss of combined water from the sodium borate decahydrate. There is sufficient combined water present in the borax molecules to allow for the dissolution of the sodium borate in its own water of crystallization when the molecules are sufficiently heated. This dissolved borax molecule then swells to a frothy mass as the water of crystallization becomes free water and boils away. After all of the water is removed by heating the sodium borate fuses to a greatly expanded solid [6]. This expansion enhances the insulative quality of the intumescent coating in addition to the expanded binder and proves the value of the borax as a blowing agent for intumescent systems.

The double peak is due to the evolution of water at two distinct temperature ranges. Different levels of hydration exist within the borax molecule. These different hydrates require different heats of crystallization and require different amounts of energy to release the moisture. Also, during

heating, some of the original decahydrate can be dehydrated into other stable or metastable hydrates.

Hidden within the large endothermic dehydration peaks is the evidence of the glass transition temperature of the binder. This glass transition is a change in state from a hard brittle polymer to one that is plastic. It is crucial that the glass transition temperature is reached at the time the blowing agent is most reactive. As the binder softens, the rapid evolution of disassociated water molecules expands the polymer leaving insulative voids. As the temperature of the binder rises, the binder hardens and chars and conforms to the new expanded state.

After the endothermic reaction involving the dehydration of the molecule is completed, any further reaction is related to the destruction of the polymeric binder. At about 300°C there is a small endotherm. This could be due to the sodium contained in the borax reacting with the polymer in a saponification soap-making reaction.

After this temperature has been exceeded, the endotherm begins to rise rapidly. This rapid endothermic increase is caused by the carbonization of the binder. The rigid interlocking structure of the polymer is being broken; large amounts of energy are required to break the polymeric chains. The amount of heat absorbed by the char at temperatures greater than 450°C is significantly higher in curve B than that exhibited by the "rerun" sample, curve C. This indicates that formation of the char results in the absorption of heat in chemical bond breaking reactions that are irreversible, meaning the bonding structure does not return to its preheated condition with cooling. However, the relatively high energy absorption per unit mass of the "formed" char (curve C) suggests that reversible bond breaking reactions do occur during cooling and reheating. Curve C is reproduced if the DSC experimented is repeated on the sample.

Comparing the DSC curve (Figure 14) with the TGA (Figure 8) curve shows the correlation between them. A large weight loss occurs at the temperatures where the borax is dissolving and boiling away the water of crystallization. Between 300-375°C, another large mass loss is observed which signals the onset

of the destruction of the binder. After this large weight loss, there is a more gradual, but steady, weight loss as the coating is heated. This weight loss is consistent with the endothermic reaction of further thermal decomposition of the polymeric binder. This latter weight loss is due to the breaking and releasing of that portion of the polymer molecule that is not carbonaceous such as sulfur, hydrogen, oxygen, and nitrogen.

Tables 13 through 17 list heat absorption properties as a function of temperature for five of the intumescent paint formulations. The specific energy absorbed by the carbonized char, C_{char}, is listed first. This term includes heat consumed in reversible chemical bond breaking and increasing internal energy of the sample. From the data available there is no way to discern the portion of energy going to each process (bond breaking or temperature increase). The energy absorbed in irreversible bond breaking, C_{chem}, is listed next. An effective specific heat, C_p^*, represents the total specific energy absorbed by the sample (neglecting enthalpy changes) per degree increase in temperature for the "virgin" material. Note that at the lower temperatures (in the temperature range of the endotherms, release of the blowing agent and intumescence), C_p^* generally is different and lower than C_{char}. In this lower temperature range, C_p^* is calculated from the difference in the reference curve and a straight line connecting the DSC curve before and after the endotherm(s). C_{char} is computed from the difference in the reference curve and the response curve of the experiment conducted on the residual (char) material remaining in the DSC holder, e.g., curve C in Figure 14. As seen in Figure 14, the "char" curve falls beneath the "virgin" curve. curve B. However, since the calculation of the specific heats uses the mass of the sample, and the residual mass is always less than the "virgin" mass, C_{char} is typically higher than the coating specific heat C_p^*; this is reflected in Tables 13-17.

Comparisons can be made, as a function of temperature, between the C_p's of the different formulations. The following discussion is representative of the types of comparisons which can be made.

Figure 16 shows effective specific heat as a function of temperature for two paints (526 and 736) which have a common filler, sodium metasilicate, but

Table 13. Specific Heats and Energy Absorbed in Bond Breaking for ID 513

MATERIAL: 513 Borax--Polysulfide/Epoxy--Glass Fiber

Temperature	C_{char} (cal/g-°C)	C_{chem} (cal/g-°C)	C_p* (cal/g-°C)
90°C	0.72	0	0.61
150°C	0.78	0.04	0.82
210°C	1.08	0.08	1.16
270°C	1.43	0.29	1.72
330°C	2.01	1.09	3.10
390°C	2.86	1.28	4.14
450°C	3.71	1.32	5.03
510°C	4.71	2.79	7.50
570°C	5.14	7.93	13.07

Table 14. Specific Heats and Energy Absorbed in Bond Breaking for ID 526

MATERIAL: 526 Sodium Metasilicate--Neoprene--Glass Fiber

Temperature	C_{char} (cal/g-°C)	C_{chem} (cal/g-°C)		C_p* (cal/g-°C)	
		Test 1	Test 2	Test 1	Test 2
90°C	0.50	0	0.01	0.40	0.51
150°C	0.60	0.05	0.17	0.65	0.77
210°C	0.80	0.02	0.01	0.82	0.81
270°C	1.11	0	0	1.01	0.87
330°C	1.30	0.12	0	1.42	1.15
390°C	1.61	0.62	0.36	2.23	1.97
450°C	2.01	2.04	1.85	4.05	3.86
510°C	2.51	5.49	4.29	8.00	6.80
570°C	3.02	6.43	5.33	9.45	8.35

Table 15. Specific Heats and Energy Absorbed in Bond Breaking for ID 736

MATERIAL: 736 Sodium Metasilicate--Foundrez/Epoxy--Glass Fiber

Temperature	C_{char} (cal/g-°C)	C_{chem} (cal/g-°C)	C_p* (cal/g-°C)
90°C	0.33	0	0.29
150°C	0.45	0	0.29
210°C	0.69	0	0.44
270°C	1.13	0	0.73
330°C	1.44	0	1.24
390°C	1.80	1.30	3.10
450°C	2.10	2.73	4.83
510°C	2.69	5.34	8.03
570°C	2.84	9.19	12.03

Table 16. Specific Heats and Energy Absorbed in Bond Breaking for ID 746

MATERIAL: 746 Borax--Flexible Epoxy--Glass Fiber

Temperature	C_{char} (cal/g-°C)	C_{chem} (cal/g-°C)		C_p* (cal/g-°C)	
		Test 1	Test 2	Test 1	Test 2
90°C	0.80	0	0	0.37	0.30
150°C	1.04	0	0	0.51	0.60
210°C	1.56	0	0	0.88	1.07
270°C	2.19	0	0	0.85	1.24
330°C	2.96	0	0	2.51	2.65
390°C	3.48	0.81	1.58	4.29	5.06
450°C	4.00	2.88	4.14	6.88	8.14
510°C	4.00	6.87	10.00	10.87	14.00
570°C	3.48	10.40	18.02	13.88	21.50

Table 17. Specific Heats and Energy Absorbed in Bond Breaking for ID 753

MATERIAL: 753 Borax--Polyurethane Resin--Glass Fiber

Temperature	C_{char} (cal/g-°C)	C_{chem} (cal/g-°C)		C_p*(cal/g-°C)	
		Test 1	Test 2	Test 1	Test 2
90°C	0.23	0	0.16	0.19	0.39
150°C	0.41	0	0.26	0.33	0.67
210°C	0.64	0	0.10	0.62	0.74
270°C	0.88	0.27	1.28	1.15	2.16
330°C	1.11	0.75	2.59	1.86	3.70
390°C	1.17	1.04	3.05	2.21	4.22
450°C	1.31	2.0	4.91	3.31	6.22
510°C	1.51	3.80	8.00	5.31	9.51
570°C	1.51	6.21	12.30	7.72	13.80

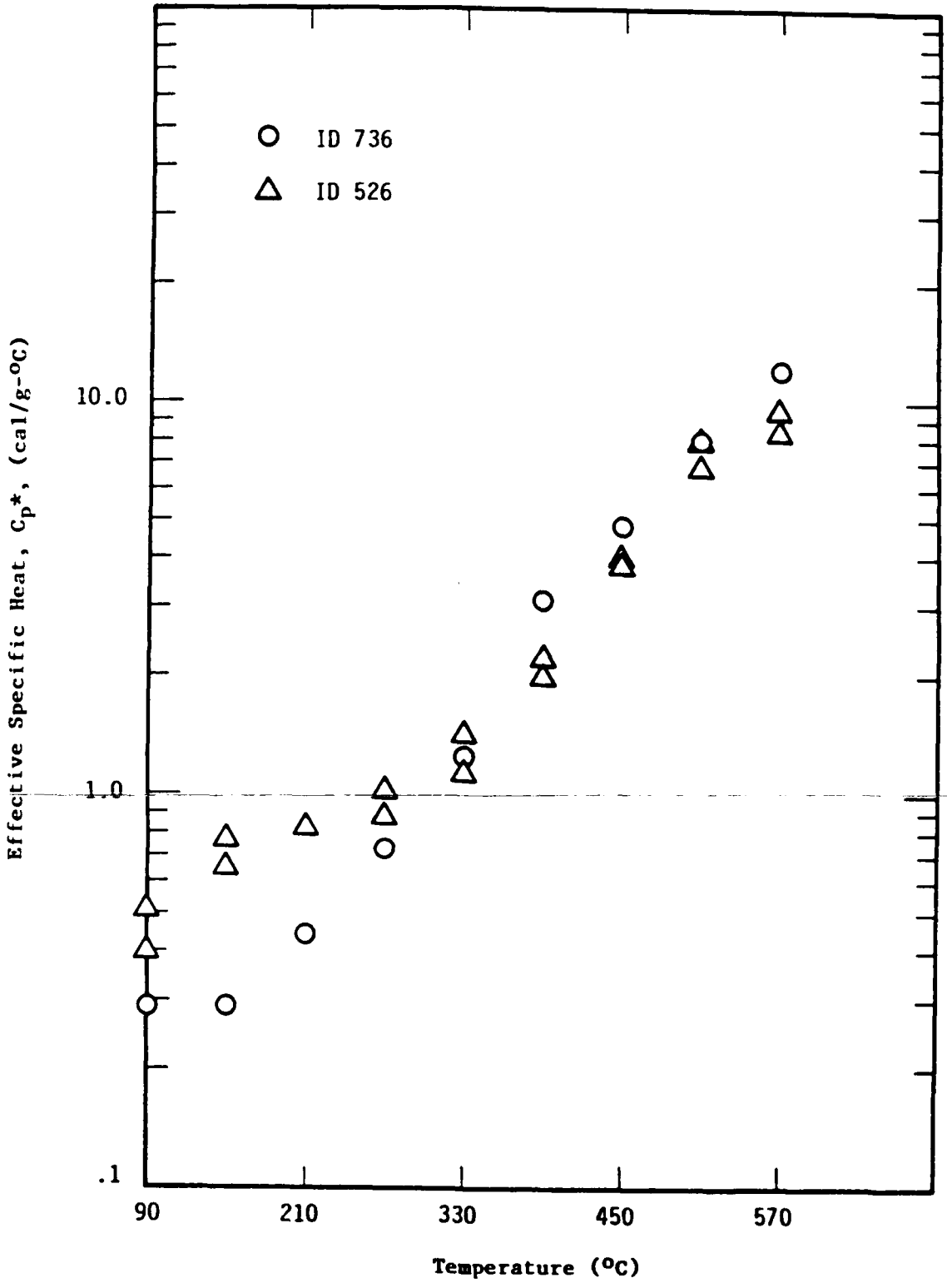

Figure 16. Absorbed Heat of Formulations with Common Filler, Different Binder

different binders. Formulation 526 contained 69% filler with a neoprene binder while formulation 736 had 56% filler with a Foundrez/epoxy binder. There appears to be no significant difference in the energy absorbed between the two formulations, except in the temperature region where intumescence is occurring. Differences in the plasticizing of the binder could account for the spread in the heat absorbed between 90°C and 250°C, i.e., the differences in heat absorption may reflect some of the dynamics of intumescence. Otherwise, the type of binder has little influence on the heat consumed.

Figure 17 shows effective specific heat versus temperature for two formulations with a common binder but different fillers. The paint with borax absorbs more heat per gram than the one with sodium metasilicate, indicating the filler material plays a role in the amount of heat absorbed by the formulation.

The specific energy per degree absorbed in the breaking of chemical bonds is shown in Figure 18. As temperature increases, the heat consumed in bond breaking gradually increases. The irreversible, endothermic restructuring of the complex polymeric chains in the char absorbs a great deal more energy than previously thought. This process may take an important contribution to the effectiveness of the paint's overall thermal protection, except that the density is quite low due to mass loss and expansion.

Table 18 lists the measured enthalpy changes for a number of samples. Paints with borax filler show two distinct peaks in the DSC records, indicating two levels of hydration. Formulations with a common filler show enthalpy changes of similar magnitude. Several of the samples were replicated to determine the accuracy of the measurements. The strong variation found in the data may be due to local inhomogeneities, or partial dehydration of the formulations during storage (the samples were stored for approximately two years). The samples were chipped from coated coupons, and may differ in their moisture content depending on whether the sample came from along the surface or from the interior. Some of the bound water in the formulation may have slowly diffused into the air over the storage time. Similar variability in the heat absorbed was also seen in "fresh" but cured samples, as described in

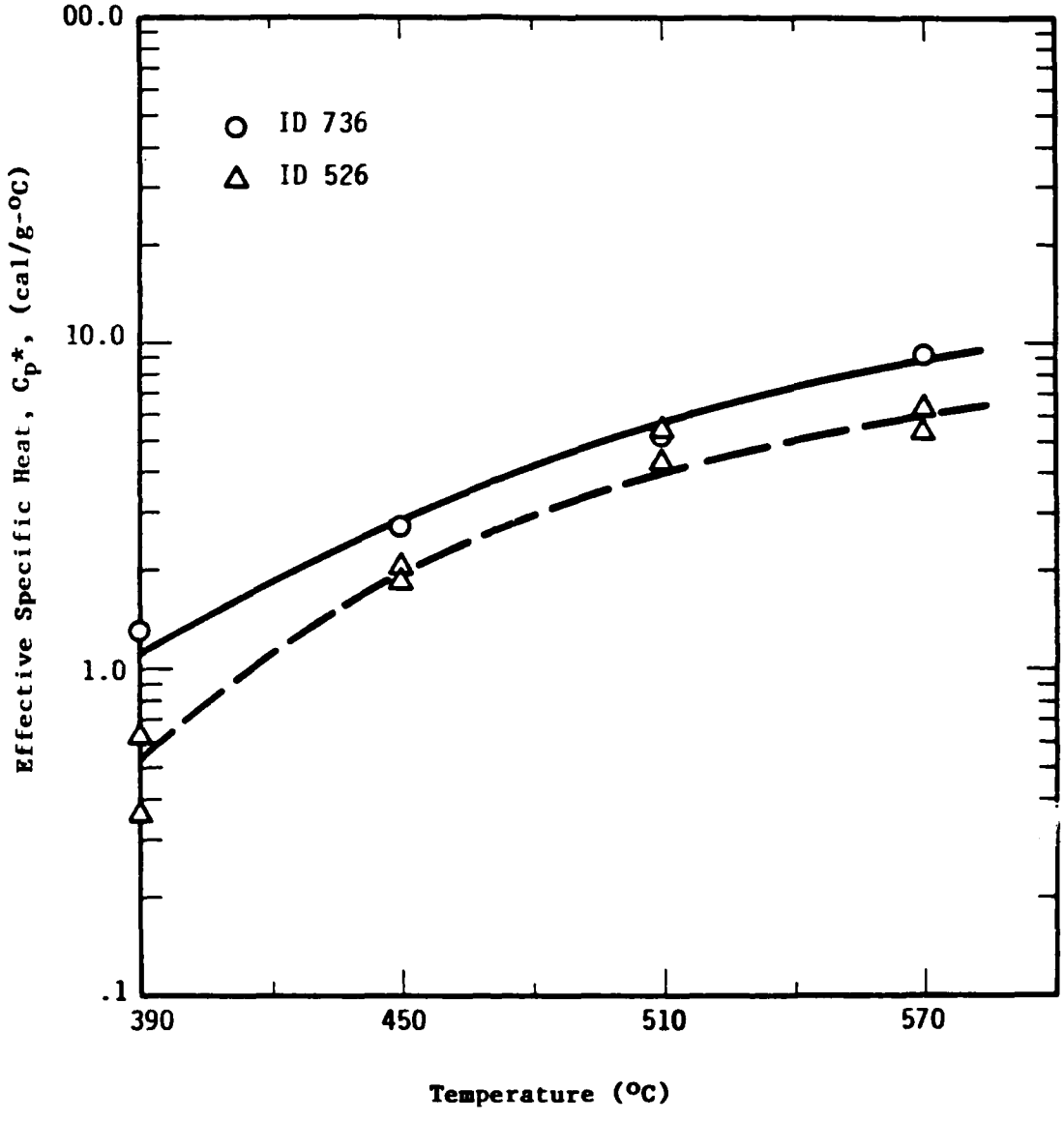

Figure 17. Absorbed Heat of Formulations with Common Binder, Different Filler

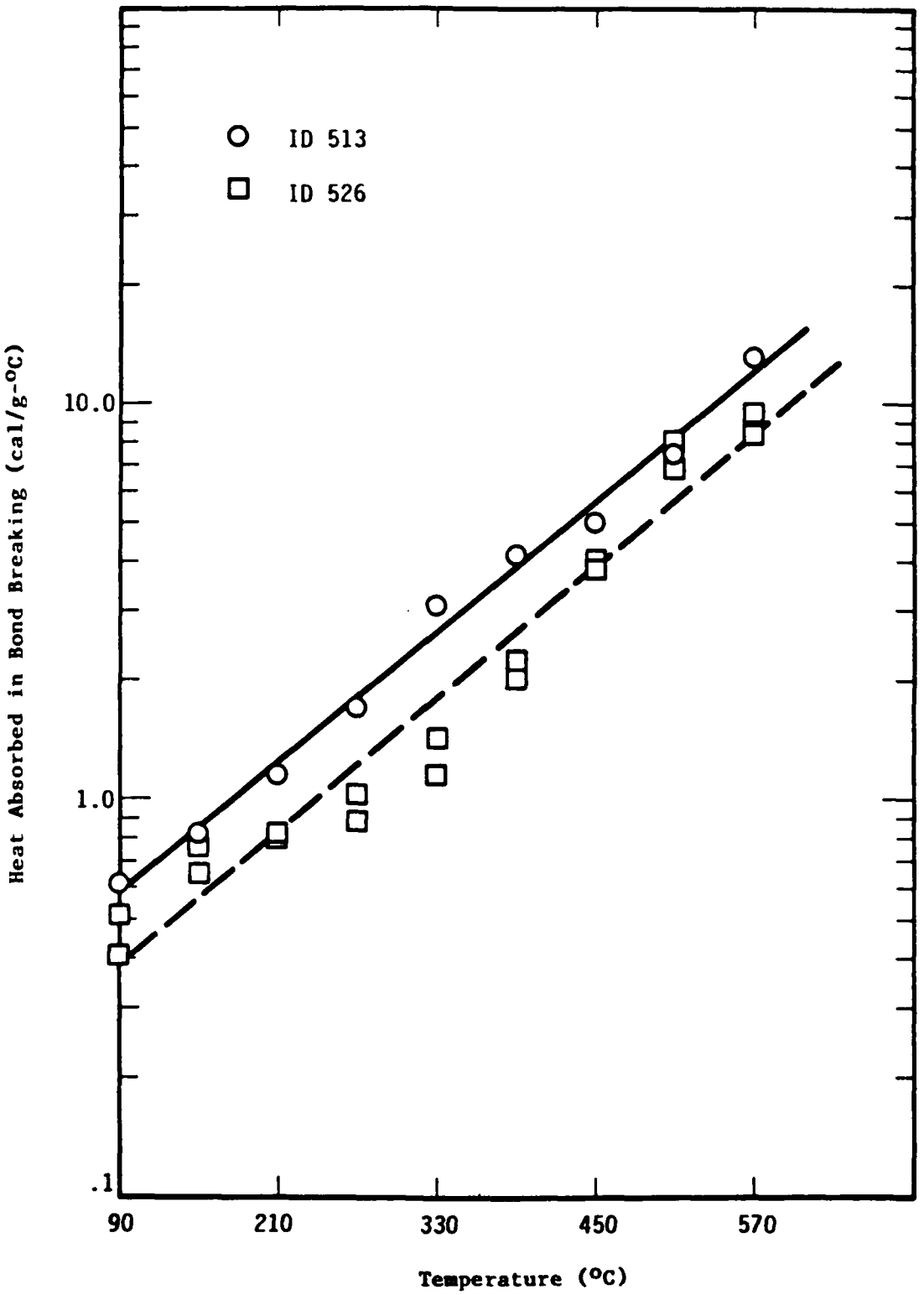

Figure 18. Heat Absorbed in Chemical Bond Breaking

Table 18. Enthalpy Changes During Intumescence

Filler Material	Temperature (°C)	Enthalpy Change (cal/g)
Borax 753	137	1597
Borax 753	171	279
Borax 753*	138	1834
Borax 753*	170	758
SMS 526	138	703
SMS 526*	103	453
Borax 513	141	1319
Borax 513	164	515
SMS 746	120	886
SMS 736	133	576

*Indicates repeat test.

the next section. We thus conclude that the variation is due to local inhomogeneities of small samples.

4.0 PRESSURE DEPENDENCE OF INTUMESCENCE

4.1 Introduction

Thermal performance of an intumescent coating depends, in part, upon the degree of expansion of that coating when subjected to intense heat. This correlation between thermal performance and expansivity is not absolute, however. Some coating systems with a limited amount of expansion exhibit better thermal insulative qualities than other coatings that expand greatly. Thus, factors other than expansivity contribute to thermal performance; however, an effort to understand the mechanics of expansion should help in a better understanding of the role of various parameters in thermal performance.

The degree of expansion of an intumescent coating depends upon the internal pressure built up within that coating by the action of heating, such as from flame impingement. This increase in internal pressure occurs when water vapor or other gases are liberated within the coating by heating. As the coating is heated, the binder matrix also softens allowing it to expand, or intumesce, from the pressure forces of the released gases. The release of these gases could be inhibited by the application of pressure, i.e., pyrolysis might well be self-limiting. This is illustrated by the familiar example of the increase in the boiling point of water as increasing amounts of pressure are applied. In this study, we attempt to ascertain the effect pressure has upon the pyrolysis reaction crucial to the intumescent process. In particular, the question asked is: Can the vaporization of crystallized water from the intumescent coating be retarded by pressure?

4.2 Approach

Ideally, it would have been desirable to run TGA's as a function of several different chamber pressures to determine if gas evolution was suppressed or shifted. Unfortunately, TGA devices are not readily amenable to pressurized testing. However, the DSC can be pressurized. We make the reasonable assumption that gas evolution is associated with the large endothermic peaks, interpreting the peaks as the energy absorbed in the release of the blowing agents. Therefore, by comparing the shapes and

temperature position of the enthalpy peaks for samples run at different pressures, it is inferred whether or not gas evolution is suppressed.

Three types of coatings were selected for analysis, all of which have bound water that acts as the blowing agent. Selection of these three coating types was based upon their thermal performance during testing in the T-3 firebox test, their workability, and their adhesion properties. The three coatings selected were designated 513, 1, and 7, respectively; the formulations are listed in Table 11. Coating 513 contains borax ($Na_2B_4O_2 \cdot 10H_2O$) as the blowing agent; formulation 1 contains aluminum sulfate ($Al_2SO_4 \cdot 18H_2O$) as the blowing agent; and formulation 7 contains sodium perborate ($NaBO_3 \cdot 4H_2O$) as the blowing agent. Borax loses its crystallized water within the temperature range of 75°C to 320°C. Most of the water is released before the material is heated to 150°C. At 150°C, the vapor pressure of saturated water is 83.7 psig. Aluminum sulfate octydecahydrate dehydrates at 87°C. Water vapor exerts a pressure of 23.8 psig at this temperature. For sodium perborate, dehydration occurs within the temperature range of 130°C-150°C; again, the maximum water vapor pressure is 83.7 psig. The TGA's for the three formulations are shown in Figures 8, 10, and 13 respectively.

Analyses to determine the temperature range of the reaction and the heat of reaction (ΔH) were performed on each of the three coatings using a DSC. Each of the materials were analyzed at ambient pressure (0 psig) for a control comparison. To determine pressure dependence, the materials were analyzed at 100 psig in the DSC. Since the maximum vapor pressure of the water being driven from the intumescing coatings is 83.7 psig, a pressure of 100 psig is sufficient to pressurize the system during analysis and possibly alter the rate of reaction ΔH. Coating 1 was also analyzed at 25 psig because of its low dehydration temperature and resultant low water vapor pressure of 23.8 psig. At 25 psig, the pressure exerted upon the sample is almost in equilibrium with the vapor pressure of the water leaving the material.

DSC measurements were carried out on a Dupont 9900 thermal analysis system fitted with a pressure DSC accessory module. Approximately 4.0 mg of a sample was weighed into an aluminum hermetic pan. An identical empty pan served as reference. Samples were run without lids. The samples were then

heated at a rate of 10°C/min to 500°C. All samples were purged in a flowing atmosphere of purified Argon. The area under each curve for the individual samples was integrated to obtain the heat of vaporization.

4.3 Results

Figures 19-24 represent typical thermographs. All the test specimens show characteristic endothermic absorption peaks below 200°C; the number and spacing of the peaks depends upon the active intumescing agent. Though thermographs were obtained over the entire temperature range, Figures 19-24 are expanded to the temperature range where the evolution of the water is prominent. The amount of heat absorbed, ΔH, in the pyrolyzation, or dehydration, is given for each endothermic peak by integrating the area within the peak. It is important to note that the value of ΔH given in the figures is normalized to the original mass, i.e., mass loss has not been explicitly accounted for in the integration procedure. The temperatures associated with the endothermic peaks are also given in the figures. All the thermographs are given in the Appendix; Table 19 summarizes the data contained in the thermographs.

Examining the results in Table 19, it is evident that there exists scatter in ΔH within each sample--this was also observed in the results given in Table 18 in Section 3.4. Except for the scatter, ΔH is independent of pressure, or if there is any pressure dependence, it is hidden within the experimental scatter. This result is not unexpected, i.e., the total quantity of heat absorbed in the endothermic reaction is not a function of pressure. The temperature of the onset of the pyrolysis reactions is also independent of pressure. However, examination of the upper temperature limit leads to the conclusion that there is a slight increase in the range over which heat absorption occurs for formulations 513 and 1; no shift is seen in formulation 7.

An interpretation of the thermophysics is made from examining the shapes of the enthalpy peaks at 0 and 100 psig. Figures 19 and 20 (formulation 513) shows that some of the energy absorbed in the first peak at 0 psig has been shifted into the second peak at 100 psig, i.e., dehydration has been affected

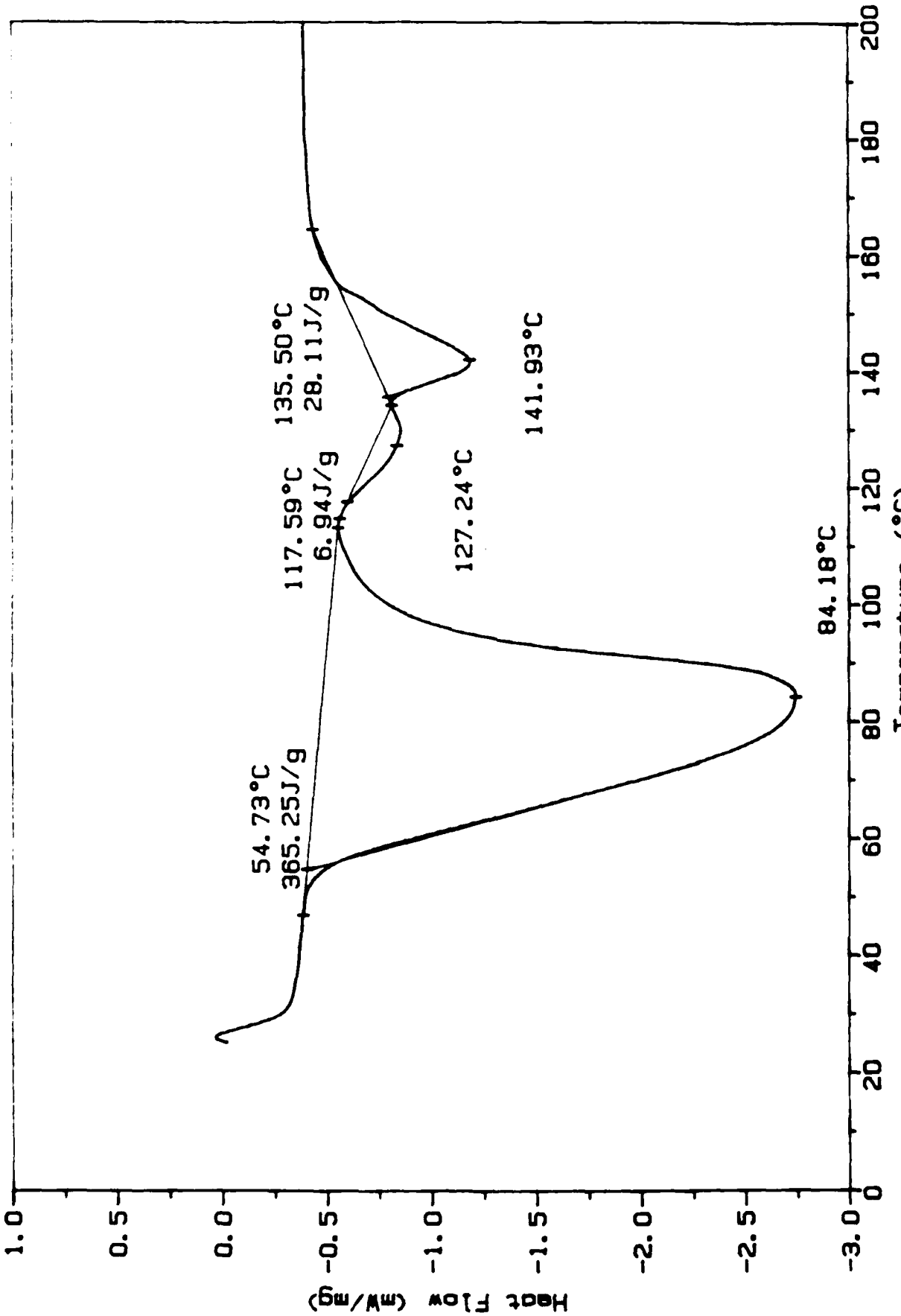

Figure 19. Thermograph for Formulation 513: 0 psig

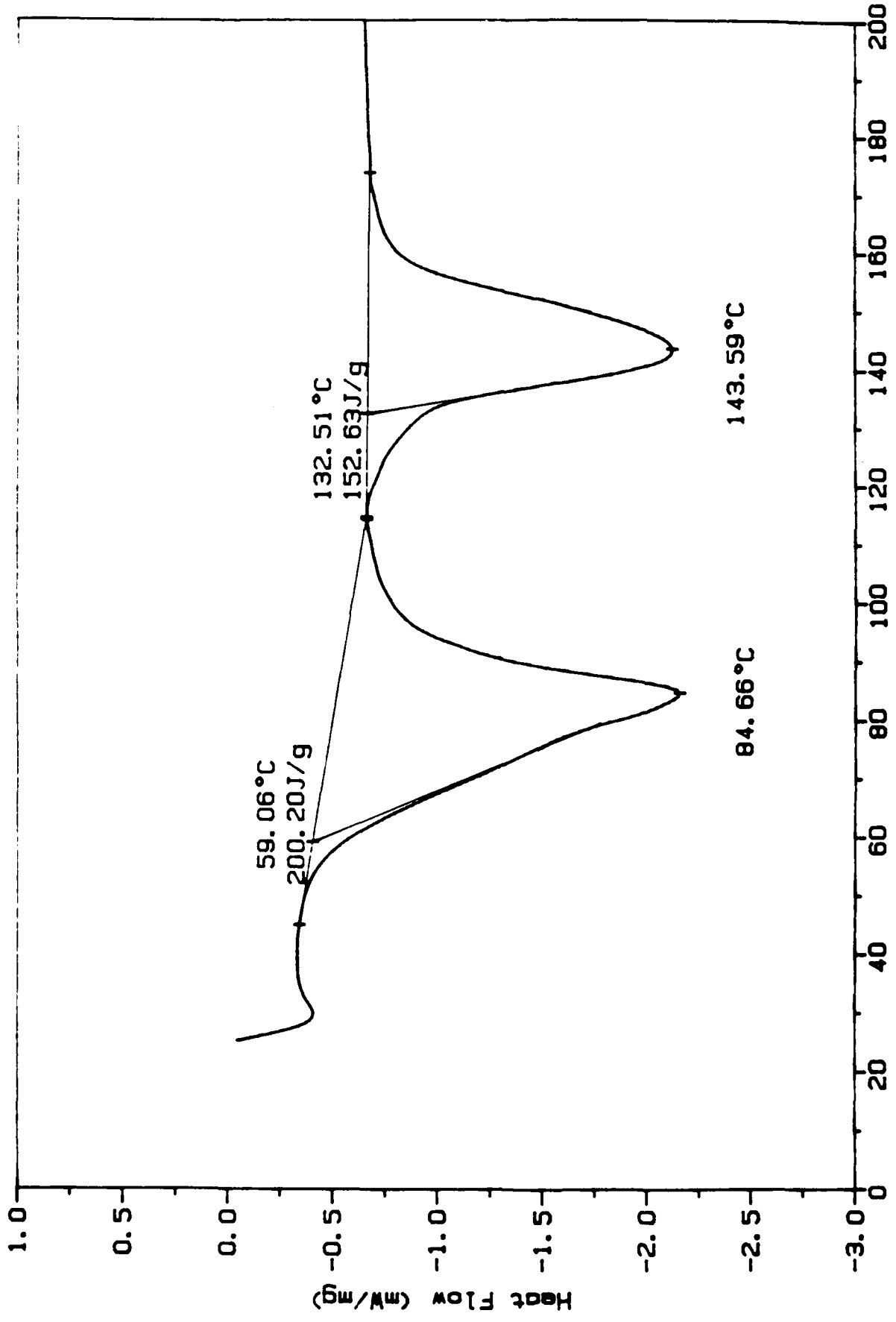

Figure 20. Thermograph for Formulation 513: 100 psig

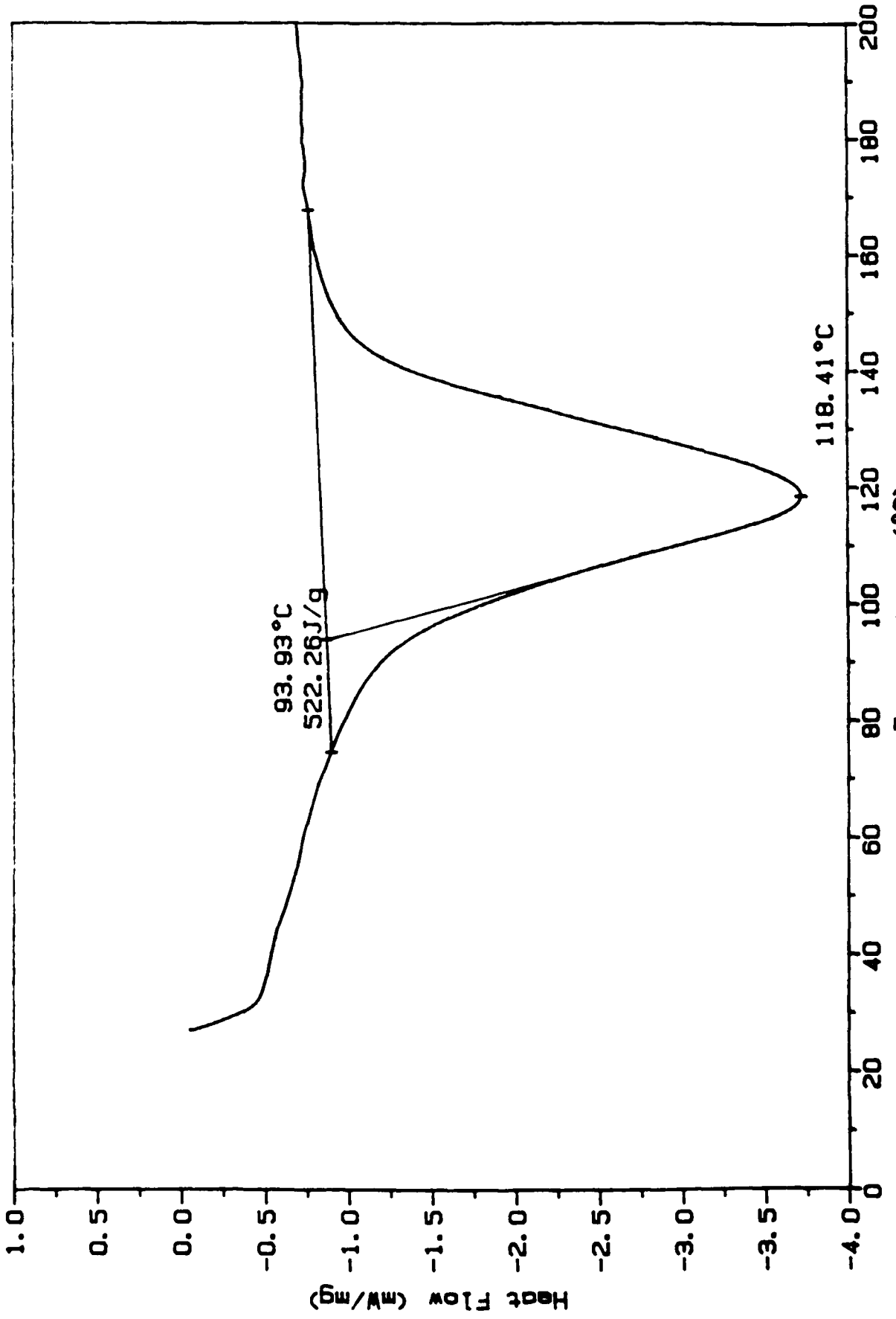

Figure 21. Thermograph for Formulation 1: 0 psig

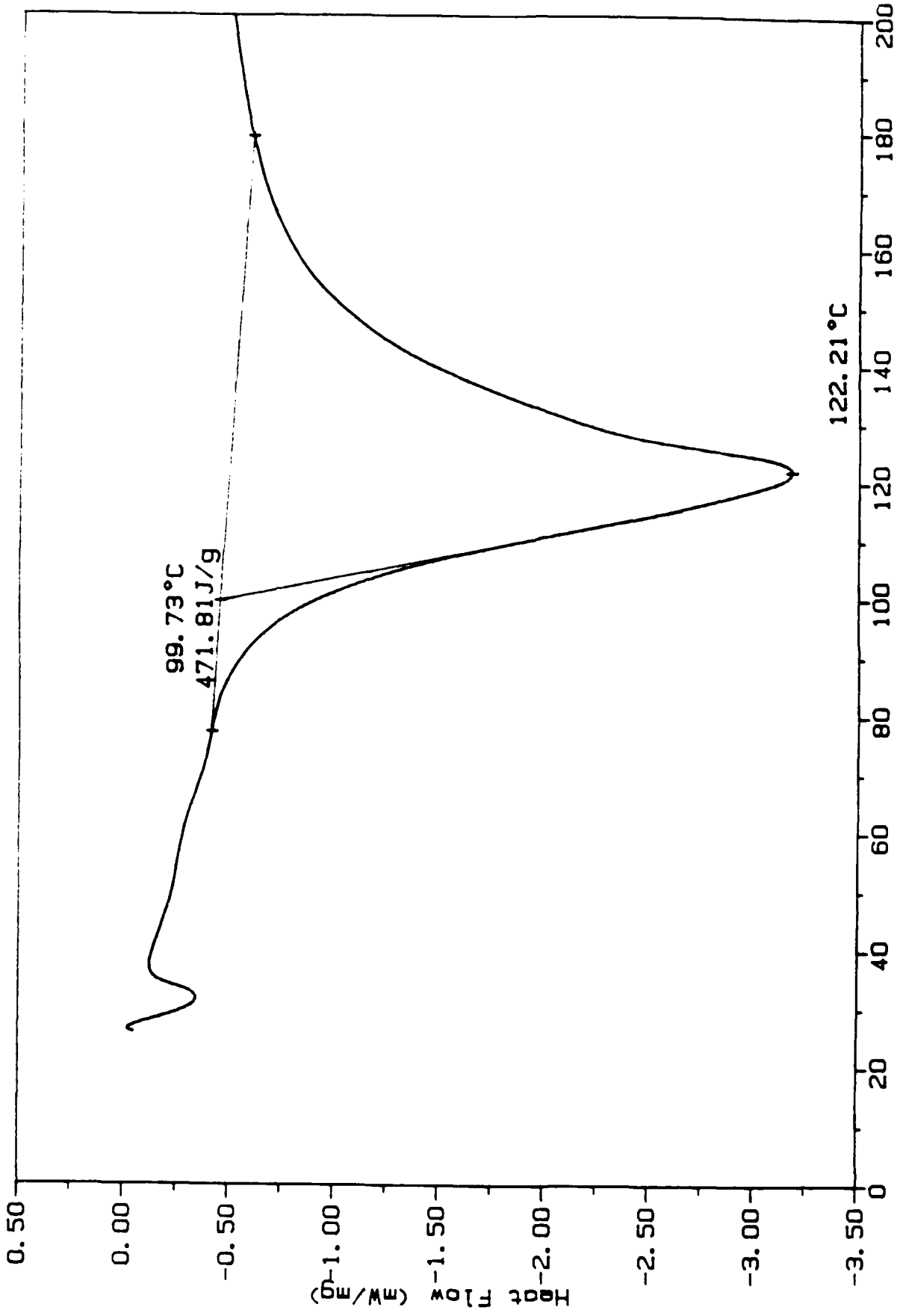

Figure 22. Thermograph for Formulation 1: 100 psig

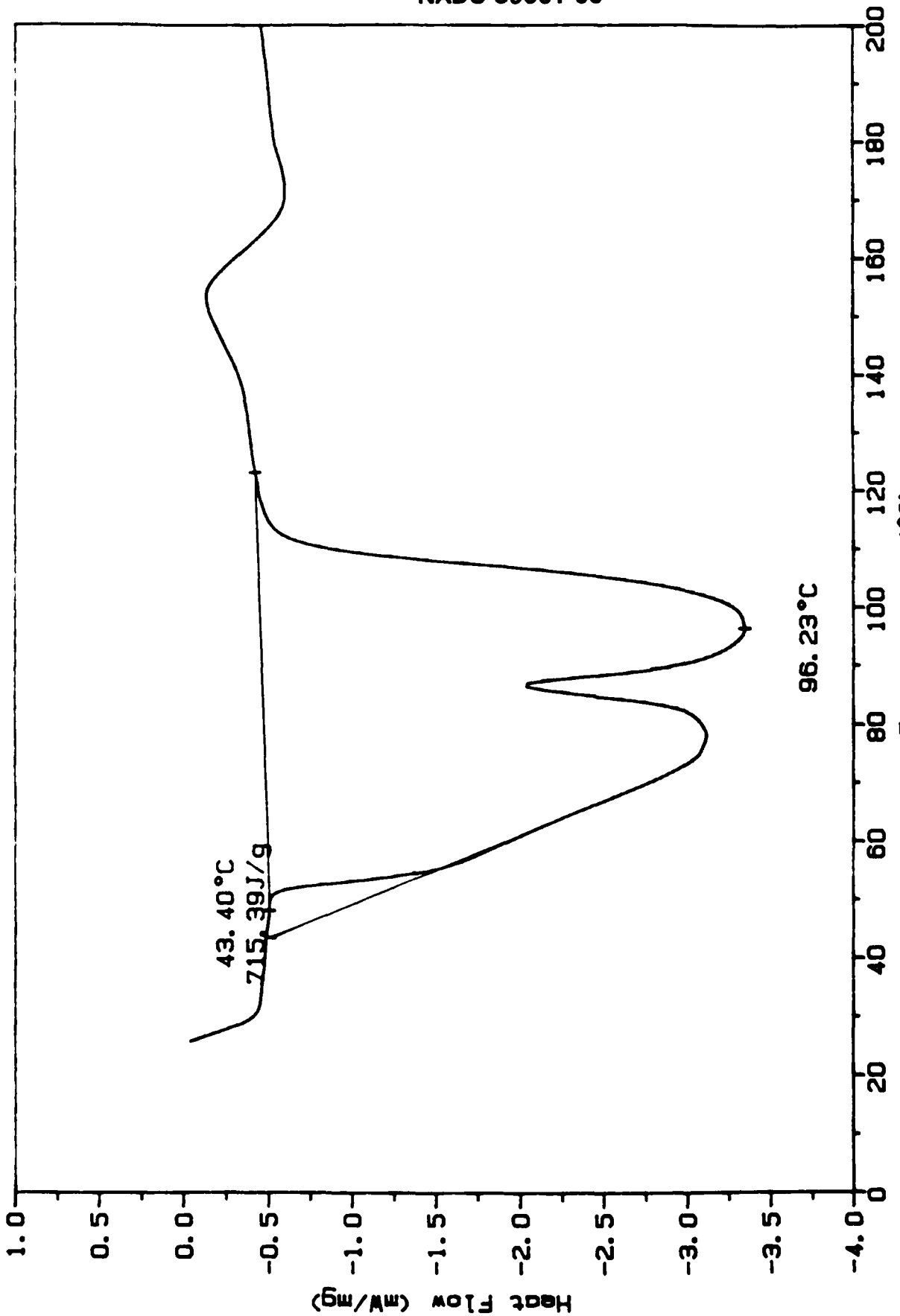

Figure 23. Thermograph for Formulation 7: 0 psig

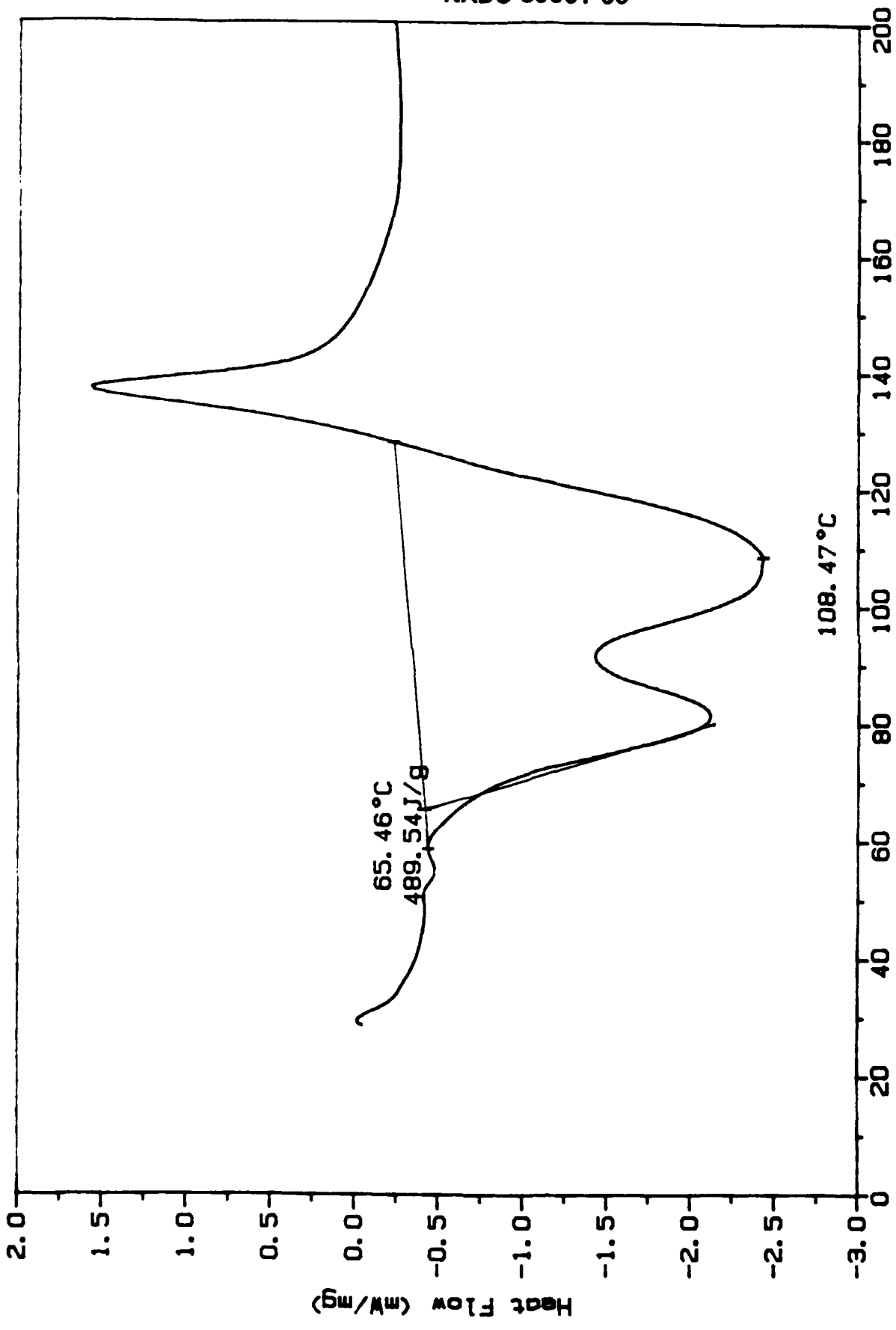

Figure 24. Thermograph for Formulation 7: 100 psig

Table 19. Pressure Dependence of Intumescence

Type	Sample ID No.	Heat of Vaporization ΔH (J/g)	Reaction Temp Range (°C)	Pressure (psig)	Sample Wt (mg)
513	0.	398.66	51-161	0	4.40
	0.29	370.35	52-114	0	4.30
	0.30	357.96	54-113	0	3.90
	0.31	400.94	52-113	0	4.30
	100.05	352.78	51-171	100	4.00
	100.06	310.41	52-172	100	3.20
1	0.11	518.03	73-162	0	4.80
	0.12	478.56	65-162	0	4.80
	0.35	564.28	63-162	0	4.40
	0.34	544.50	70-160	0	4.80
	25.19	530.92	63-162	25	4.80
	100.09	495.59	73-180	100	4.60
	100.10	471.81	77-179	100	4.40
7	0.15	698.22	51-116	0	4.40
	0.32	*851.61	57-128	0	4.50
	0.33	*849.95	57-129	0	4.00
	100.07	579.50	56-123	100	4.20
	100.08	500.51	60-128	100	4.30

*Possible moisture increase in sample due to change in storage conditions.

by pressure. Assuming that gas release is concurrent with energy absorption, this would indicate that the rate of gas evolution is somewhat pressure dependent, shifting the release of the blowing agent to a slightly higher temperature. For formulation 7, Figures 21 and 22, the pressure affect has resulted in an endothermic peak which is more "rounded" on the high temperature side, again suggesting that gas evolution might be shifted slightly by pressure. Figures 23 and 24 represent the energy absorbed for formulation 1. A barely resolved double peak is observed in Figure 23; the energy absorbed has shifted from one peak to the second peak which has become broader at the higher pressure. Also, the very slight exothermic peak at approximately 150°C at 0 psig is accented at 100 psig. (The test run at 25 psig looked exactly like the 0 psig test, reference the data in the Appendix.

From the observations of the thermographs, it appears that there is a slight temperature shift in release of the blowing agent due to the presence of pressure. Though the differences in endotherms are fairly dramatic, the pressure was quite high (100 psig), and the actual shift in temperatures is less than 20°C. This slight shift in temperature probably has a negligible effect on the intumescent process itself. Though the "fluidity" of the binder may be affected marginally, gas release is continuous over this 20°C range. It is therefore concluded that pressure generated by the liberation of the blowing agent does not self-limit intumescence.

5.0 EXPERIMENTAL DATA AND THE CHAR THERMAL CONDUCTIVITY

5.1 Introduction

The coated coupons were subjected to the heat flux from the NASA T-3 box at NADC [2]. A chromel-alumel thermocouple was attached to the back center section of the coated test plate prior to testing; the emf output as a function of time was plotted directly as temperature versus time on a chromel-alumel compensated chart recorder. The plates were exposed to a heat flux of approximately 2.7 cal/cm^2-s, with approximately 90 percent of the incident flux being radiative [2]. The temperature-time responses of the insulated coupons are shown in Figures 25-31; the formulations are listed in Table 11. There is some uncertainty as to time zero for each test since these were not marked on the chart paper. For the most part, the data are generally consistent, e.g., more coating material provides more thermal protection. Also, repeat tests were conducted for each coating material and these tests showed good reproducibility. A few anomalies do exist, however, Figure 31. The record trace of sample coupon 1-1A indicates that something has happened to either the coating or the thermocouple. The long plateaux of tests 513-2A and 513-3A are inconsistent with previous data collected at SwRI using the NASA EX-1C-82 formulation. The curve for 1-3A also appears to be "drawn out" in time. Possible explanations are: (1) the data truly are valid; (2) the test specimen was not exposed to the proper heat flux; or (3) there was poor thermal contact between the thermocouple and the metal substrate. The third explanation would seem to be the most reasonable.

As noted in previous work, an intumescent front forms which limits the heat flux transmitted to the plate. The temperature of the plate tends to plateau at a temperature characteristic of the intumescing front. After the front has reached the plate, the temperature then begins to increase; in fact, the temperature rise, to a very good approximation, is linear with time. It is this observation that permits an estimate to be made of an effective thermal conductivity of the residual char material.

Traditional guarded hot plate experiments to measure the thermal conductivity, though simple in theory, are difficult in practice because of

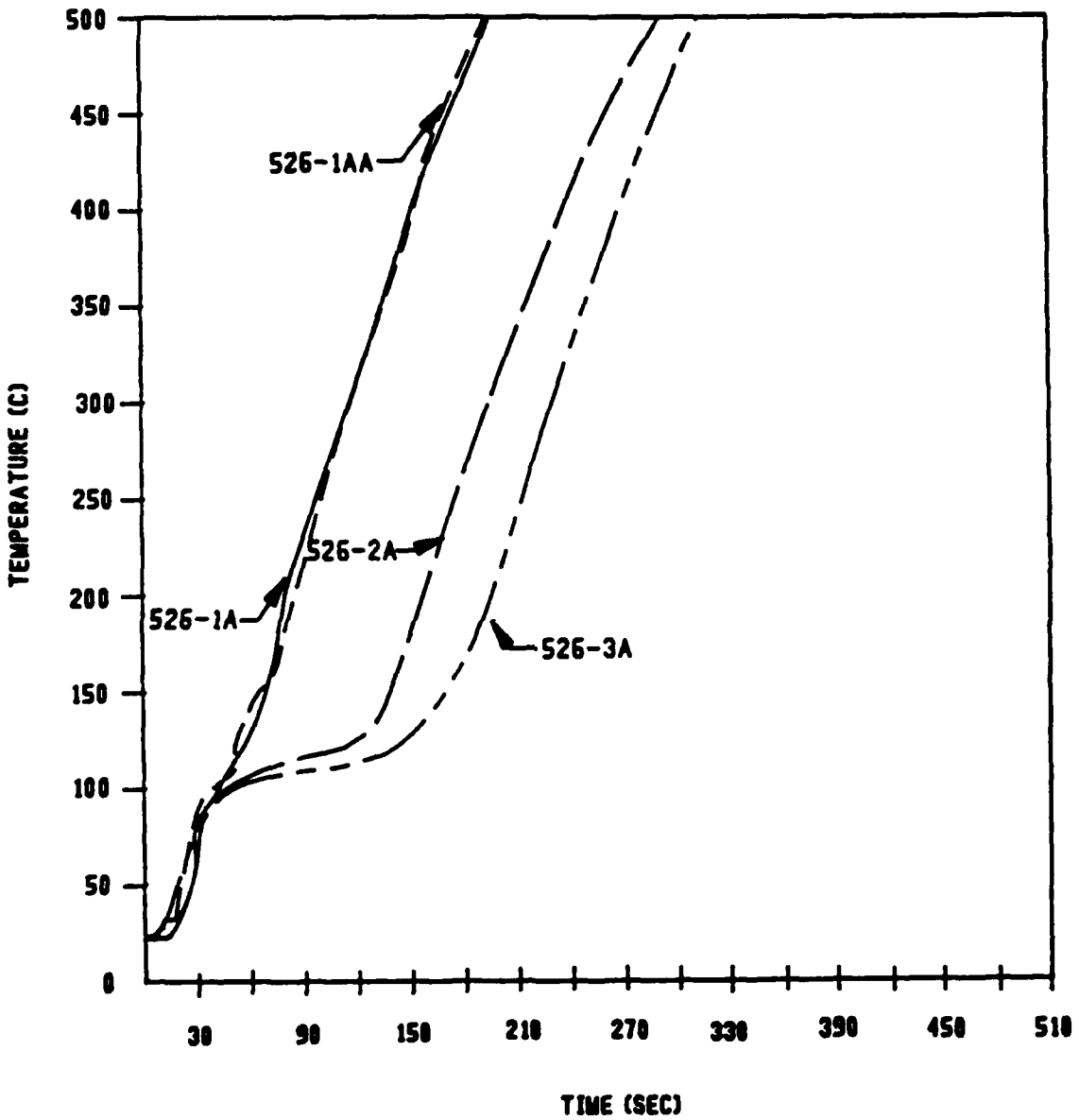

Figure 25. Temperature-Time Experimental Data: Formulation 526

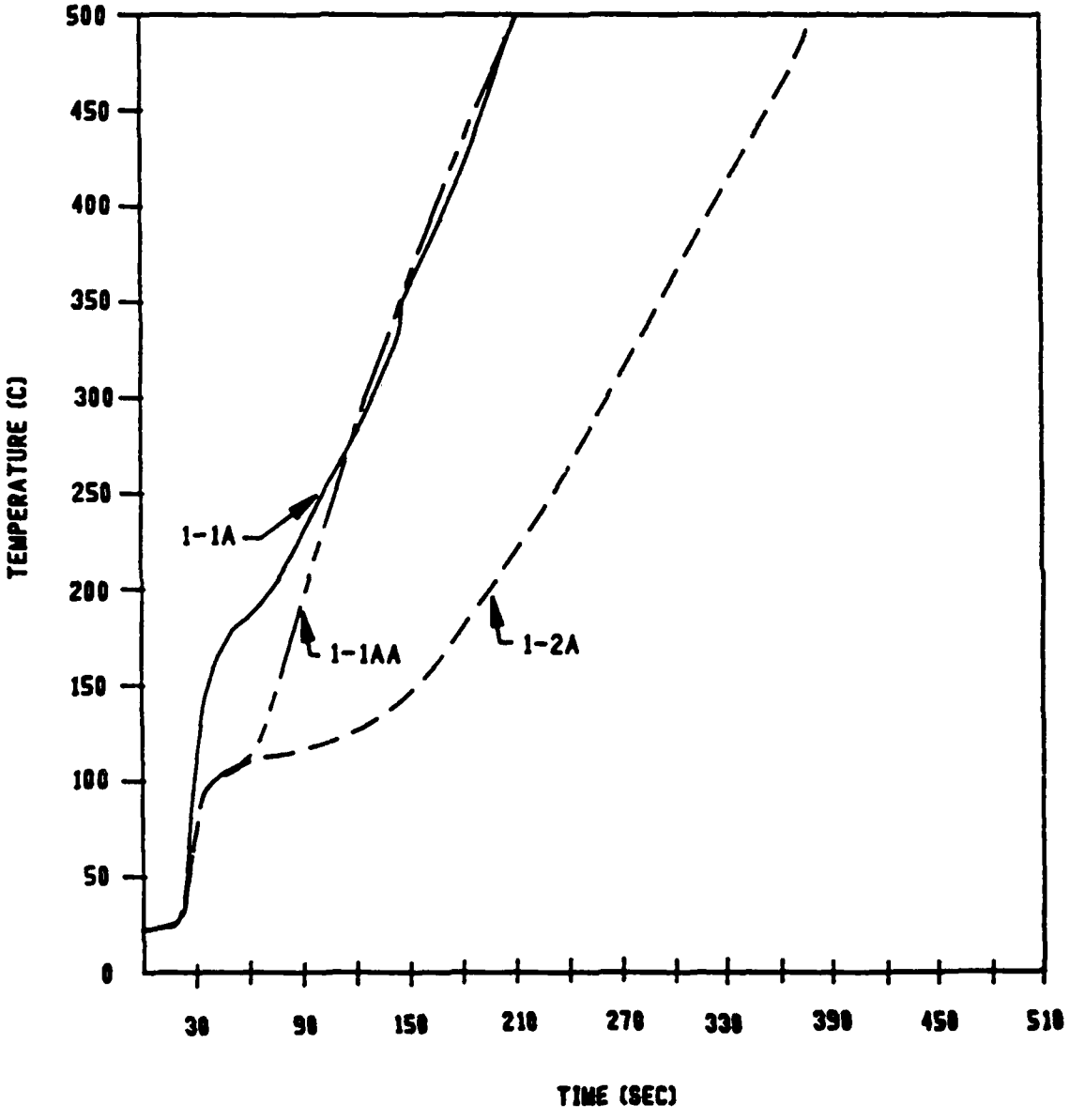

Figure 26. Temperature-Time Experimental Data: Formulation 1

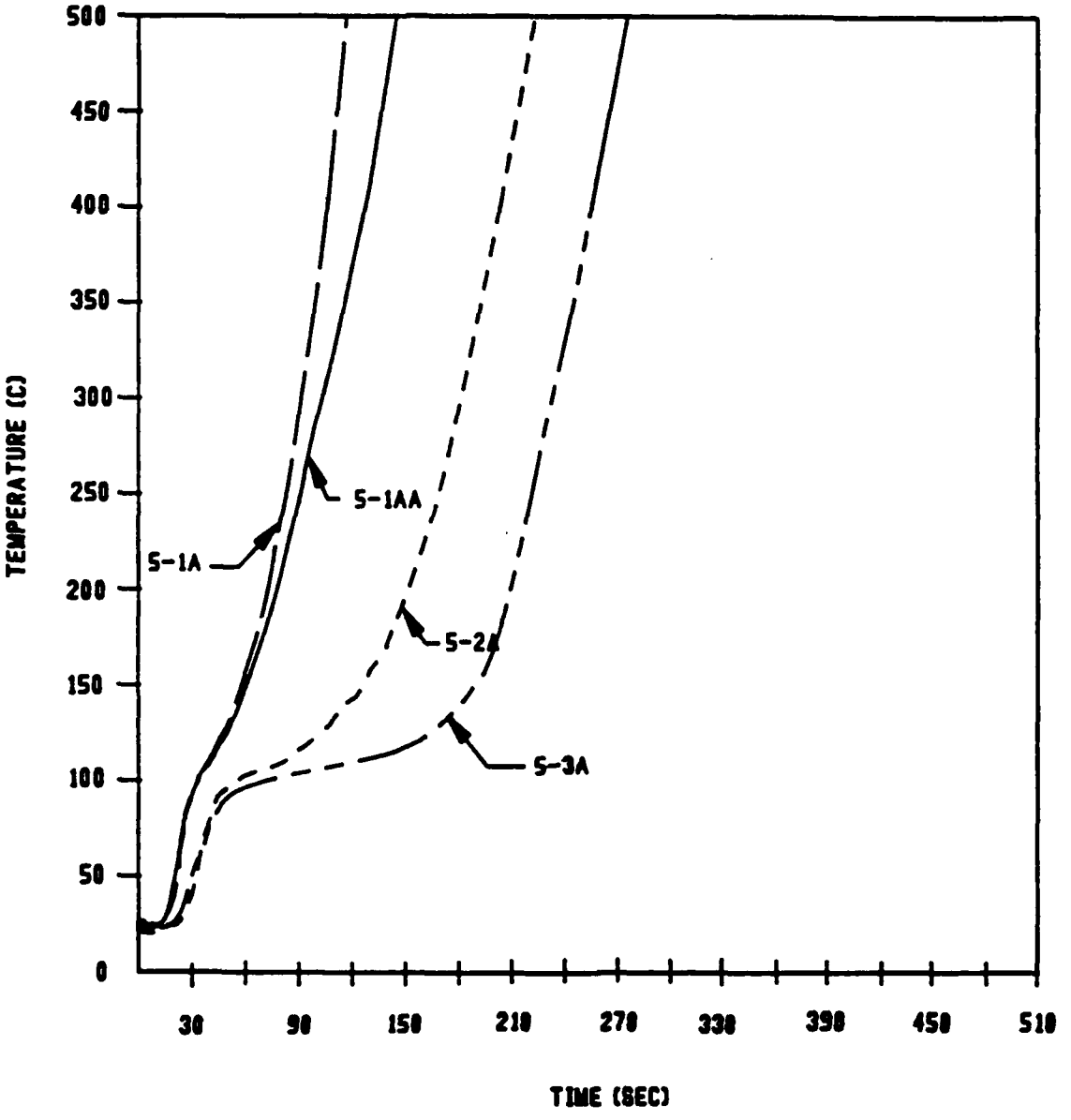

Figure 27. Temperature-Time Experimental Data: Formulation 5

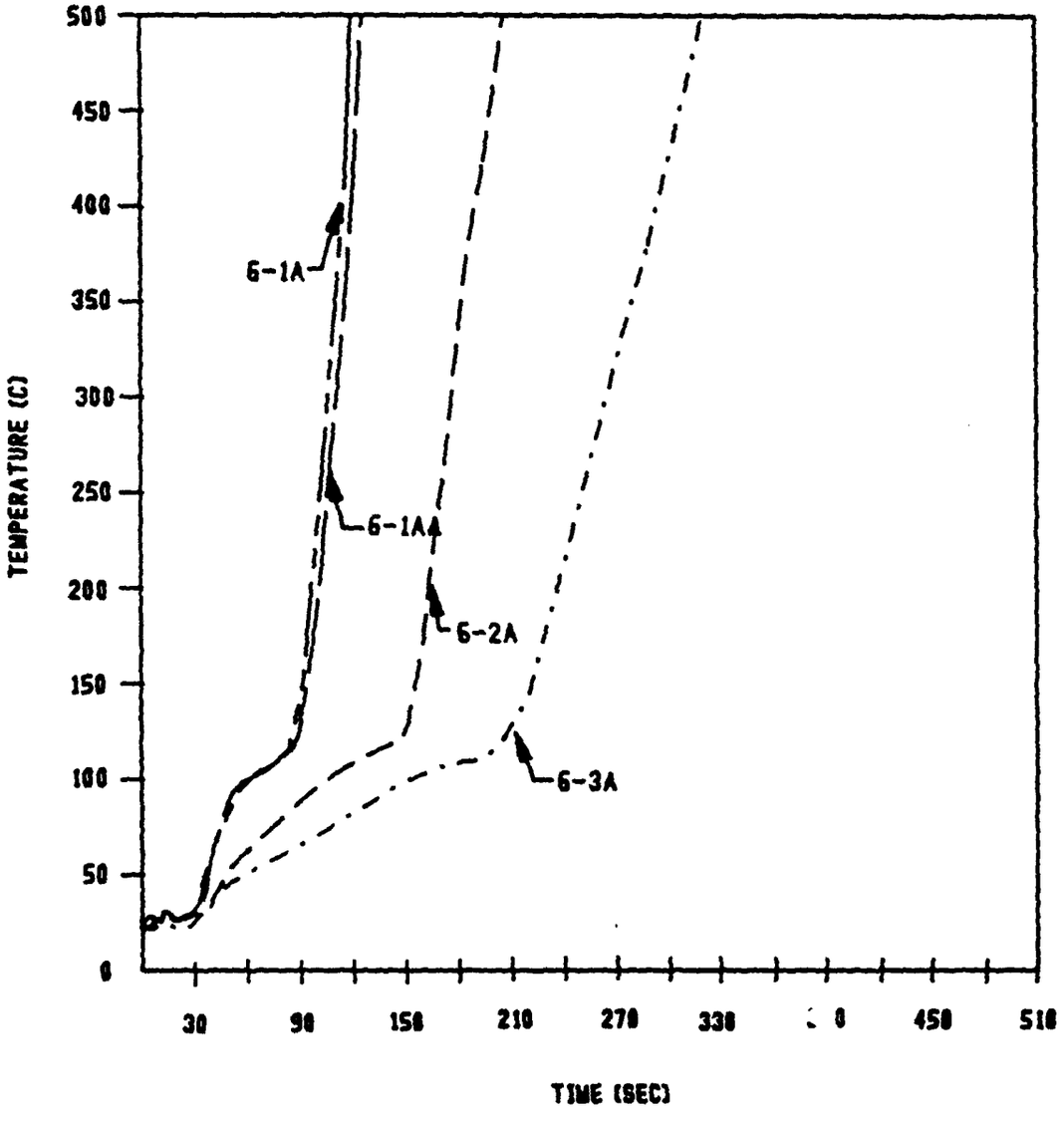

Figure 28. Temperature-Time Experimental Data: Formulation 6

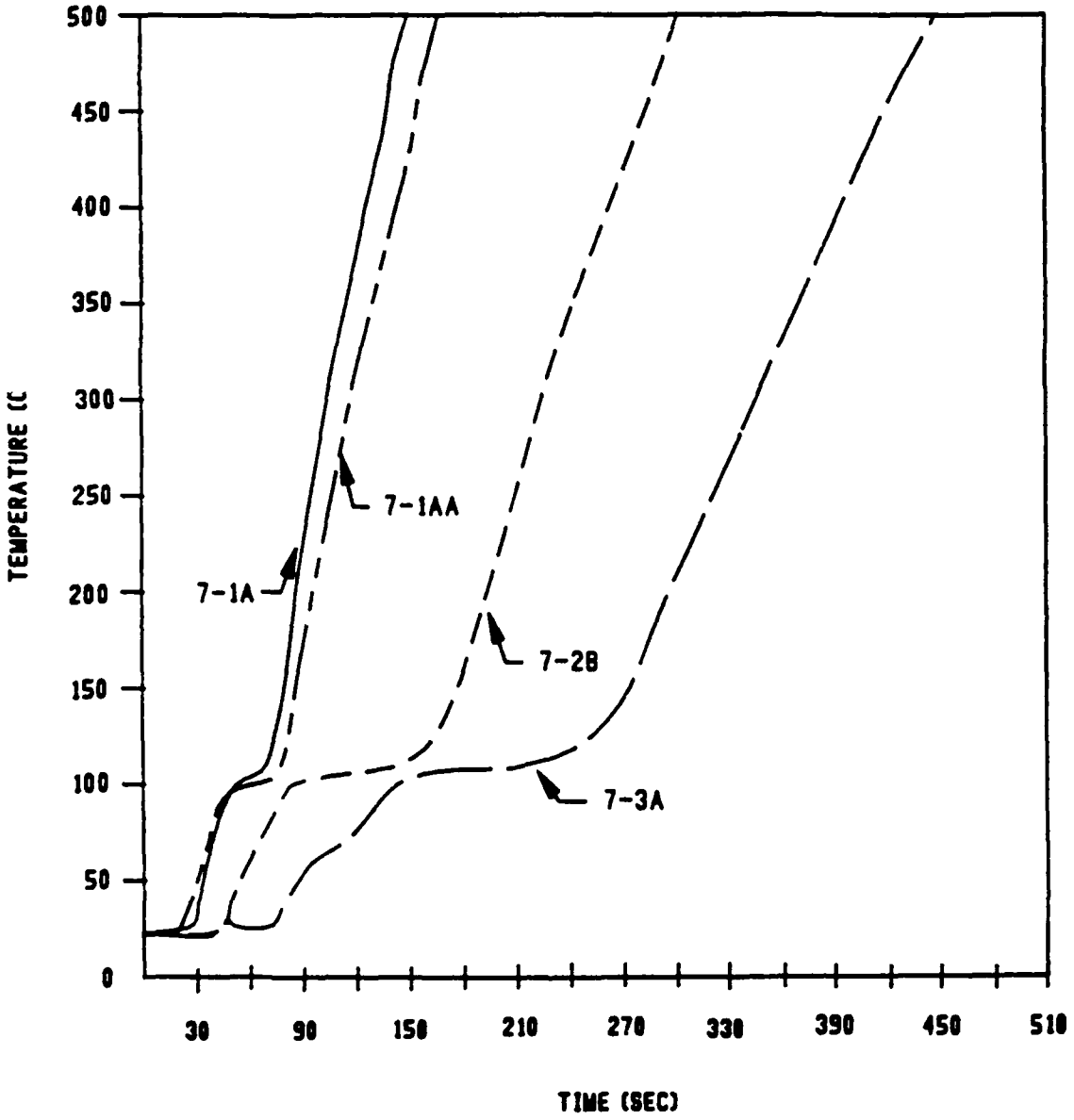

Figure 29. Temperature-Time Experimental Data: Formulation 7

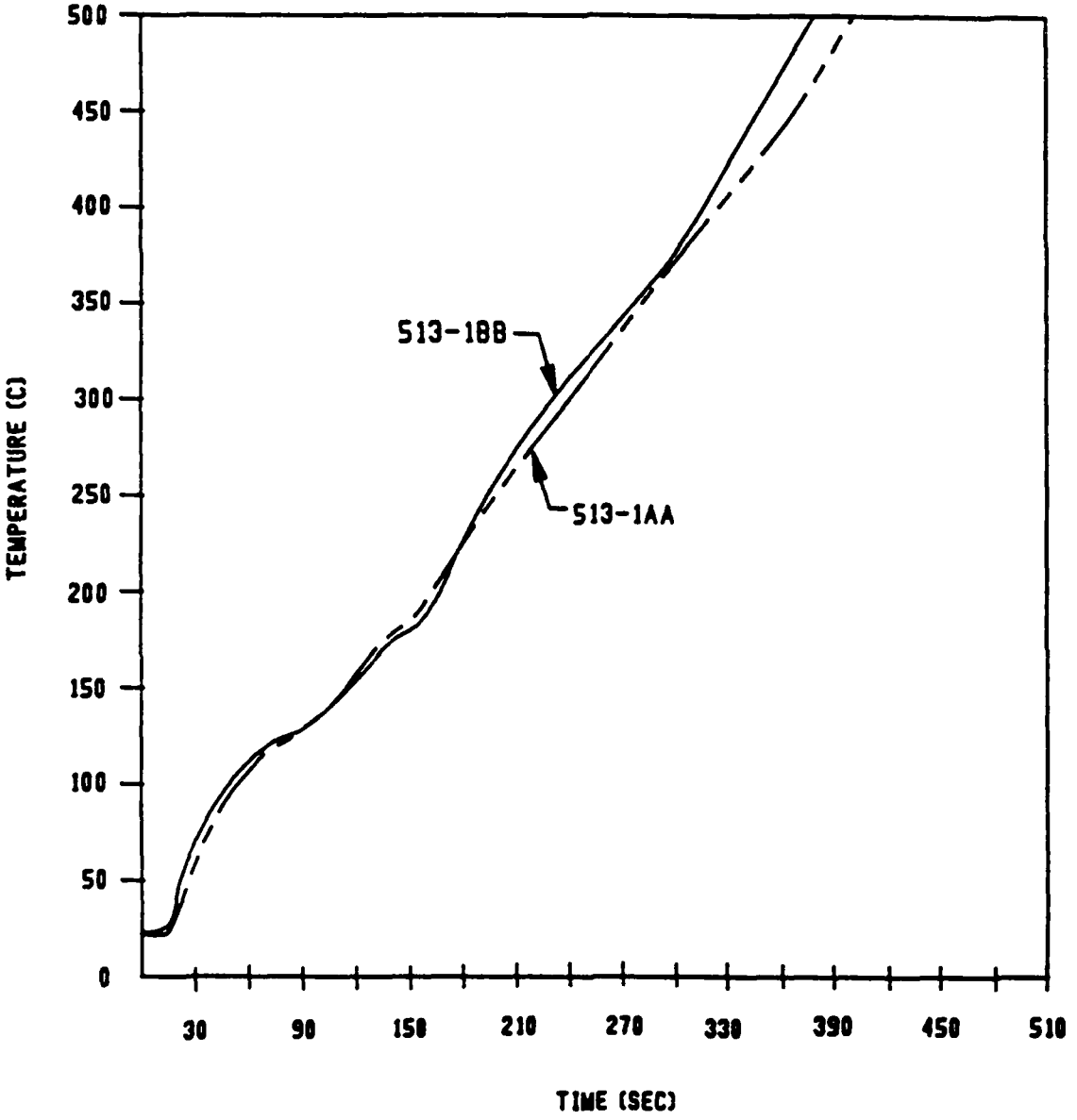

Figure 30. Temperature-Time Experimental Data: Formulation 513

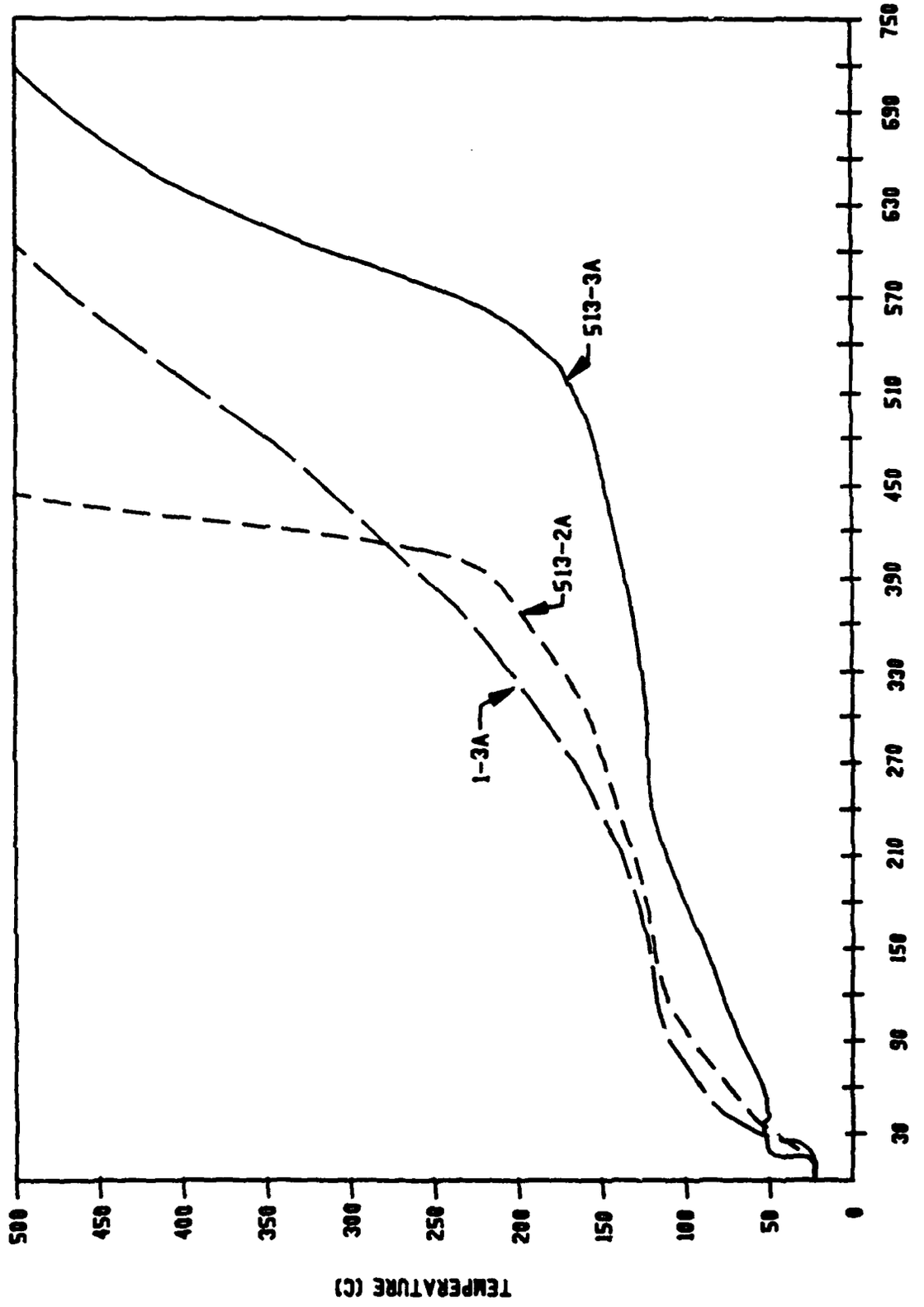

Figure 31. Temperature-Time Experimental Data (Anamalous Results)

extraneous heat paths, particularly at elevated temperatures [7]. Also, the techniques with regard to guarded hot plate experiments are not applicable for thermal systems which intumesce. Instead, a procedure has been developed to estimate an effective thermal conductivity of chars for reasonably efficient intumescent systems. This procedure relies on the temperature-time response of the coated flat coupons combined with a one-dimensional heat transfer analysis.

A variety of pre- and post-test measurements were made which are used in the procedure to estimate the effective thermal conductivity; these measurements are tabulated in Table 20. Either because of adhesion problems, or during removal of the coupons from the test fixture, a significant portion of the char fell off some of the coupons. Thus, a final char thickness could not be determined for approximately one-third of the tests; these tests are denoted by a dash in the appropriate columns. However, the remaining mass could be determined. The ratio of final to initial mass (m_f/m_o) is given in the last column of Table 20. Comparison of these values with the ratios of mass from the TGA experiments, Figures 8-13, support the conclusion that a considerable portion of the coating was ablated or fell off for formulations 1 and 6.

We also present an analysis for an estimate of the thermal conductivity based on a simple model that the char is a porous solid; this model requires an estimate for the density of the char. Densities were computed from the thicknesses and the area of the coated coupons; the initial and final densities are given in Table 21. Also listed in Table 21 are the temperatures of the intumescent front T* [2,3], and the time the front reached the substrate, t*. All analyses procedures assume that the coating is completely char material for times greater than t*.

5.2 Analytical Development

The increase in the internal energy of the steel substrate can be computed by a simple energy balance:

$$(\rho C_p \tau_p)_p \frac{dT_p}{dt} = \dot{q}_{in} \qquad (1)$$

Table 20. Coating Thicknesses and Masses

No.	Initial thick (cm) (t_o)	Final thick (cm) (t_f)	$\frac{t_f}{t_o}$	Initial coating mass (g)	Final coating mass (g)	$\frac{m_f}{m_o}$
513-1BB	0.152	0.996	6.55	11.21	6.53	0.583
513-1AA	0.155	1.430	9.23	10.85	6.18	0.570
513-2A	0.302	1.631	5.40	21.59	12.96	0.600
513-3A	0.457	1.788	3.91	33.04	18.67	0.565
526-1A	0.150	0.361	2.41	6.36	4.24	0.667
526-1AA	0.152	0.279	1.84	7.58	5.92	0.781
526-2A	0.310	0.361	1.17	14.86	12.80	0.861
526-3A	0.457	0.361	0.79	22.43	17.96	0.801
1-1A	0.150	---	---	8.34	4.97	0.596
1-1AA	0.152	---	---	7.86	4.06	0.517
1-2A	0.307	0.955	3.11	16.90	11.08	0.656
1-3A	0.460	1.034	2.25	26.16	19.77	0.756
5-1A	0.157	0.201	1.28	7.86	1.59	0.202
5-1AA	0.155	---	---	7.44	1.54	0.207
5-2A	0.307	---	---	16.59	4.52	0.272
5-3A	0.457	---	---	25.09	6.32	0.252
6-1A	0.157	---	---	8.20	3.00	0.366
6-1AA	0.157	---	---	7.93	2.62	0.330
6-2A	0.302	---	---	16.73	6.85	0.409
6-3A	0.457	---	---	25.21	11.69	0.464
7-1A	0.152	0.201	1.32	7.26	3.56	0.490
7-1AA	0.147	0.279	1.90	7.29	3.36	0.461
7-2A	0.305	0.279	0.92	15.60	9.65	0.619
7-3A	0.452	0.361	0.80	22.89	16.40	0.716

Contract No. N62269-85-C-0245
NADC-89061-60

Table 21. Coating Densities, T* and t*

No.	ρ_i (g/cm^3)	ρ_f (g/cm^3)	T* (°C)	t* (s)
513-1BB	1.270	0.113	122	79
513-1AA	1.206	0.074	121	72
513-2A	1.231	0.137	122	170
513-3A	1.245	0.180	121	270
526-1A	0.730	0.202	118	51
526-1AA	0.859	0.365	118	56
526-2A	0.826	0.611	121	112
526-3A	0.845	0.857	118	126
1-1A	0.958	---	---	---
1-1AA	0.890	---	110	60
1-2A	0.948	0.200	110	60
1-3A	0.980	0.329	110	95
5-1A	0.862	0.136	110	33
5-1AA	0.826	---	110	33
5-2A	0.931	---	116	90
5-3A	0.945	---	121	166
6-1A	0.900	---	108	60
6-1AA	0.870	---	111	84
6-2A	0.954	---	118	147
6-3A	0.950	---	112	197
7-1A	0.822	0.305	103	66
7-1AA	0.850	.220	103	77
7-2A	0.881	0.596	107	138
7-3A	0.872	0.782	107	211

where T_p is the temperature of the plate, $(\rho C_p)_p$ is the product of the plate density and specific heat, τ_p is the thickness of the steel substrate, t is time, and $\dot{q}_{in}$ is the heat flux into the plate. It is assumed that the back of the plate is well insulated such that little heat is lost off the back of the plate, i.e., an adiabatic boundary condition. Equation (1) is valid at all times, however, the experimental observation is that the temperature-time response of the plate is, to first order, linear after completion of intumescence, e.g., Figure 25; this leads to several simplifications.

5.3 Estimate of Surface Temperature

One of the assumptions inherent in Eq. (1) is that little heat is absorbed by the char, i.e., the heat absorbed by the char is negligible compared to the heat absorbed by the metal substrate. This is true largely because the char density is quite small. Therefore, the temperature profile through the char is essentially linear, implying that whatever heat is "absorbed" at the surface of the char goes into heating the substrate. The heat flux absorbed at the surface, however, is limited by the difference in flame temperature and surface temperature. The heat flux from the heat source can be written as:

$$\dot{q}_{in} = \varepsilon_s \sigma(\varepsilon_F T_F^4 - T_s^4) + H_g(T_F - T_s) \qquad (2)$$

where T_F is the flame temperature, ε_F is the flame emissivity, ε_s is the surface emissivity, H_g is the heat transfer coefficient, and σ is the Stefan-Boltzmann constant. The left-hand side of Eq. (2) can be replaced by $(\rho C_p \tau_p)_p dT/dt$, Eq. (1). Thus, an estimate of T_s is made by solving the nonlinear equation:

$$\varepsilon_s \sigma(\varepsilon_F T_F^4 - T_s^4) + H_g(T_F - T_s) = (\rho C_p \tau_p)_p \frac{dT_p}{dt} \qquad (3)$$

The thermal environment of the furnace used for testing the insulated coupons is the NASA T-3 firebox [2], characterized by the approximate conditions given in Table 22. Properties of the steel substrate are also given in Table 22. As already mentioned, these flame conditions result in an initial heat flux to

Table 22. Flame and Substrate Properties

Flame Properties

T_F: 1226 K

ε_F: 1.0

ε_s: 0.8

H_g: 2.84×10^{-4} cal/cm^2-s-°C

Substrate Properties

ρ_p: 7.84 g/cm^3

$(C_p)_p$: 0.1 cal/g-°C

τ_p: 0.1575 cm

an ambient (20°C) surface of 2.68 cal/cm^2-s with radiation providing 90 percent of the heat flux.

The slope dT_p/dt in Eq. (3) is determined from the experimental data, and is listed in Table 23 for the formulations tested. An iterative algorithm was written to obtain T_s, Eq. (3), using the data from Table 22 and the dT_p/dt values given in Table 23. These estimates for the surface temperatures are also listed in Table 23. We note here that an uninsulated coupon would have a dT_p/dt rate of approximately 22°C/s, substantially higher than any of the values in Table 23. The dT_p/dt data for the coated plates for which no final coating thickness could be determined would seem to indicate that the coating must have fallen off the substrate during removal of the coupon from the test fixture, i.e., the temperature-time data, even after intumescence, indicates that an insulative barrier was present.

5.4 Determination of an Effective Char Thermal Conductivity

As already indicated, $\dot{q}_{in}$ is approximately a constant. This heat flux into the substrate plate can be written as:

$$\dot{q}_{in} = k_c \left.\frac{\partial T_c}{\partial x}\right|_{x=0} \tag{4}$$

where k_c is the conductivity of the char and T_c is the char temperature. The simplest representation for the temperature distribution through the char consistent with $\dot{q}_{in}$ being a constant is a linear temperature profile, i.e.:

$$T_c(x) = (T_s - T_p)\cdot x/\tau_c + T_p \tag{5}$$

where T_c is the char temperature, T_s is the surface temperature, τ_c is the thickness of the char, and x is the coordinate (x = 0 is the plate/char interface). Note that Eq. (5) gives T_p at x = 0, and T_s at x = τ_c. The derivative dT_c/dx is computed from Eq. (5), which is then inserted into Eq. (4) yielding:

Table 23. Post-intumescent Slope, Surface Temperature, and Effective Thermal Conductivity

No.	dT_p/dt (°C/s)	T_s(K)	$(k_c)_1$ (cal/cm-s-°C)	$(k_c)_2$ (cal/cm-s-°C)
513-1BB	1.22	1218	1.97×10^{-4}	2.53×10^{-4}
513-1AA	1.32	1217	3.04	3.91
513-2A	7.39	1166	24.6	31.7
513-3A	2.32	1209	7.05	9.09
526-1A	3.31	1201	1.83	2.36
526-1AA	2.84	1204	1.27	1.63
526-2A	2.72	1206	1.55	1.99
526-3A	2.99	1203	1.80	2.31
1-1A	2.06	1211	---	---
1-1AA	3.09	1202	---	---
1-2A	1.54	1215	2.62	3.37
1-3A	1.16	1218	2.39	3.09
5-1A	3.56	1199	1.18	1.21
5-1AA	5.79	1180	---	---
5-2A	3.86	1196	---	---
5-3A	1.95	1198	---	---
6-1A	8.44	1157	---	---
6-1AA	9.26	1149	---	---
6-2A	6.38	1175	---	---
6-3A	3.19	1202	---	---
7-1A	4.88	1188	1.48	1.91
7-1AA	4.41	1192	1.97	2.54
7-2A	3.09	1202	1.36	1.76
7-3A	1.95	1212	1.18	1.52

$$\dot{q}_{in} = \frac{k_c(T_s - T_p)}{\tau_c} \tag{6}$$

Replacing $\dot{q}_{in}$ in Eq. (1) with Eq. (6), gives an equation which can be integrated over time to yield:

$$\frac{T_p - T_s}{T_p^* - T_s} = e^{-m(t-t^*)} \qquad t > t^* \tag{7a}$$

$$m = k_c/[\tau_c(\rho C_p \tau_p)_p] \tag{7b}$$

where T_p^* and t^* are the temperature and time at the beginning of the linear portion of the temperature-time history after intumescence.

The exponential in Eq. (7a) can be approximated by a series expansion:

$$\frac{T_p - T_s}{T_p^* - T_s} = 1 - m(t - t^*) + \frac{m^2(t-t^*)^2}{2} + O((t-t^*)^3) \tag{8}$$

Equation (8) is the basic equation from which estimates for the thermal conductivity are made. Two approximations will be presented: a first-order approximation, and a more accurate second-order approximation.

5.4a First-Order Approximation

A first-order approximation for the thermal conductivity of the char is made by keeping only the terms through (t-t*) in Eq. (8):

$$T_p = T_p^* + m(T_s - T_p^*)(t - t^*) \tag{9}$$

with m given by Eq. (7b). Equation (9) states that the temperature response of the plate should be linear with time for early times after intumescence is complete. This same conclusion was stated in the discussion of the Frontal Model, described in Refs. 2 and 3.

The char thermal conductivity can be found by differentiating Eq. (9) with respect to time and solving for k_c:

$$(k_c)_1 = \frac{\tau_c(\rho C_p \tau_p)_p}{(T_s - T_p^*)} \frac{dT_p}{dt} \qquad (10)$$

The slope dT_p/dt is determined from the experimental data and is given in Table 23. Using this first-order approximation, k_c's were determined for the various formulations and are tabulated in Table 23. Equation (7a) is plotted in Figure 32, along with Eq. (9) for comparison, using a typical value for k_c. Note that the data traces in Figures 25-31 only go to 500°C while the ordinate axis goes to 1000°C in Figure 32.

5.4b Second-Order Approximation

The difficulty with the preceding analysis is that it underestimates the thermal conductivity of the char. Examination of typical thermal responses of the coated substrates, e.g., Figure 25 does indicate that there is some curvature to the temperature-time responses, though the curvature is more pronounced for some than others. The temperature data were collected to approximately 500°C, and it is seen, even in Figure 25, that the curvature is just becoming pronounced by 500°C.

The accuracy with which the data can be read from the output of the strip chart recorder does not warrant anything better than a straight-line curve fit to the post-intumescent temperature-time data; but, the straight-line response can be viewed as a linear "least squares" fit to a response with a slight amount of curvature. With this viewpoint, it is possible to obtain a second-order accurate approximation of the thermal conductivity for the char.

The procedure follows that outlined above through Eq. (8), where terms are kept through second-order in time, i.e.,

$$\frac{T_p - T_s}{T_p^* - T_s} = 1 - m\alpha + m^2\alpha^2/2 \qquad (11)$$

where $\alpha = (t-t^*)$. Rearranging and solving for T_p gives:

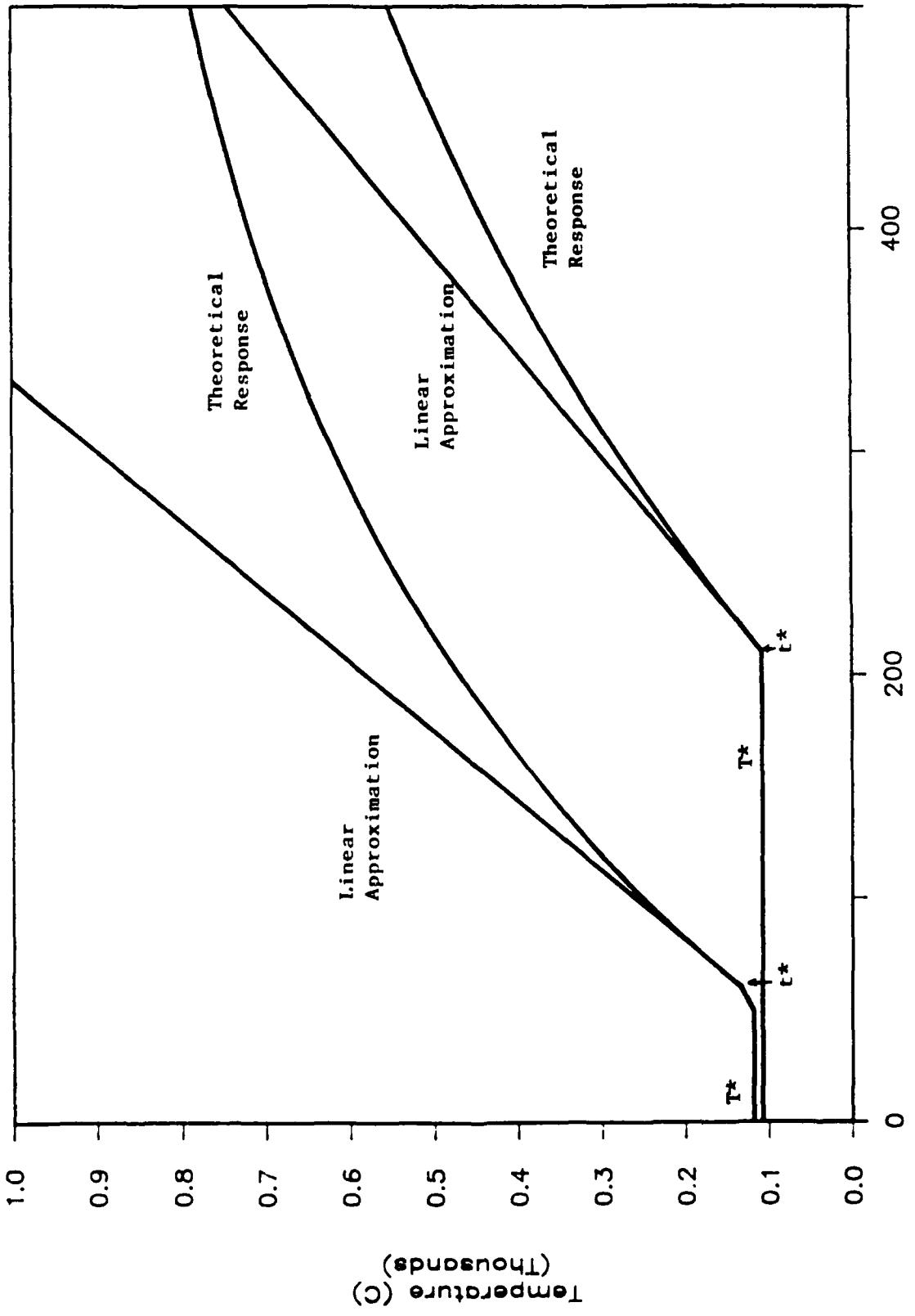

Figure 32. Temperature-Time Response First-order Approximation for the Thermal Conductivity

$$T_p = T_s + (T_p^* - T_s)[1 - m\alpha + m^2\alpha^2/2] \quad (12)$$

Let $\langle m \rangle$ be the "least-squares" slope dT_p/dt as measured from the experimental data. Taking the time derivative of Eq. (12), substituting $\langle m \rangle$ for $(dT_p/dt)/(T_s-T_p^*)$ and rearranging, gives a quadratic equation for m:

$$\alpha m^2 - m + \langle m \rangle = 0 \quad (13)$$

Solving for m gives:

$$m = \frac{1 - [1-4\alpha \langle m \rangle]^{\frac{1}{2}}}{2\alpha} \quad (14)$$

where α is the variable $(t-t^*)$. Since the discriminate must be positive, α_{max} can be found:

$$\alpha_{max} = \frac{1}{4\langle m \rangle} \quad (15)$$

Values for m are found using $\alpha = n \cdot \alpha_{max}/10$ for n = 1 to 10 in Eq. (14). The mean for these ten values are computed; this mean is then used in Eq. (7b) to determine k_c. The calculated values for $(k_c)_2$, using this second-order approximation, are given in Table 23.

Equations (7a) and (9) are plotted in Figure 33 using the second-order k_c determined from the above procedure. It is evident that the appearance of the linear estimate shown in Figure 33 is more in keeping with the general appearance of the experimental response curves, e.g., Figure 25. Typically, the second-order procedure for determining k_c leads to a 22 percent higher thermal conductivity than the first-order procedure.

Several correlations were attempted with the experimental data, e.g., thermal conductivity versus final thickness t_f, or expansion ratio t_f/t_o, but no correlation was found. We thus have concluded, within the accuracy of the data, that the thermal conductivity is virtually independent of thickness. Except for formulation 513, all the thermal conductivities are relatively consistent within a group. Further, the thermal conductivities are within a

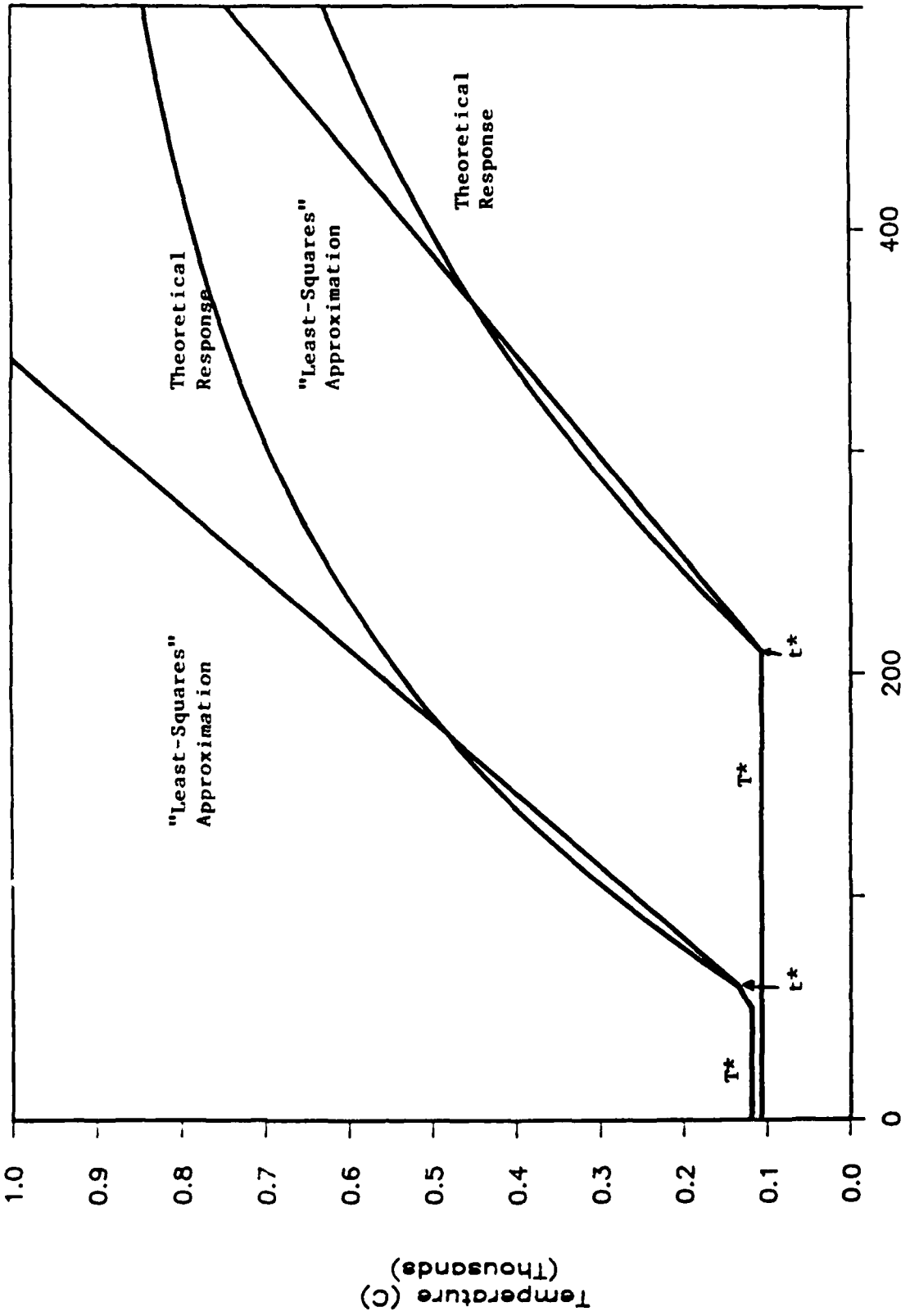

Figure 33. Second-order Approximation for the Thermal Conductivity

factor of two of an average thermal conductivity of 2.32×10^{-4} cal/cm-s-°C (ignoring the two highly variant values of 513-2A and 513-3A). This suggests that perhaps some fundamental mechanism might be responsible for the thermal conductivity. We examine a possibility in the next section.

5.5 Theoretical Consideration

The various formulations, Table 11, are comprised of a variety of constituent elements. The virgin coating system, through the application of heat, undergoes chemical decomposition, pyrolysis, chemical reactions, and expansion as it becomes a char. Predicting the exact geometrical and chemical structure of the char is an exceedingly difficult task. However, it is not unfair to state that the char consists of a considerable volume fraction of gas trapped within a carbonaceous-like material. Several simplifying assumptions and approximations can be made which permit "theoretical" estimates for the thermal conductivity; this exercise provides insights into the physical mechanisms governing the ability of the char of an intumescent coating to provide thermal protection.

Firstly, it is assumed that the char is composed solely of vapor and solid material, and that the cell size of the pores is sufficiently small that convective currents are suppressed, and that thermal radiation does not have a "direct" path through the char to the substrate. Then it is assumed that the arrangement of the solid material and vapor, integrated through the thickness of the char, can be considered as a thermal resistance network; Figure 34 is an idealized sketch of the one-dimensional model that has been adopted. Assuming a constant cross-sectional area, the equivalent thermal resistance R_{eq} of the char can be estimated by summing the thermal resistances R_i, of each layer:

$$R_{eq} = \sum_i R_i \qquad (16)$$

where the thermal resistance is given by:

$$R_i = (\Delta x)_i / (k_i A) \qquad (17)$$

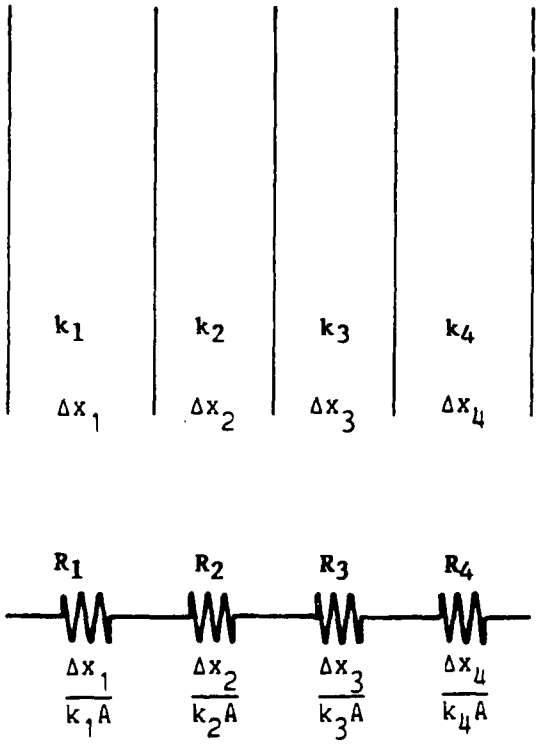

Figure 34. Schematic of Thermal Resistance Network

with $(\Delta x)_i$ and k_i beng the thickness and thermal conductivity of the i-th layer, respectively, and A is the cross-sectional area. Equation (16) can be rewritten in terms of total char thickness $(\Delta x)_{total}$ and an equivalent thermal conductivity k_{eq} for the char:

$$\frac{(\Delta x)_{total}}{k_{eq}} = \sum_i \frac{(\Delta x_i)}{k_i} \tag{18}$$

Since the solid and vapor are the only two "materials," $k_1=k_3=k_5=\ldots=k_s$ and $k_2=k_4=k_6=\ldots=k_v$ where the subscripts "s" and "v" denote the solid and vaporous materials. Therefore, Eq. (18) can be rearranged to give:

$$\frac{(\Delta x)_{total}}{k_{eq}} = \left((\Delta x)_1 + (\Delta x)_3 + (\Delta x)_5 + \ldots\right)\frac{1}{k_1} + \left((\Delta x)_2 + (\Delta x)_4 + (\Delta x)_6 + \ldots\right)\frac{1}{k_2}$$

$$= \frac{(\Delta x)_s}{k_s} + \frac{(\Delta x)_v}{k_v} \tag{19}$$

Multiplying both sides of Eq. (19) by the constant cross-sectional area A permits Eq. (19) to be written in terms of the volumes:

$$\frac{V_{total}}{k_{eq}} = \frac{V_s}{k_s} + \frac{V_v}{k_v} \tag{20}$$

Dividing both sides by the volume of the char V_{total} reduces Eq. (20) to:

$$\frac{1}{k_{eq}} = \frac{f_s}{k_s} + \frac{f_v}{k_v} \tag{21}$$

where f_s and f_v are the volume fractions of the solid and vaporous materials, respectively.

The volume fraction of solid and vapor are determined from conservation of mass:

$$m_{total} = m_s + m_v \tag{22}$$

The mass is given by the product of density ρ and volume. The bulk density, as opposed to the density of solid material, is defined to be the coating mass divided by the expanded volume of the coating. Hence, Eq. (22) can be rearranged to give:

$$\rho = \rho_s f_s + \rho_v f_v$$
$$= \rho_s f_s + \rho_v (1-f_s) \qquad (23)$$

To complete the analysis, estimates must be obtained for the volume fractions, and the densities and thermal conductivities of the solid and vaporous materials. As already indicated, the exact composition and nature of the char is unknown. We have chosen to average the thermal conductivities of a variety of types of graphite at approximately 500 K, Table 24; this average is given in Table 25. To obtain an estimate of the properties of the vapor material, the chemical constituents of several formulations were entered into a chemical equilibrium code to determine relative percentages of pyrolyzed compounds. For the materials examined, over eight-five percent (by mass) of the gases are either carbon dioxide (48%) or water vapor (38%), with the remainder being methane (12%) and hydrogen (2%). Given all the uncertainties in the exact nature of the evolutionary flow of the gases, a 50/50 mixture of water vapor and carbon dioxide was used to represent the gas; a more rigorous analysis is not warranted at this time. An average temperature of 850 K was used as representative of an average temperature for the vapor products. The properties used to represent the vapor are also listed in Table 25.

The bulk densities of the residual chars are given in Table 21. Using the values for ρ_s and ρ_v from Table 25, the volume fraction of the solid material f_s was determined, Eq. (23); these are listed in Table 26. The effective thermal conductivities then were obtained using Eq. (21); these "theoretical" thermal conductivities are also listed in Table 26.

Before comparing the theoretical values for the thermal conductivity with those obtained from analysis of the experimental temperature-time data of the coated substrates, it is noteworthy to point out that the effective thermal

Table 24. Thermal Conductivities for Graphite-like Materials [from Ref. 8]

Material	k cal/(cm-s-°C)	T (K)	ρ (g/cm^3)
Commercial Graphite	0.0750	473.0	1.65
Grade RT-0003	0.0473	500.2	1.90
Grade CS	0.0562	503.2	1.55
EY9	0.0311	478.2	1.64
British Reactor Grade Carbon	0.0535	488.2	1.62
R0025-1	0.0485	468.2	---
JTA; 14-G-1	0.0674	494.8	---
Acheson; 1	0.0514	543.2	---

Table 25. Properties for Theoretical Analysis

	ρ (g/cm^3)	k (cal/cm-s-°C)
Solid Material (from Table 24)	1.67	5.38×10^{-2}
Vapor		
CO_2	0.000630	1.55×10^{-4}
H_2O	0.000258	1.52×10^{-4}

Table 26. Theoretical Thermal Conductivities

ID	f_s(%)	k_{eq} (cal/cm-s-°C)
513-1BB	5.200	1.62×10^{-4}
513-1AA	3.418	1.59
513-2A	6.308	1.64
513.3A	8.299	1.67
526-1A	9.338	1.69
526-1AA	16.894	1.85
526-2A	28.250	2.14
526-3A	39.650	2.54
1-1A	---	---
1-1AA	---	---
1-2A	9.224	1.69
1-3A	15.220	1.81
5-1A	6.280	1.64
5-1AA	---	---
5-2A	---	---
5-3A	---	---
6-1A	---	---
6-1AA	---	---
6-2A	---	---
6-3A	---	---
7-1A	14.097	1.79
7-1AA	10.148	1.71
7-2A	27.557	2.12
7-3A	36.203	2.40

conductivity of the char material is largely controlled by the entrapped gas. This can be seen by rewriting Eq. (21) as:

$$k_{eq} = \frac{k_s k_v}{f_s k_v + f_v k_s} = \frac{k_v}{f_v}\left[1 + \frac{f_s k_v}{f_v k_s}\right]^{-1} \tag{24}$$

Equation (24) can be expanded; keeping only the first term yields:

$$k_{eq} \approx \frac{k_v}{f_v}\left(1 - \frac{f_s k_v}{f_v k_s}\right) \tag{25}$$

Inserting reasonable values for f_s and f_v, and the values for k_v and k_s from Table 25, shows that the term within the brackets of Eq. (25) is 0.9995, i.e.,

$$k_{eq} \approx \frac{k_v}{f_v} \tag{26}$$

Figure 35 is a graph of the experimentally-derived thermal conductivities versus the thermal conductivities calculated from our simple model. The solid line represents a one-to-one correspondence in the experimental and "theoretical" values. It is perhaps somewhat surprising that the theoretical model, which is based on the equivalent thermal resistance of "layers" of solid and gas, does so well in predicting the thermal conductivities. An intumescent char is a complex porous structure. Thermogravitric analysis (TGA) experiments, where a small mass is placed on a sensitive mass balance and "weighed" as a function of temperature, shows that pyrolysis of the binder continues to occur for many of the char materials out to temperatures of 1000°C. This outgassing would result in some convective cooling of the char, which may be the reason for the experimental thermal conductivities being higher than the calculated conductivities for some of the char systems. However, it is seen that the simple model does provide a reasonable estimate of the thermal conductivity. From this, we conclude that the entrapped gas is largely responsible for the small thermal conductivity of intumescent chars. An independent confirmation that the thermal conductivity might be controlled by the porosity is inferred from the thermal conductivities of porous graphites which have a thermal conductivity two orders of magnitude less than graphite at its normal density [8].

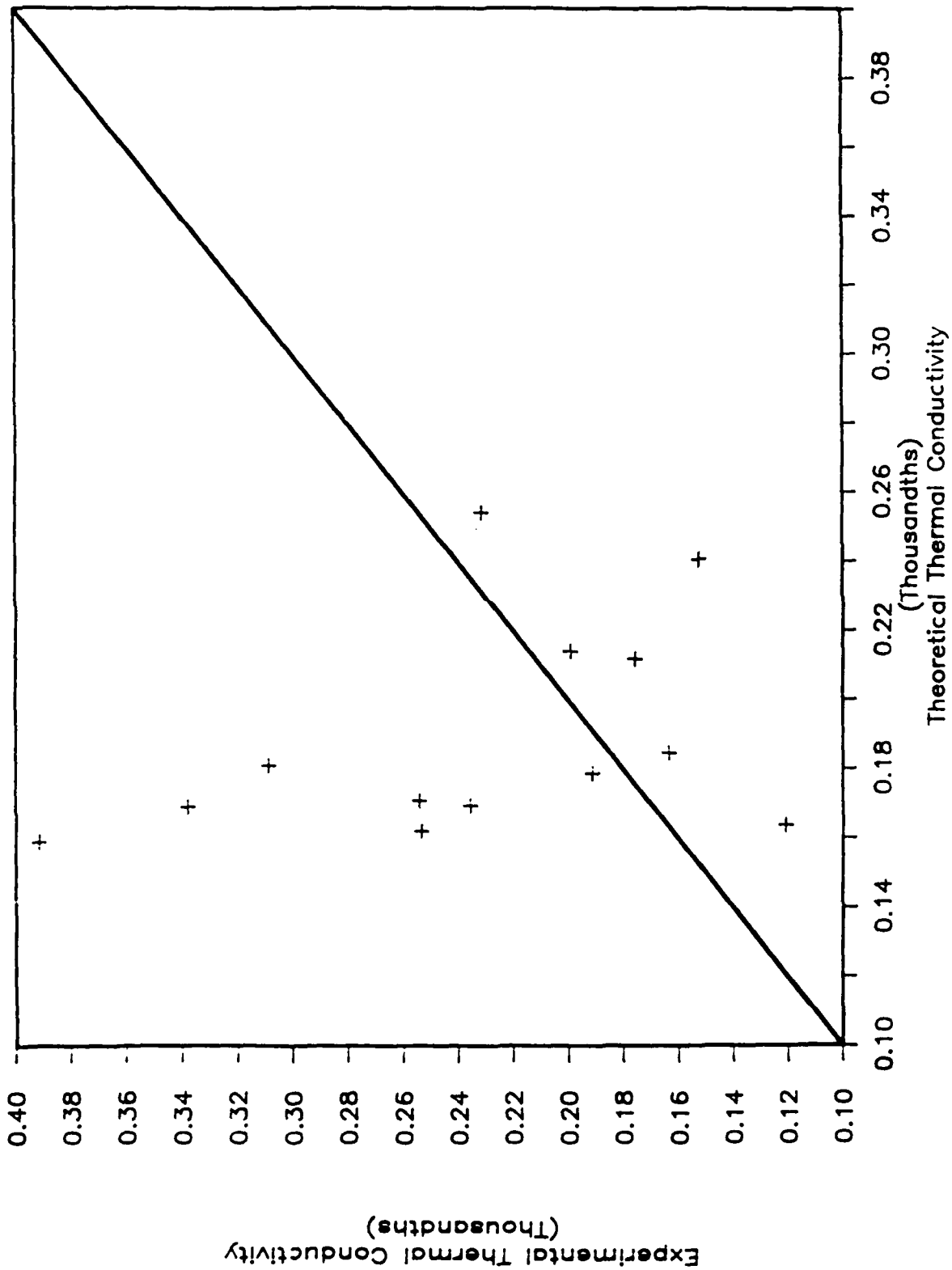

Figure 35. Comparison of Experimental versus Theoretical Thermal Conductivities

5.6 Summary

A procedure has been developed for estimating an effective thermal conductivity of intumescent systems from temperature-time data of a coated, metal substrate. The thermal conductivity obtained is a "dynamic" value in that it is calculated from data obtained from exposure of test samples to a fire-like heat flux. Both first-order and second-order procedures were presented, based on the observation that the post-intumescence temperature-time response of the substrate is quasi-linear. The data, for a variety of materials, yields an average value of 2.3×10^{-4} cal/cm-s-°C for the effective thermal conductivity of the char.

Intumescence, and the physics associated with intumescence is quite complex. However, a rather simple model for the conductive heat transfer through a porous char yields a representative approximation for the thermal conductivity of the char. An average value of 1.86×10^{-4} cal/cm-s-°C is obtained from the theoretical analysis, which only differs by approximately 20% from the experimental average. Whether this simple model accurately reflects the proper physics is unknown, but the reasonably good agreement with the experimentally-derived values is encouraging.

6.0 SUMMARY AND CONCLUSIONS

A considerable amount of research was performed in the current study. A variety of intumescent systems were formulated and examined during this effort. Several of these formulations probably warrant further study by the Navy. Specifically, all the formulations in Table 11 appear to provide good thermal protection. Though the char separated from the substrate for several of the formulations, the temperature-time data indicates that the separation occurred when removing the coupons from the test fixture since an uninsulated plate would heat at a rate of approximately 22°C/s, and the worst of the formulations (number 6) heated at 9°C/s after intumescence. Ablation may have occurred, however, for some of the formulations since the total expansion was not high for any of the formulations tested, Table 20. In fact, except for formulation 513, the expansion ratios were quite small. If ablation is the reason for small expansion ratios, a study should be conducted to examine if the addition of fibers might increase char integrity during the fire testing. Glass flake was added to several of the formulations (Table 11), however, other materials might provide a more suitable bridging mechanism for char integrity. The integrity of the formulations on a curved surface was not investigated.

A couple of points can be made concerning a comparison of formulation 513 (NASA EX-1C-82) with the other intumescent formulations. For a thin application of coating material (1.5 mm), 513 appears to be superior because of protection provided by the "char" after intumescence, as indicated by the post-intumescent slope. However, for thicker applications (3.0 and 4.6 mm), the other formulations develop a definitized intumescent front as evident by the distinct plateau in the temperature-time response of the coated coupons. This is particularly useful in protecting the substrate from the high temperatures of the heat source as self-heating of ordnance becomes irreversible in the 200-350°C range [9]. Previous work [5] seems to indicate that the borax/epoxy mixture does not develop this well-defined plateau (the responses indicated in Figure 31 are considered to be anomalous). A conclusion, then, is that these other formulations may be as good as or superior to EX-1C-82 for applications of 3.0 mm, but that EX-1C-82 is the formulation of choice for 1.5 mm applications. If the other formulations are

subject to some ablation, as discussed in the first paragraph, then the efficacy of these formulations might be improved further for both the thinner and thicker coating applications if char integrity can be maintained through the addition of a suitable bridging agent.

A study of the heat absorbed as a function of temperature has shown that considerable energy per gram of material is absorbed through bond breaking of the "polymeric" char. Though some of this energy is recovered in reversible bond linking, the binder undergoes considerable irreversible bond breaking during the initial heating and formation of the char. This energy absorption is much larger than previously thought.

The self-limiting affect of pressure on intumescence was investigated indirectly by examining the endothermic response generated by the release of the blowing agents. The temperature for the onset of the endothermic response did not change due to pressurization. However, assuming the release of the blowing agent could be correlated with heat absorbed, the gas released was spread over a slightly higher temperature range. For a couple of formulations, there was a shift of the release of the blowing agent to a slightly higher temperature as inferred from a change in the shape of the endothermic peaks with and without pressurization. However, the total shift (spread) in temperature was less than 20°C, and gas release is continuous during this temperature interval. Since the behavior of the softening binder is relatively continuous and smooth, i.e., there are no sudden transitions to "hardness", then pressurization would not seem to have a self-limiting affect on intumescence.

A model was developed to estimate the effective thermal conductivity of intumescent chars from the temperature-time response of coated coupons. For the formulations examined, an average value of 2.3×10^{-4} cal/cm-s-°C was found. To the authors' knowledge, and from examination of the literature, this is the first direct estimate of the thermal conductivity for intumescent chars. This value is two orders of magnitude smaller than for carbon or graphite. A theoretical model, based on conductive heat transfer through a porous media, gives a thermal conductivity in reasonably good agreement (within 20%) with the experimentally-derived thermal conductivity. From this,

it is inferred that the good insulating ability of intumesced chars results from the insulating quality of gas pockets within the char.

In summary, it is felt that the present study has provided several formulations which hold promise as insulative systems for the Navy. Also, the parallel studies have provided further insights into the thermophysics of intumescent systems.

7.0 REFERENCES

1. Anderson, C. E., and D. K. Wauters, "A Thermodynamic Heat Transfer Model for Intumescent Systems," **International Journal of Engineering Science**, Vol. 22, No. 7, pp. 881-889, 1984.

2. Anderson, C. E., J. Dziuk, Jr., W. A. Mallow, and J. Buckmaster, "A Study of Intumescent Reaction Mechanisms," **Journal of Fire Sciences**, Vol. 3, No. 3, pp. 161-194, 1985.

3. Buckmaster, J., C. E. Anderson, and A. Nachman, "A Model for Intumescent Systems," **International Journal of Engineering Science**, Vol. 24, No. 3, pp. 263-276, 1986.

4. Anderson, C. E. and D. K. Wauters, "Intumescent Reaction Mechanisms: An Analytic Model," NADC-82211-60, Naval Air Development Center, Warminster, PA, May, 1983.

5. Anderson, C. E., J. Dziuk and J. Buckmaster, "A Study of Intumescent Reaction Mechanisms," NADC-84170-60, Naval Air Development Center, Warminster, PA, August 1984.

6. Kemp, P. H., "The Chemistry of Borates, Part I," Borax Consolidated Limited, 1956, p. 31.

7. Holman, J. P., **Experimental Methods for Engineers**, Third Edition, McGraw-Hill, 1978.

8. **Thermophysical Properties of Matter, Volume 2: Thermal Conductivity: Nonmetallic Solids**, edited by Y. J. Toulonkian, R. W. Powell, C. Y. Ho, and P. G. Klemens, IFI/Plenum, Plenum Publishing Company, 1970.

9. Dobratz, B. M., "LLNL Explosives Handbook. Properties of Chemical Explosives and Explosive Simulants," UCRL-57997, Lawrence Livermore National Laboratory, Livermore, CA, 1981.

APPENDIX: PRESSURIZED DSC THERMOGRAPHS

The following pages contain the thermographs from the DSC experiments conducted to investigate any if pressure dependence might self-limit inumtescence. The ID number for each test, listed in Table 19, appears in the upper right hand corner of each figure besides the label "File:". The formulation number appears first. A dash then separates the formulation number and the pressure at which the test was conducted. The sample numbers have no significance beyond an identification number during sample preparation. For example, 1-0.35 is formulation 1 conducted at a pressure of 0 psig (sample 35), whereas 7-100.08 is formulation 7 conducted at 100 psig (sample 8).

Each test has two figures. The first figure represents the thermograph over the entire temperature range at which the test was conducted, which was nominally 25°C to 500°C. The second figure represents an enlargement of the curves between 0 and 200°C, providing more detail of the endothermic peaks.

Sample: COATING 513
Size: 4.40 mg
Method: DSC 10
Comment: PRESSURE DEPENDENCE OF INTUMESCENCE 06-8766-006

DSC

File: A:513.0
Operator: VDB
Run date: 07/23/87 12:45

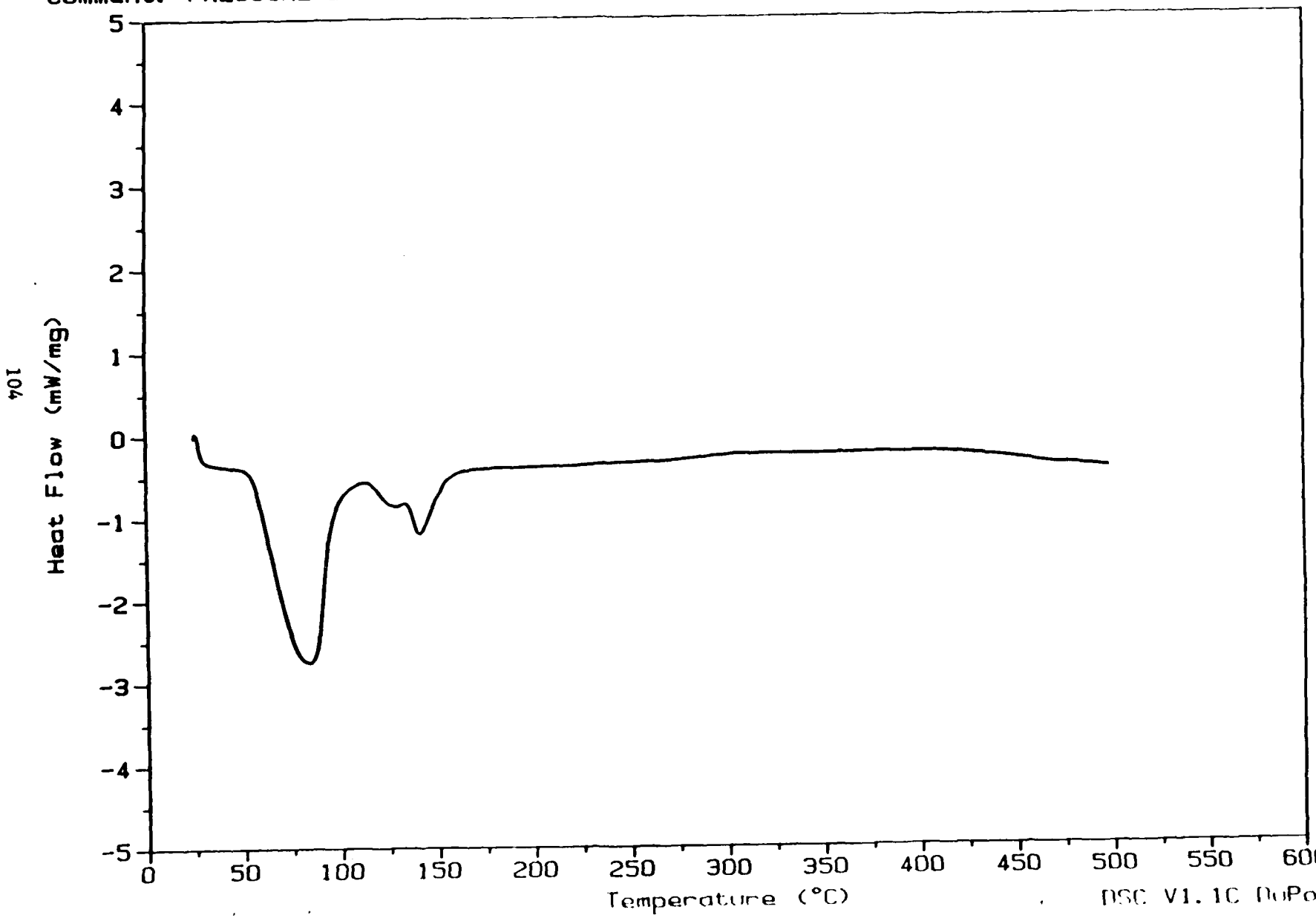

NADC-89061-60

Sample: COATING 513
Size: 4.40 mg
Method: DSC 10
Comment: PRESSURE DEPENDENCE OF INTUMESCENCE 06-8766-006

DSC

File: B:513.0
Operator: VDB
Run date: 07/23/87 12:45

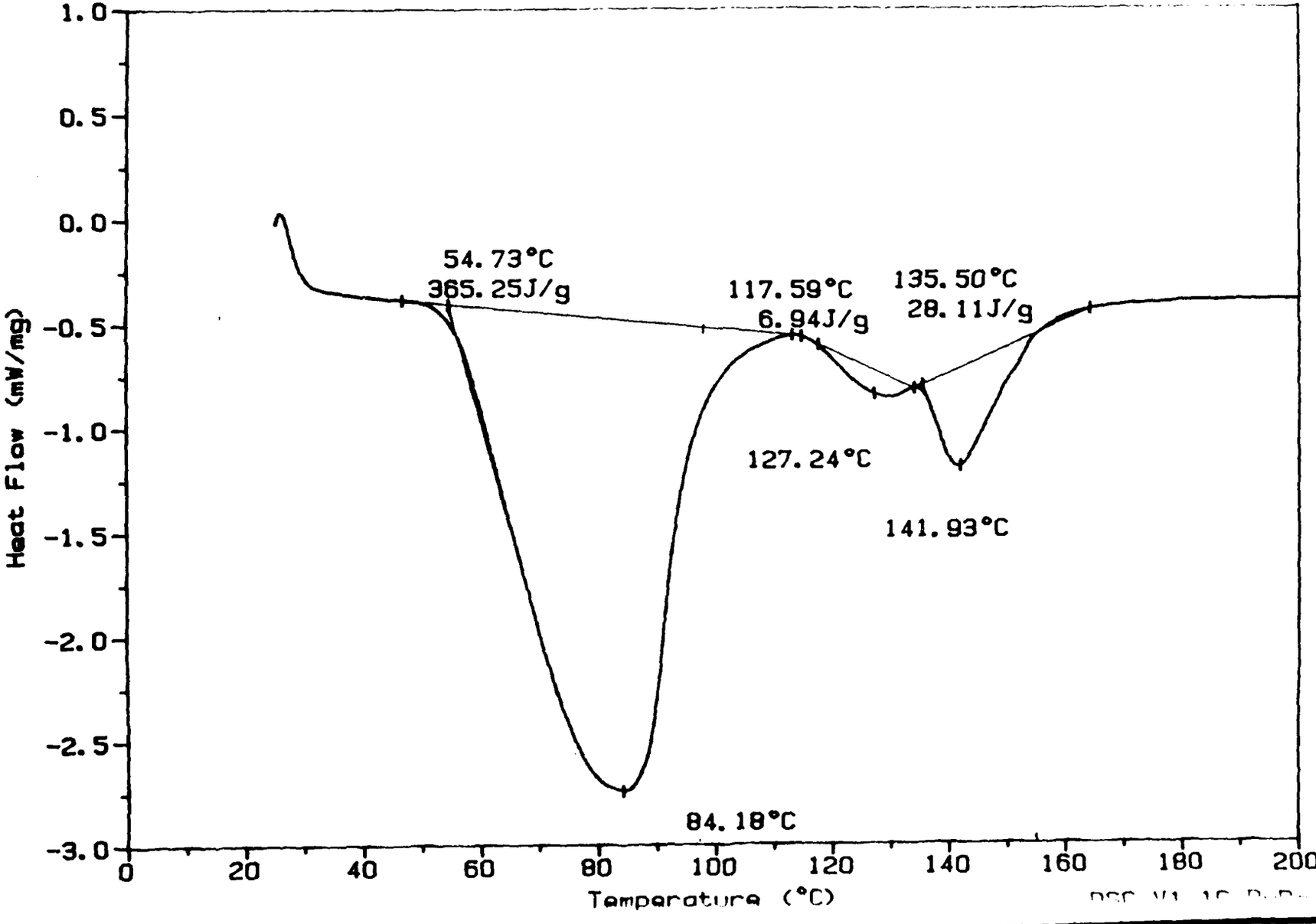

Contract No. N62269-85-C-0245
NADC-89061-60

Sample: COATING 513
Size: 4.30 mg
Method: DSC 10
Comment: PRESSURE DEPENDENCE OF INTUMESCENCE 06-8766-006

DSC

File: A:513-0.29
Operator: VDB
Run date: 08/13/87 09:19

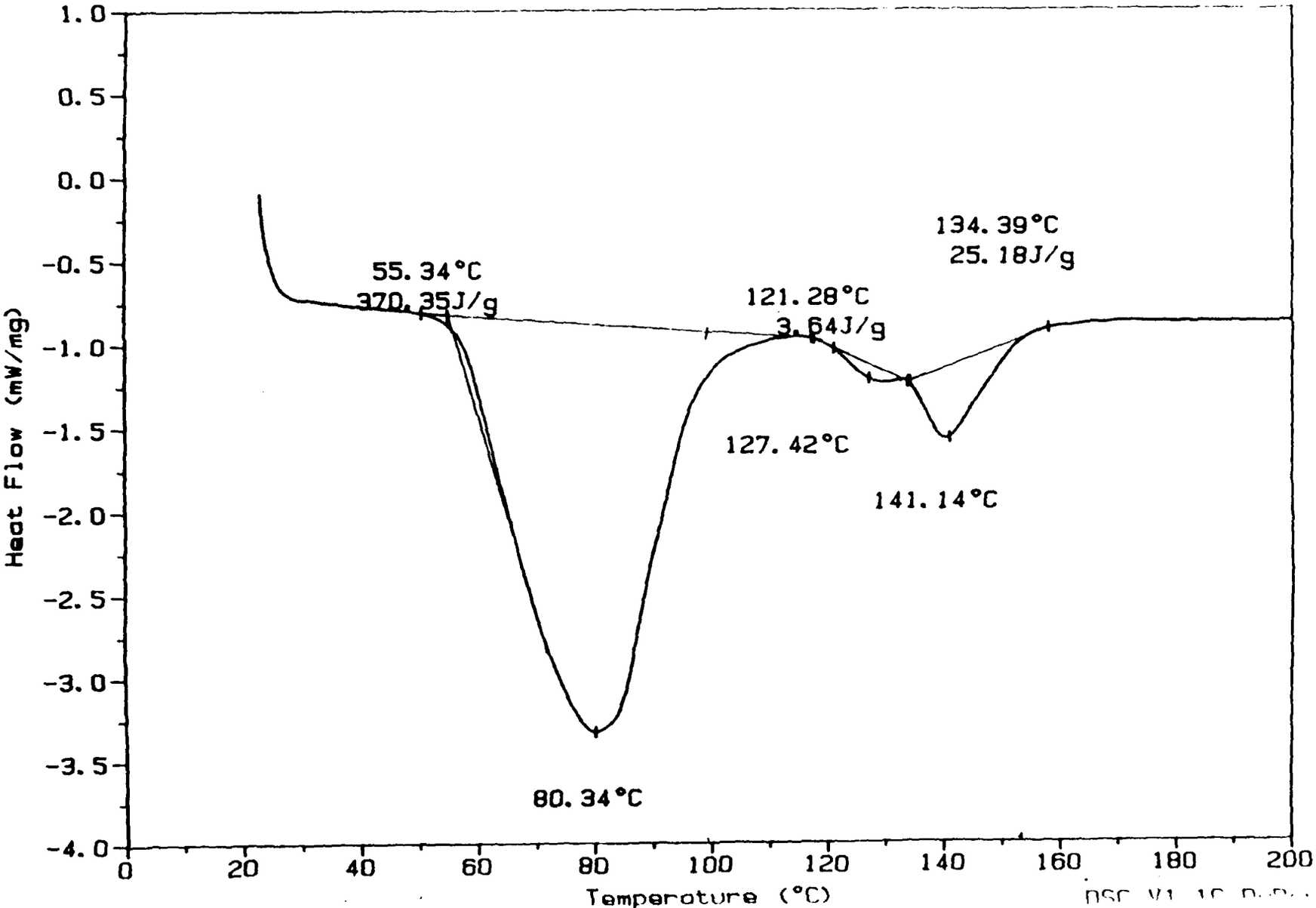

Contract No. N62269-85-C-0245
NADC-89061-60

Sample: COATING 513
Size: 3.90 mg
Method: DSC 10
Comment: PRESSURE DEPENDENCE OF INTUMESCENCE 06-8766-006

DSC

File: A:513-0.30
Operator: VDB
Run date: 08/13/87 10:40

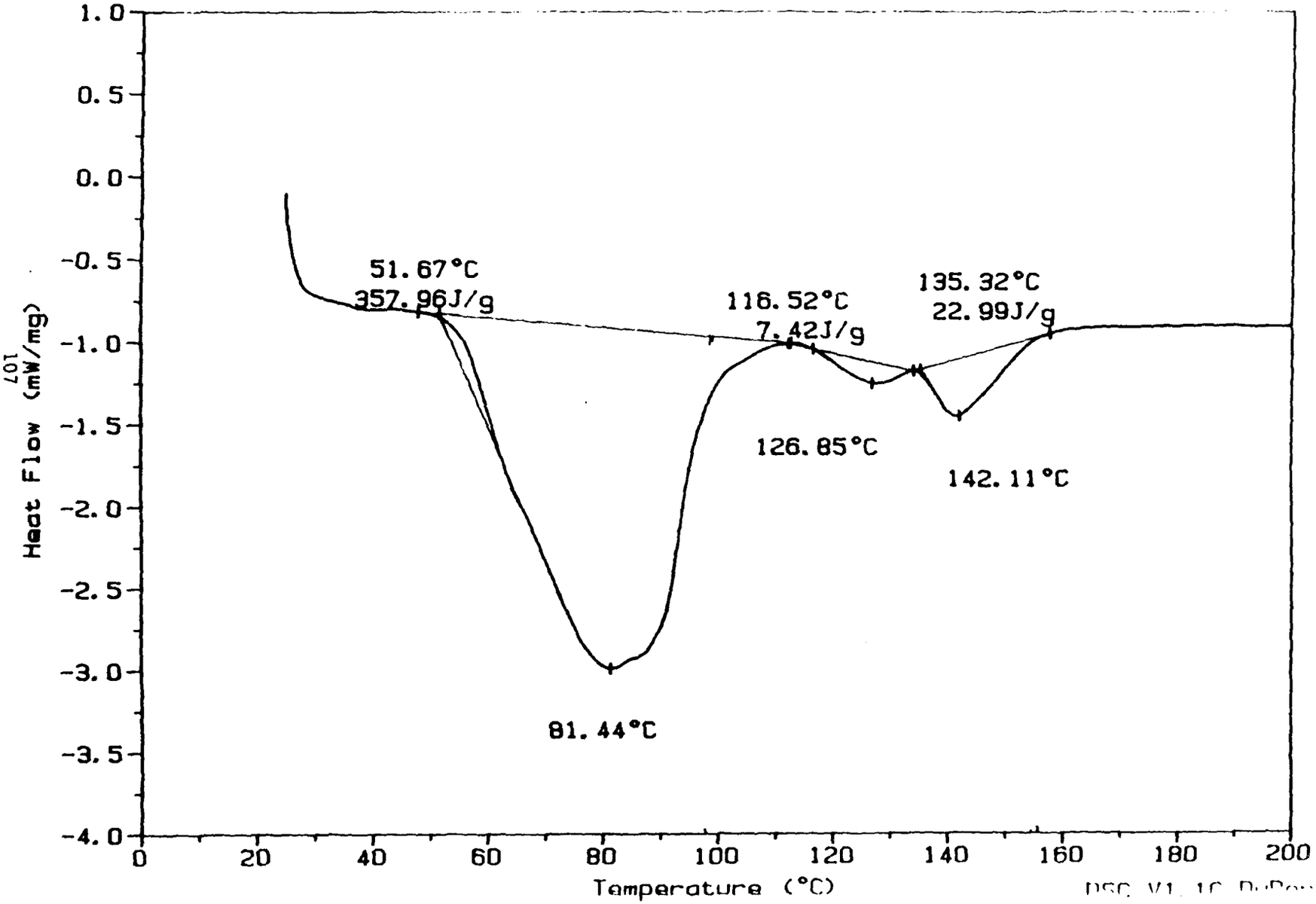

Contract No. N62269-85-C-0245
NADC-89061-60

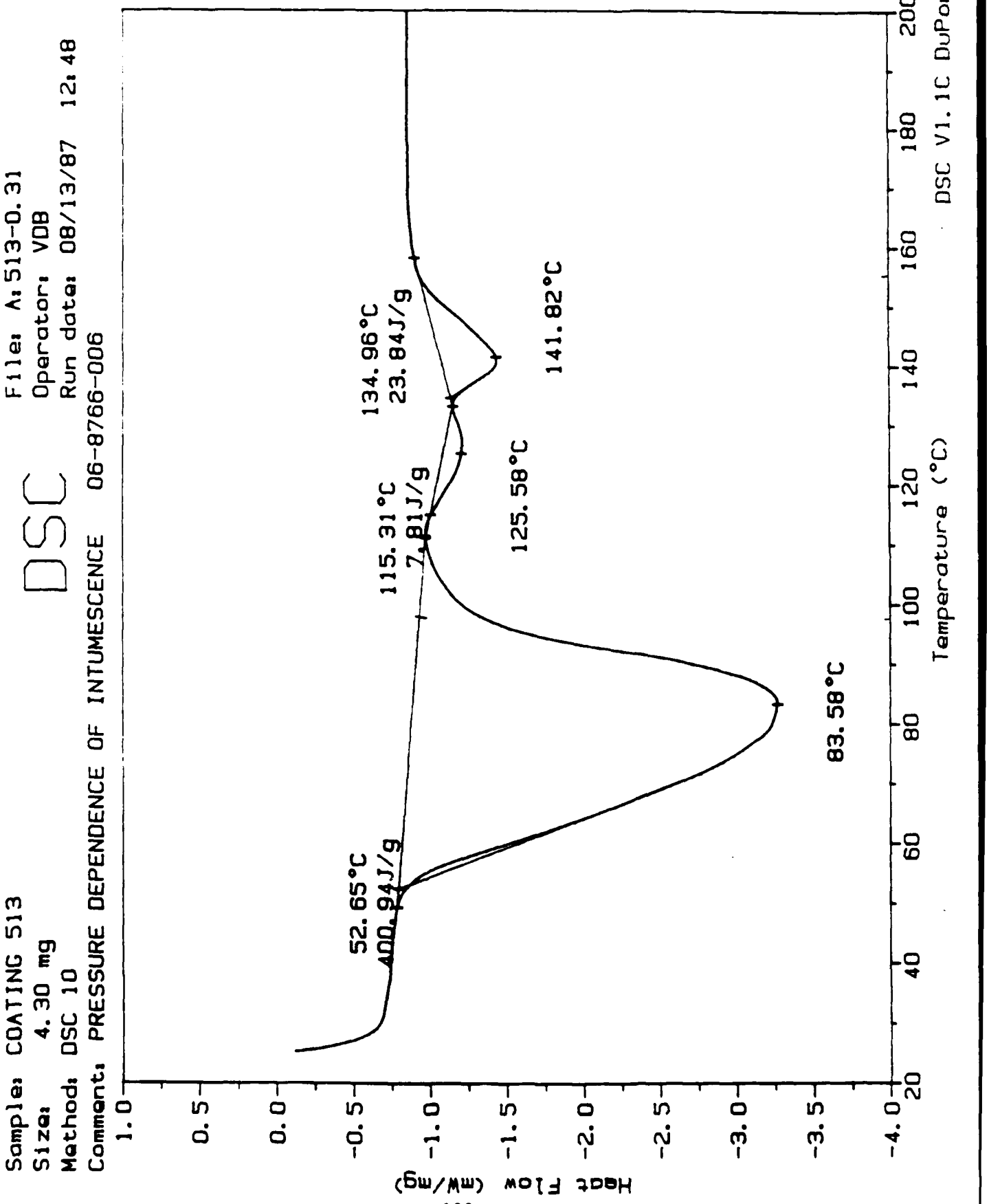
Sample: COATING 513
Size: 4.30 mg
Method: DSC 10
Comment: PRESSURE DEPENDENCE OF INTUMESCENCE 06-8766-006
File: A:513-0.31
Operator: VDB
Run data: 08/13/87 12:48
DSC
52.65°C
400.94J/g
115.31°C
7.81J/g
134.96°C
23.84J/g
125.58°C
141.82°C
83.58°C
Heat Flow (mW/mg)
Temperature (°C)
DSC V1.1C DuPont 9900

Sample: COATING 513
Size: 4.00 mg
Method: DSC 10
Comment: PRESSURE DEPENDENCE OF INTUMESCENCE 06-8766-006

DSC

File: A:513-100.05
Operator: VDB
Run date: 07/20/87 10:19

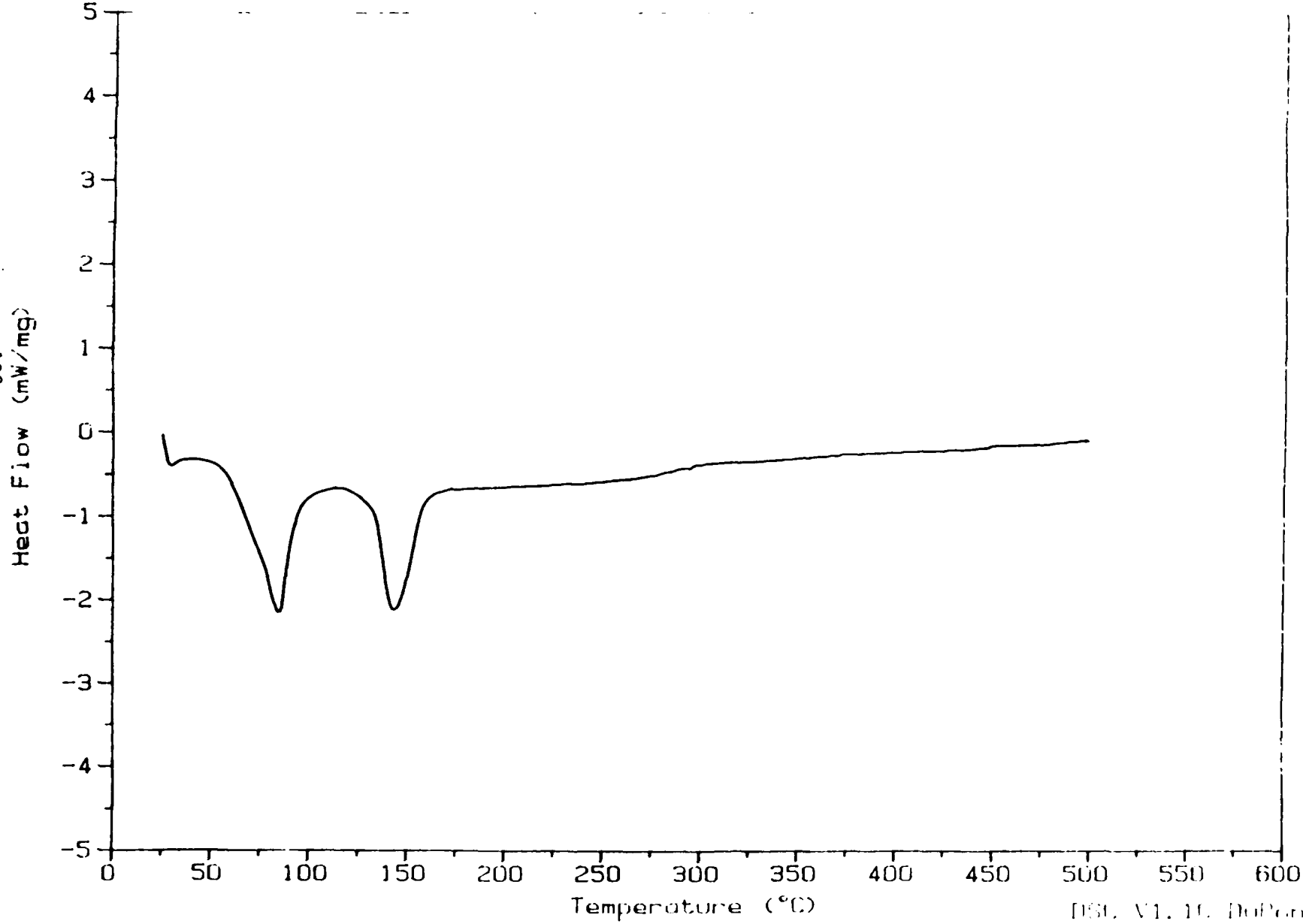

DSC, V1.1C DuPont 9900

Contract No. N62269-85-C-0245
NADC-89061-60

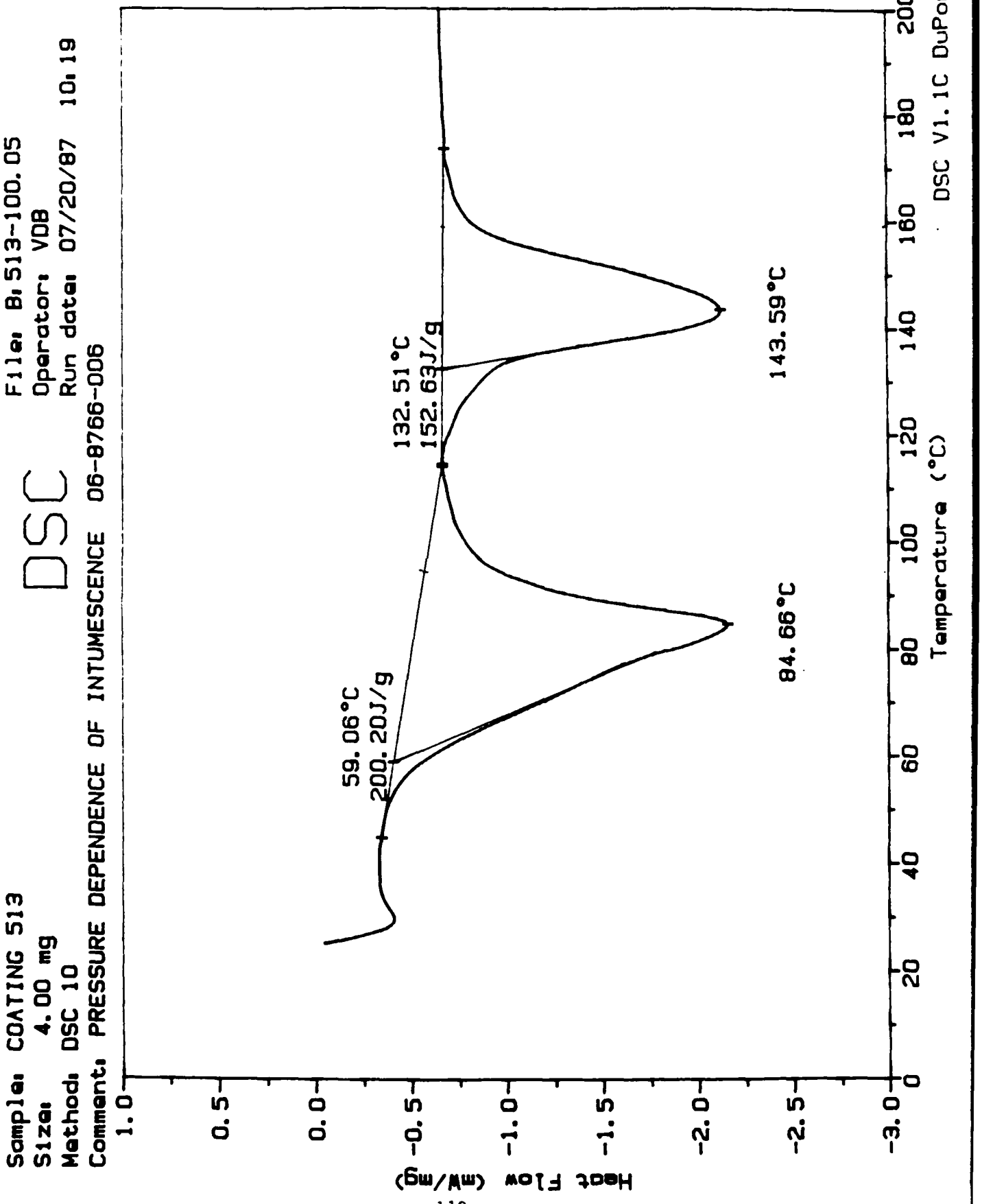
Sample: COATING 513
Size: 4.00 mg
Method: DSC 10
Comment: PRESSURE DEPENDENCE OF INTUMESCENCE 06-8766-006
File: B:513-100.05
Operator: VDB
Run date: 07/20/87 10:19
DSC
59.06°C
200.20J/g
84.66°C
132.51°C
152.63J/g
143.59°C
Heat Flow (mW/mg)
Temperature (°C)
DSC V1.1C DuPont 9900

Sample: COATING 513
Size: 3.20 mg
Method: DSC 10
Comment: PRESSURE DEPENDENCE OF INTUMESCENCE 06-8760-006

DSC

File: A:513-100.06
Operator: VDB
Run date: 07/20/87 12:44

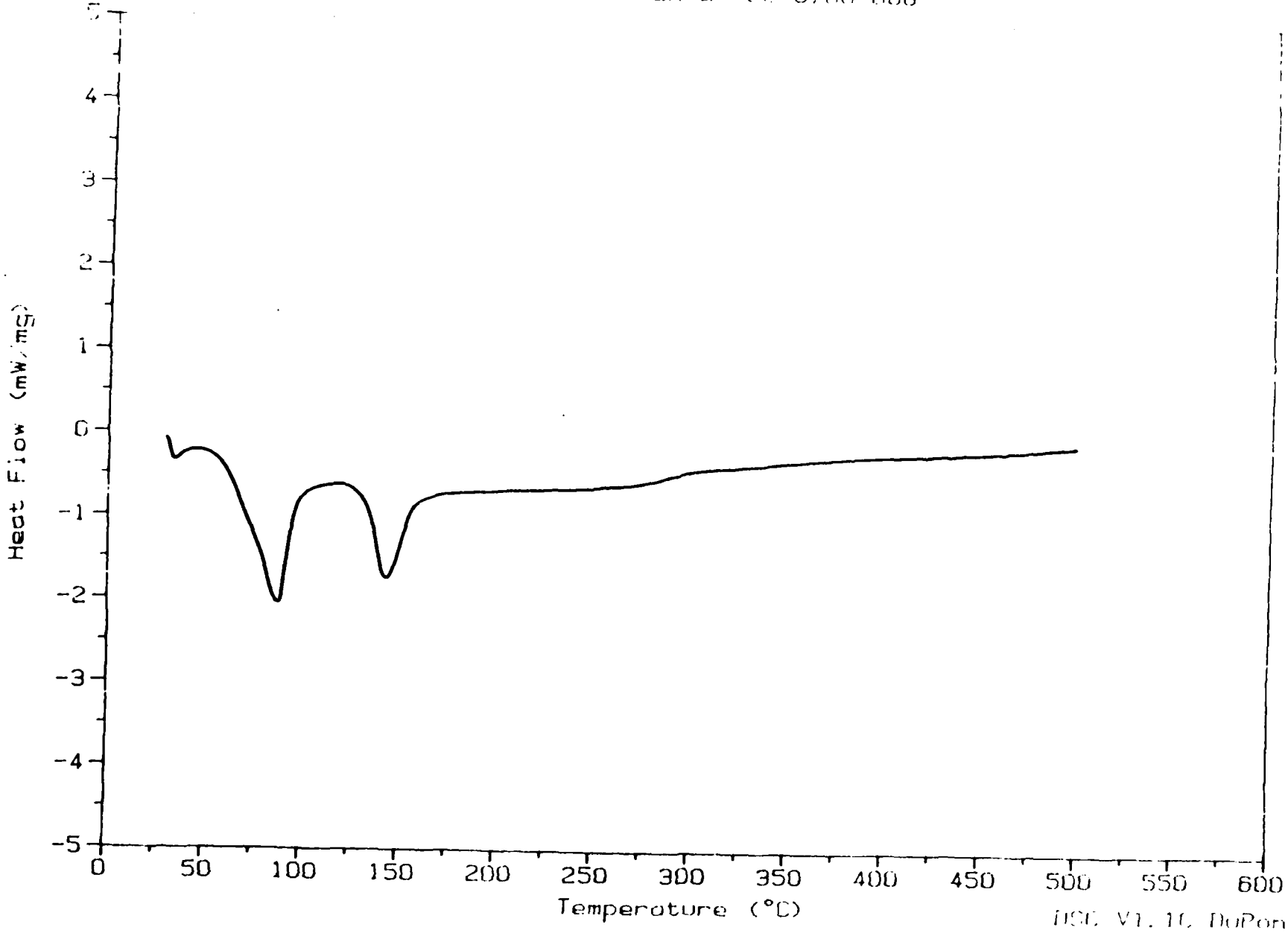

DSC V1.1C DuPont 9900

111

Contract No. N62269-85-C-0245
NADC-89061-60

Sample: COATING 513
Size: 3.20 mg
Method: DSC 10
Comment: PRESSURE DEPENDENCE OF INTUMESCENCE 06-8766-006

DSC

File: A:513-100.06
Operator: VDB
Run date: 07/20/87 12:44

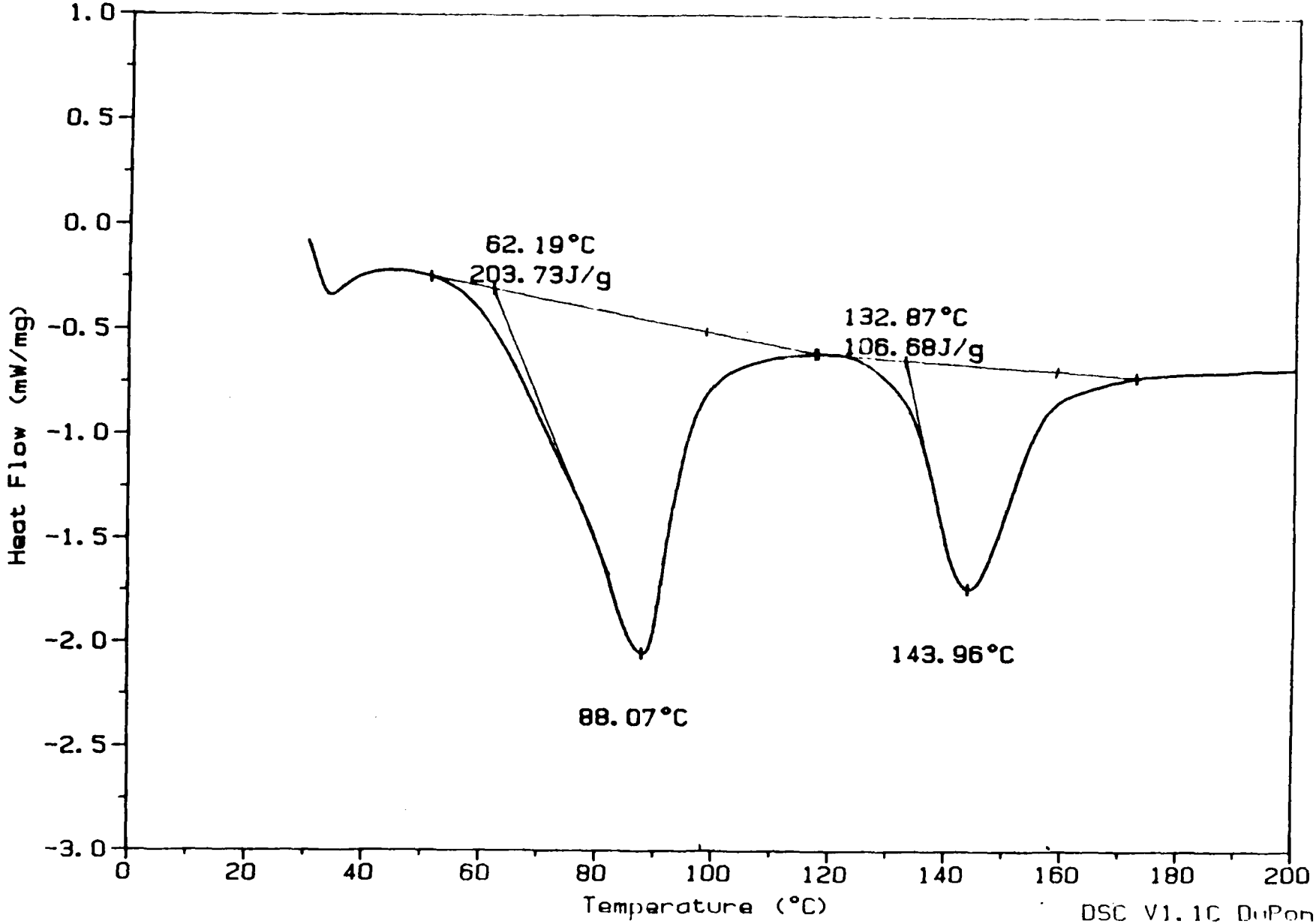

DSC V1.1C DuPont 9900

Contract No. N62269-85-C-0245
NADC-89061-60

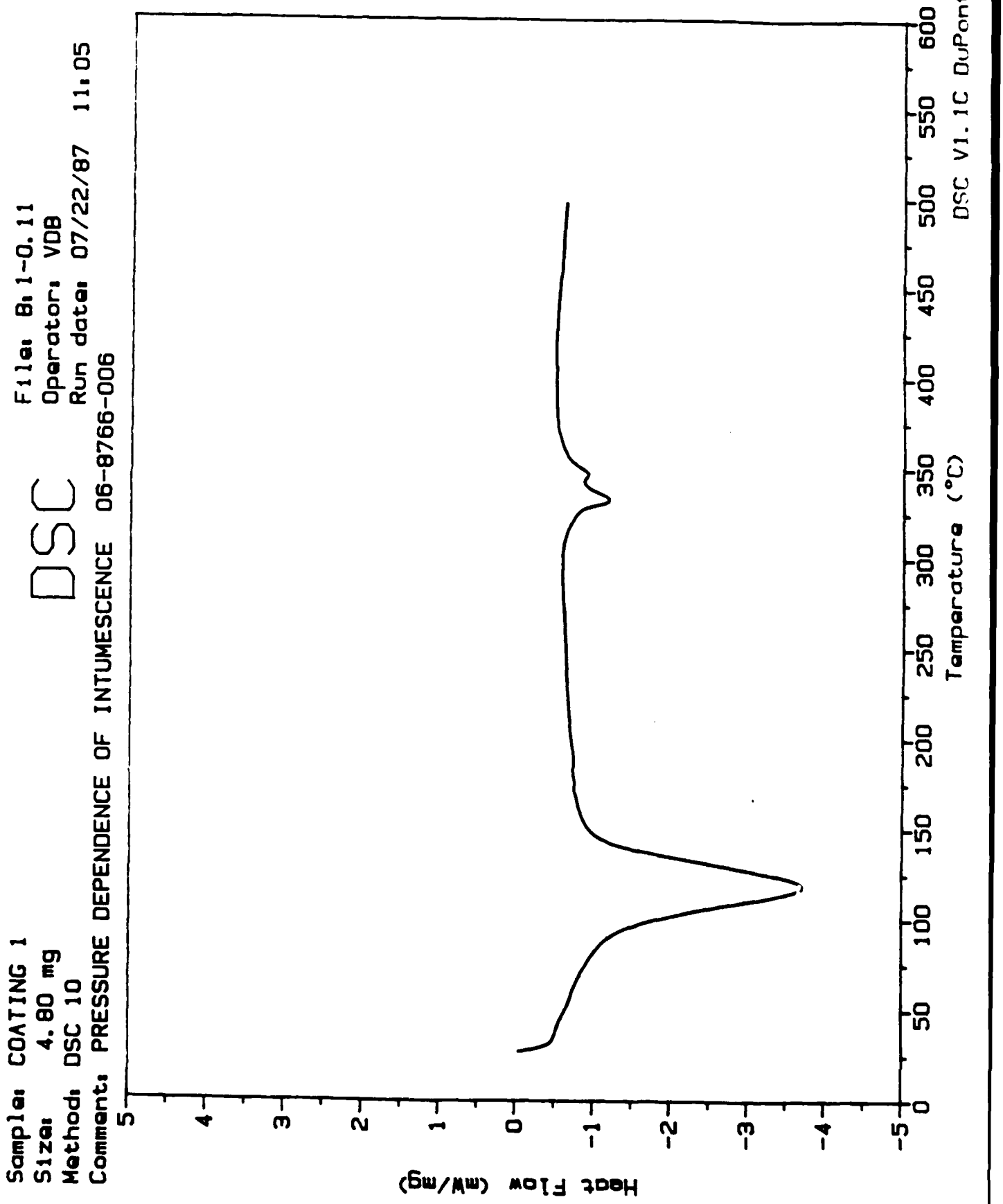
Sample: COATING 1
Size: 4.80 mg
Method: DSC 10
Comment: PRESSURE DEPENDENCE OF INTUMESCENCE 06-8766-006
DSC
File: B:1-0.11
Operator: VDB
Run date: 07/22/87 11:05
Heat Flow (mW/mg)
5
4
3
2
1
0
-1
-2
-3
-4
-5
0
50
100
150
200
250
300
350
400
450
500
550
600
Temperature (°C)
DSC V1.1C DuPont 9900

Sample: COATING 1
Size: 4.80 mg
Method: DSC 10
Comment: PRESSURE DEPENDENCE OF INTUMESCENCE 06-8766-006

DSC

File: B:1-0.11
Operator: VDB
Run date: 07/22/87 11:05

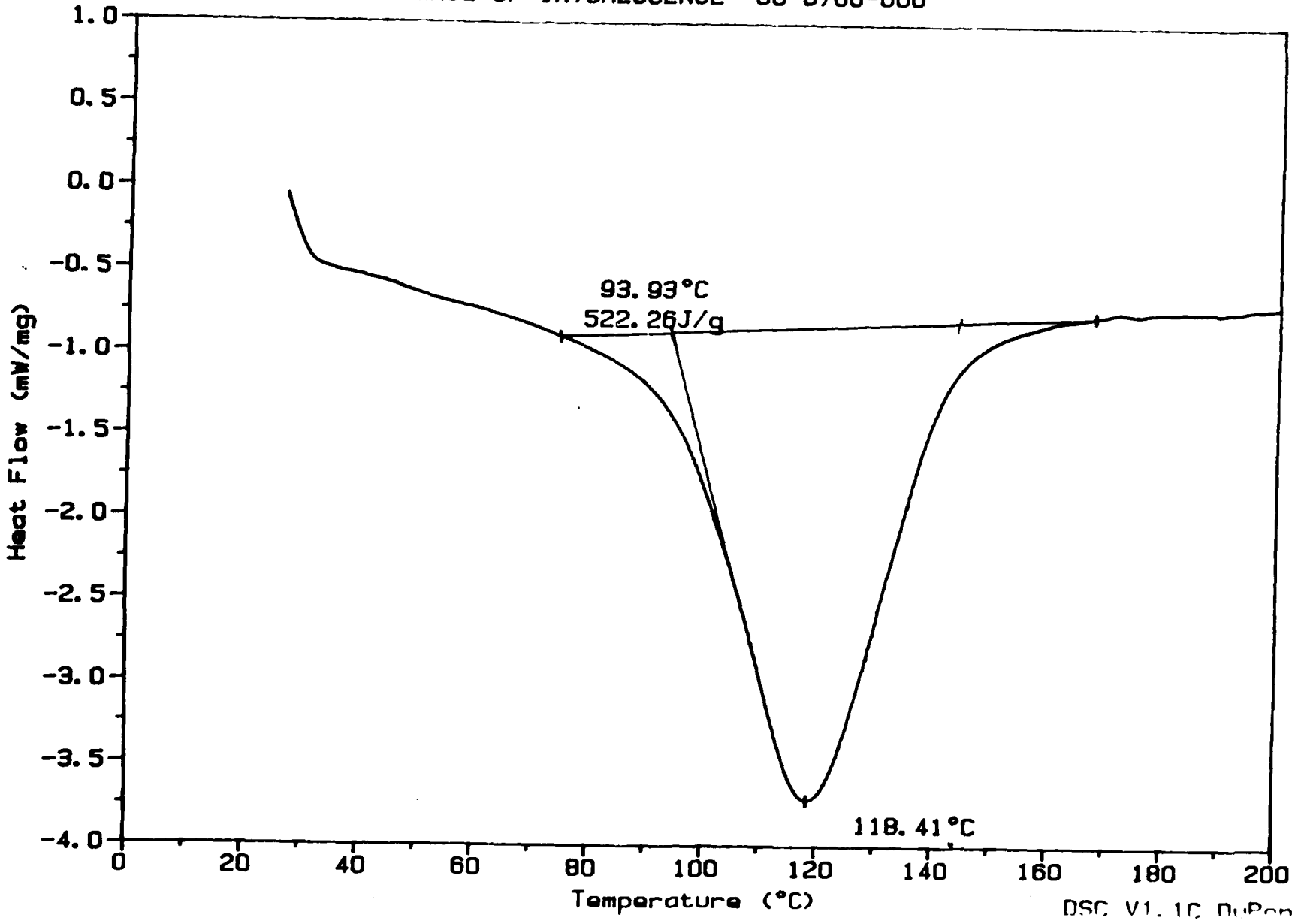

Contract No. N62269-85-C-0245
NADC-89061-60

DSC V1.1C DuPont 2000

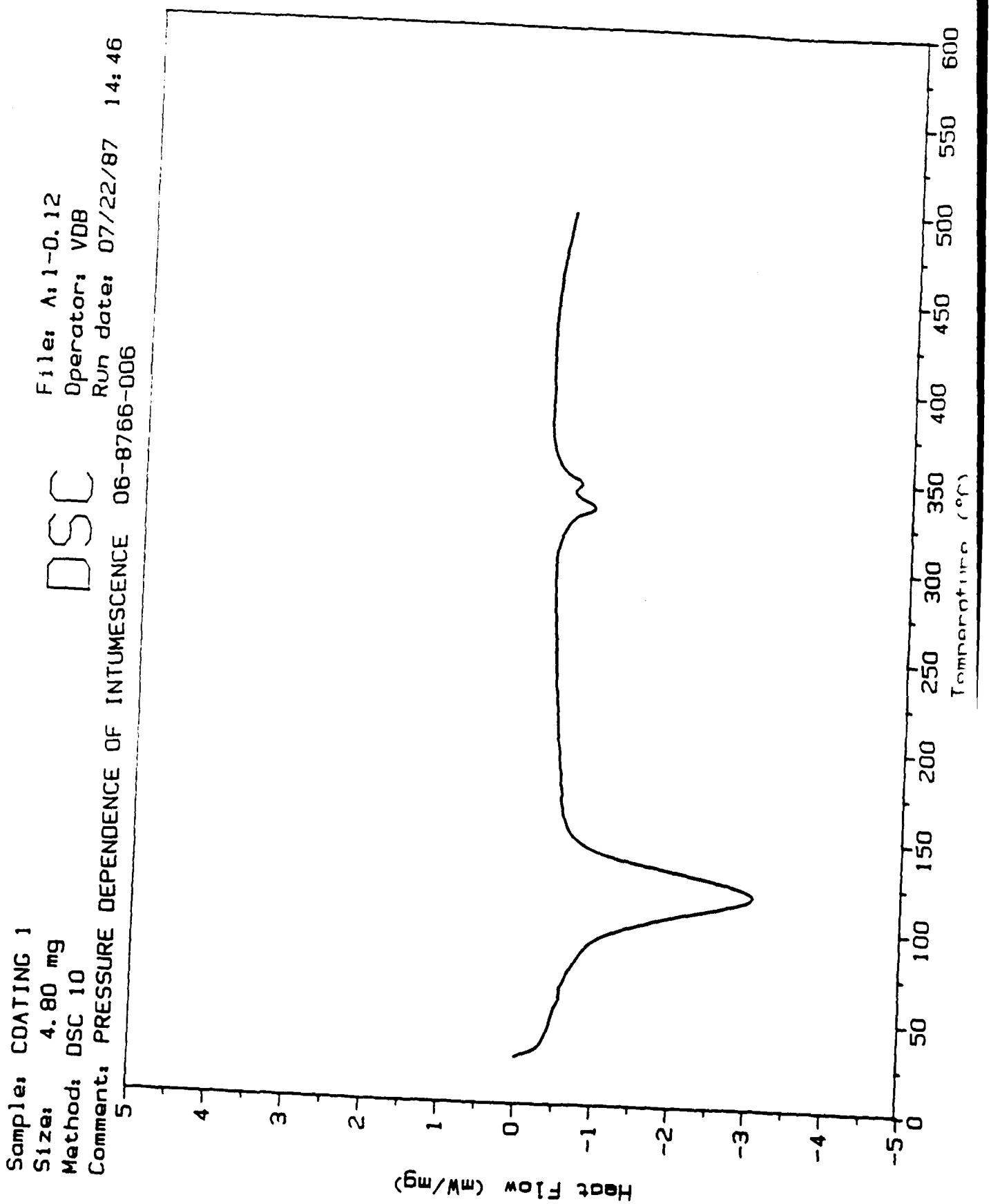
Sample: COATING 1
Size: 4.80 mg
Method: DSC 10
Comment: PRESSURE DEPENDENCE OF INTUMESCENCE 06-8766-006
DSC
File: A:1-0.12
Operator: VDB
Run date: 07/22/87 14:46
Heat Flow (mW/mg)
5
4
3
2
1
0
-1
-2
-3
-4
-5
0
50
100
150
200
250
300
350
400
450
500
550
600
Temperature (°C)

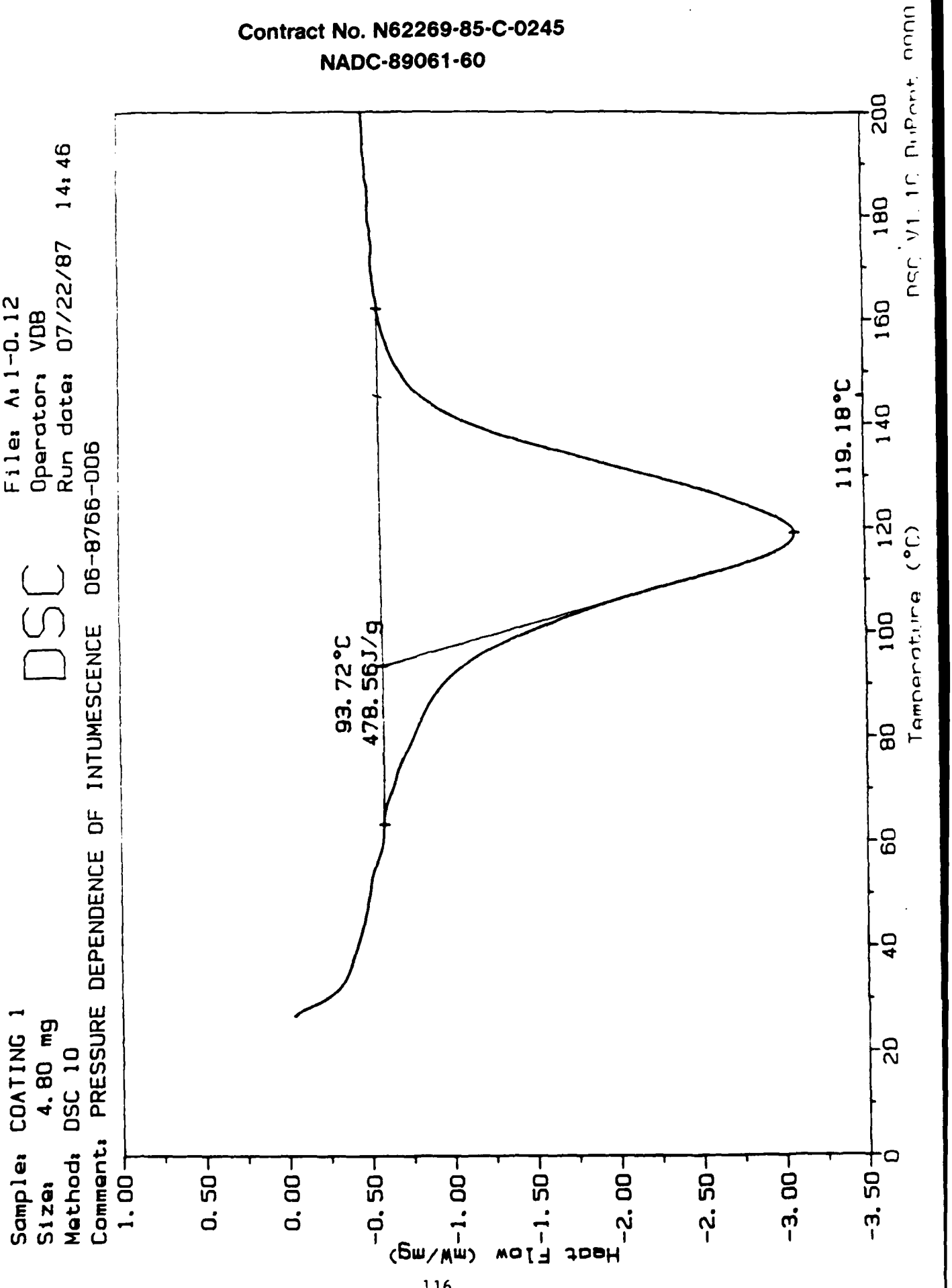
Sample: COATING 1
Size: 4.80 mg
Method: DSC 10
Comment: PRESSURE DEPENDENCE OF INTUMESCENCE 06-8766-006
File: A:1-0.12
Operator: VDB
Run data: 07/22/87 14:46
DSC
93.72°C
478.56J/g
119.18°C
Heat Flow (mW/mg)
Temperature (°C)
1.00
0.50
0.00
-0.50
-1.00
-1.50
-2.00
-2.50
-3.00
-3.50
0
20
40
60
80
100
120
140
160
180
200

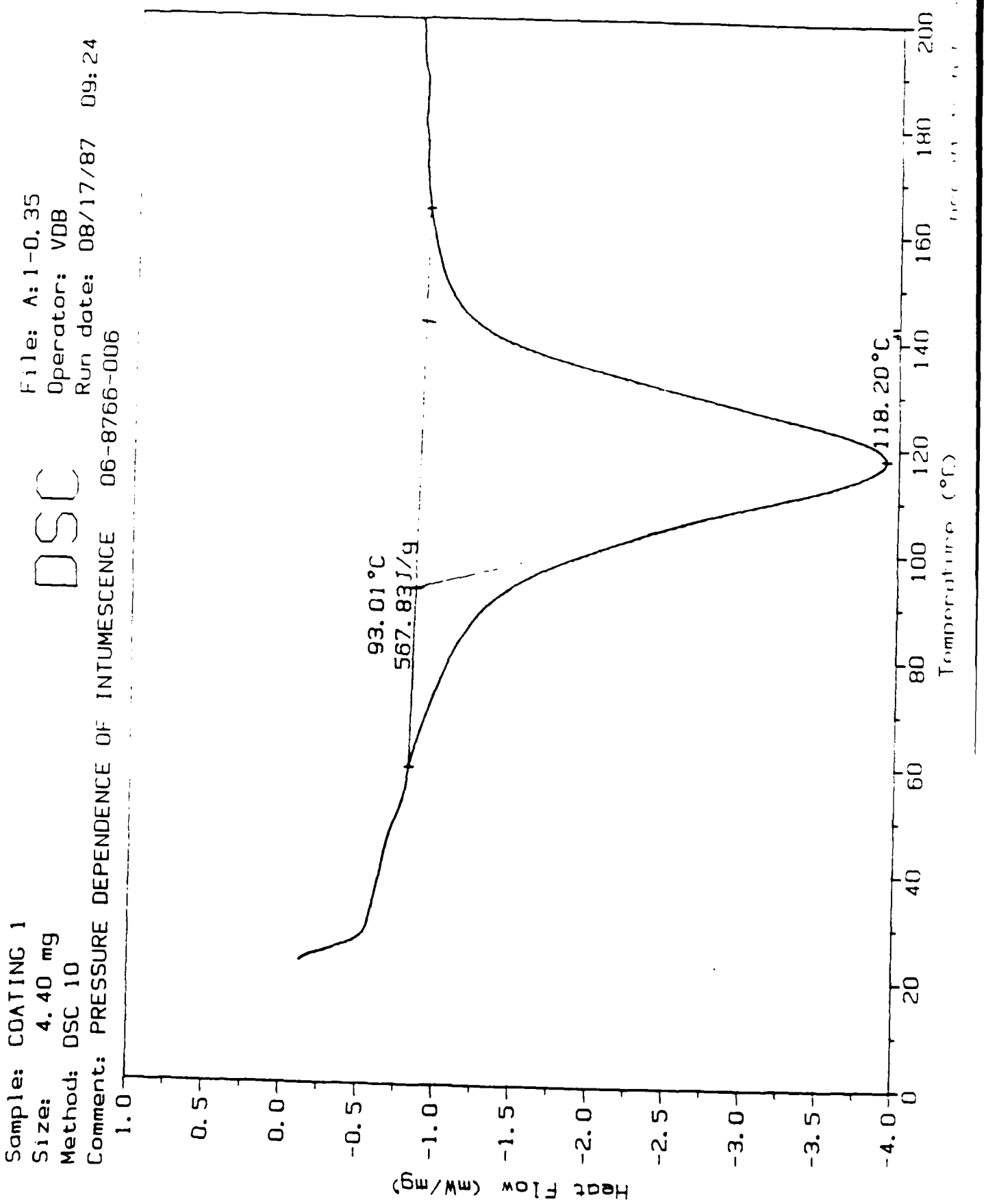
Sample: COATING 1
Size: 4.40 mg
Method: DSC 10
Comment: PRESSURE DEPENDENCE OF INTUMESCENCE 06-8766-006
DSC
File: A:1-0.35
Operator: VDB
Run date: 08/17/87 09:24
93.01°C
567.83 J/g
118.20°C
Heat Flow (mW/mg)
Temperature (°C)
1.0
0.5
0.0
-0.5
-1.0
-1.5
-2.0
-2.5
-3.0
-3.5
-4.0
0
20
40
60
80
100
120
140
160
180
200

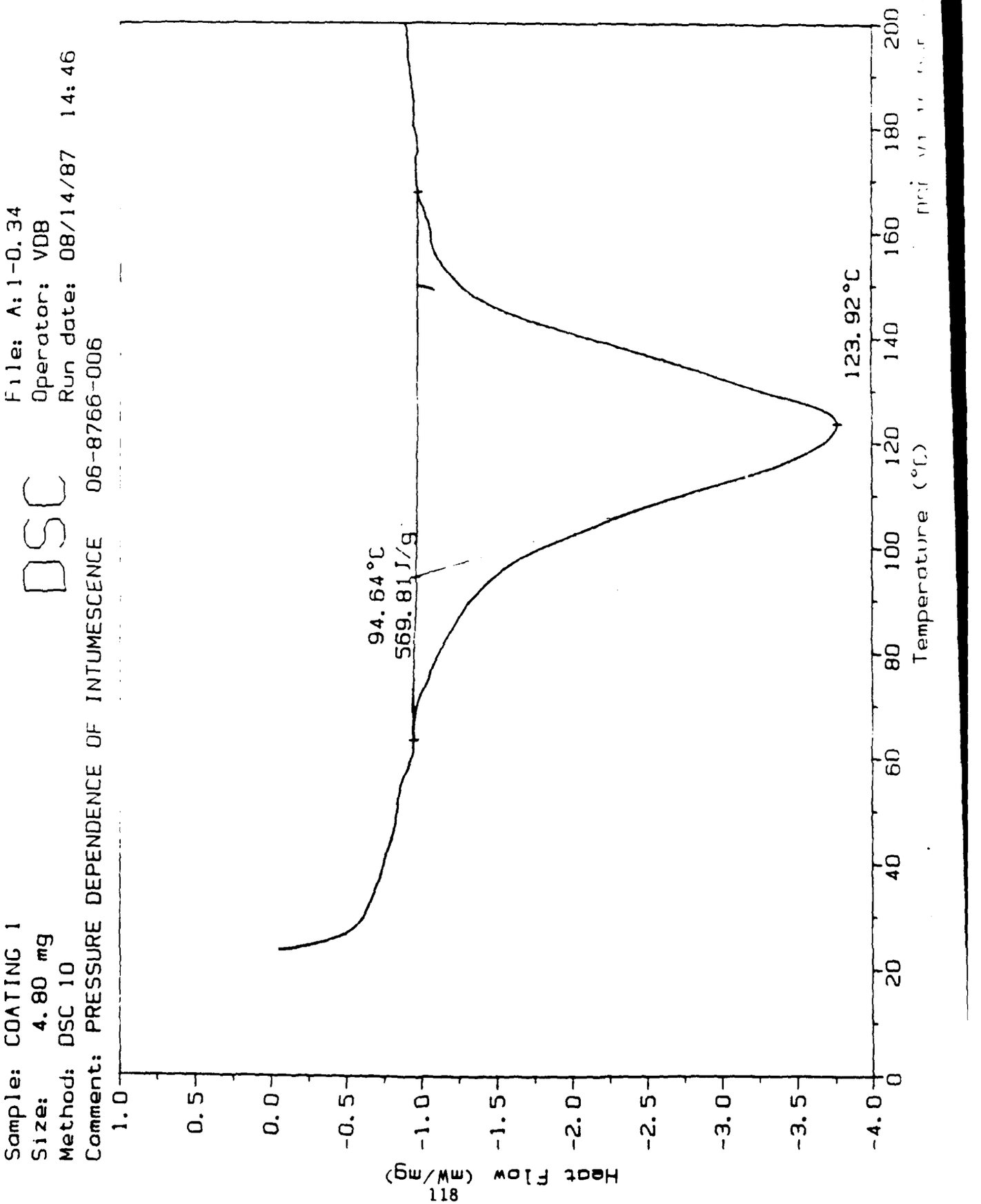
Sample: COATING 1
Size: 4.80 mg
Method: DSC 10
Comment: PRESSURE DEPENDENCE OF INTUMESCENCE 06-8766-006
DSC
File: A:1-0.34
Operator: VDB
Run date: 08/14/87 14:46
94.64°C
569.81 J/g
123.92°C
Heat Flow (mW/mg)
Temperature (°C)
1.0
0.5
0.0
-0.5
-1.0
-1.5
-2.0
-2.5
-3.0
-3.5
-4.0
0
20
40
60
80
100
120
140
160
180
200

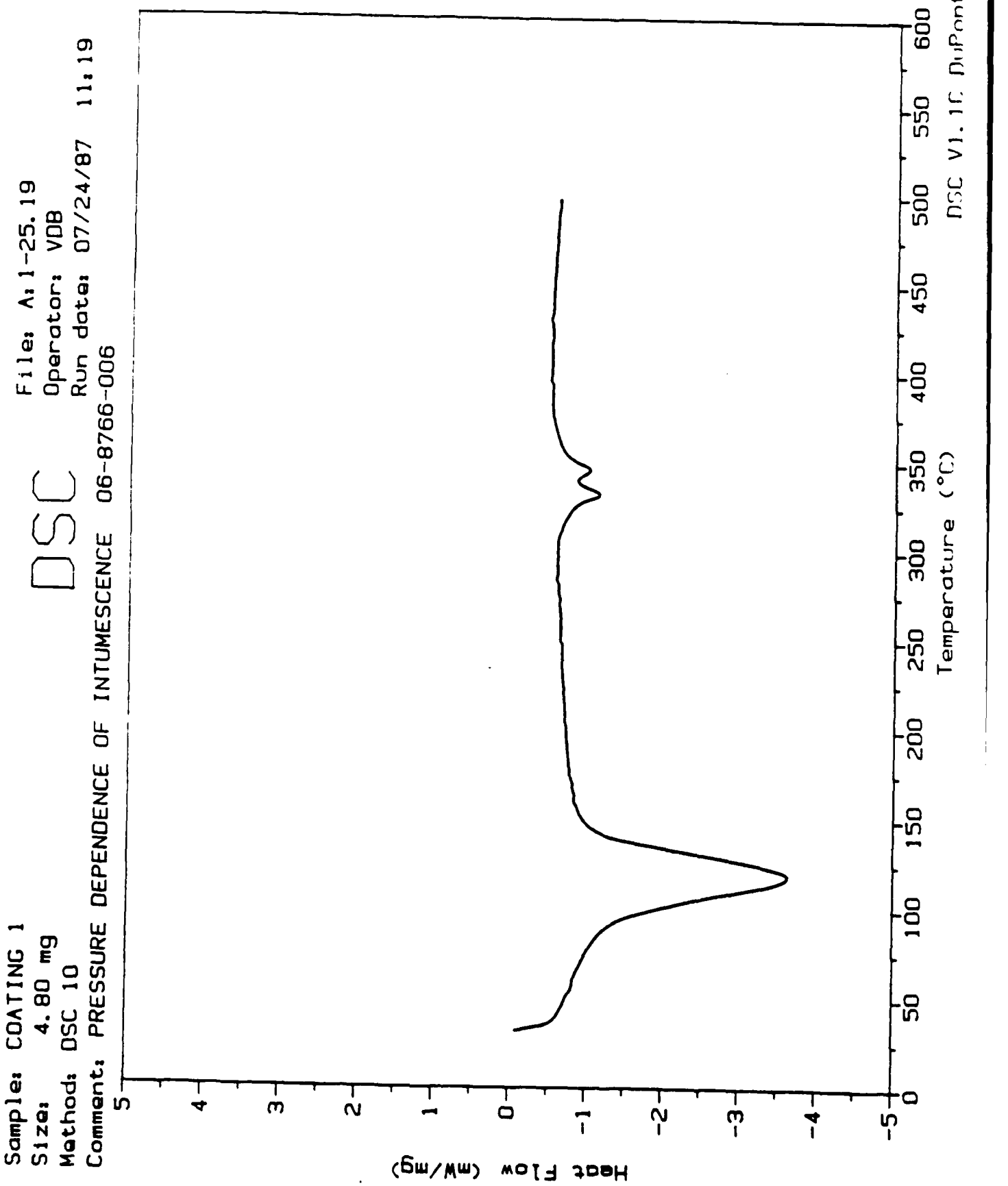
Sample: COATING 1
Size: 4.80 mg
Method: DSC 10
Comment: PRESSURE DEPENDENCE OF INTUMESCENCE 06-8766-006
DSC
File: A:1-25.19
Operator: VDB
Run date: 07/24/87 11:19
Heat Flow (mW/mg)
Temperature (°C)
DSC V1.1F DuPont 9900

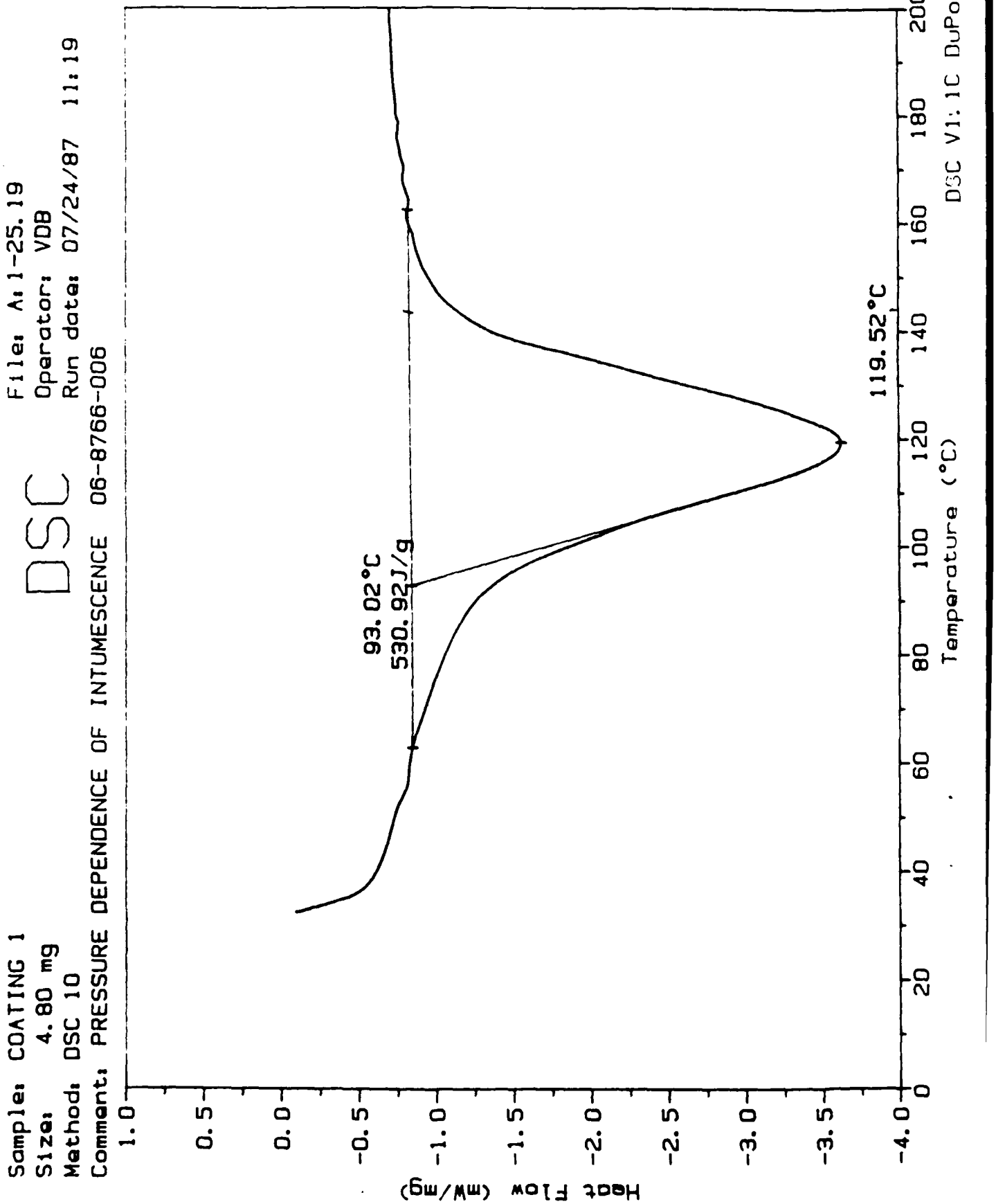
Sample: COATING 1
Size: 4.80 mg
Method: DSC 10
Comment: PRESSURE DEPENDENCE OF INTUMESCENCE 06-8766-006
File: A:1-25.19
Operator: VDB
Run date: 07/24/87 11:19
DSC
93.02°C
530.92J/g
119.52°C
Heat Flow (mW/mg)
Temperature (°C)
DSC V1.1C DuPont 9900

Sample: COATING 1
Size: 4.60 mg
Method: DSC 10
Comment: PRESSURE DEPENDENCE OF INTUMESCENCE 06-8766-006

DSC

File: B:1-100.09
Operator: VDB
Run date: 07/21/87 14:57

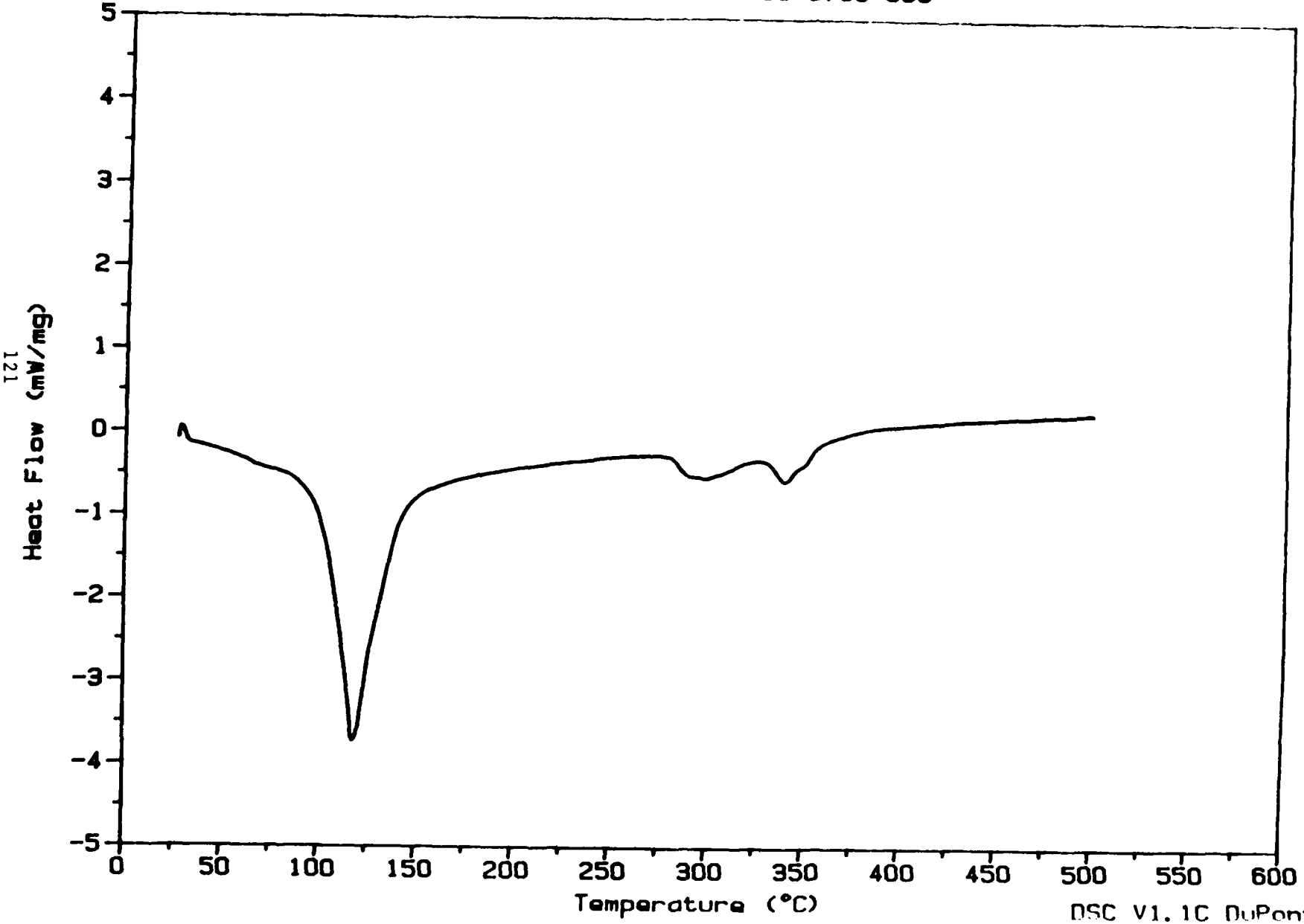

DSC V1.1C DuPont 9900

Contract No. N62269-85-C-0245
NADC-89061-60

Sample: COATING 1
Size: 4.60 mg
Method: DSC 10
Comment: PRESSURE DEPENDENCE OF INTUMESCENCE 06-8766-006

DSC

File: B:1-100.09
Operator: VDB
Run date: 07/21/87 14:57

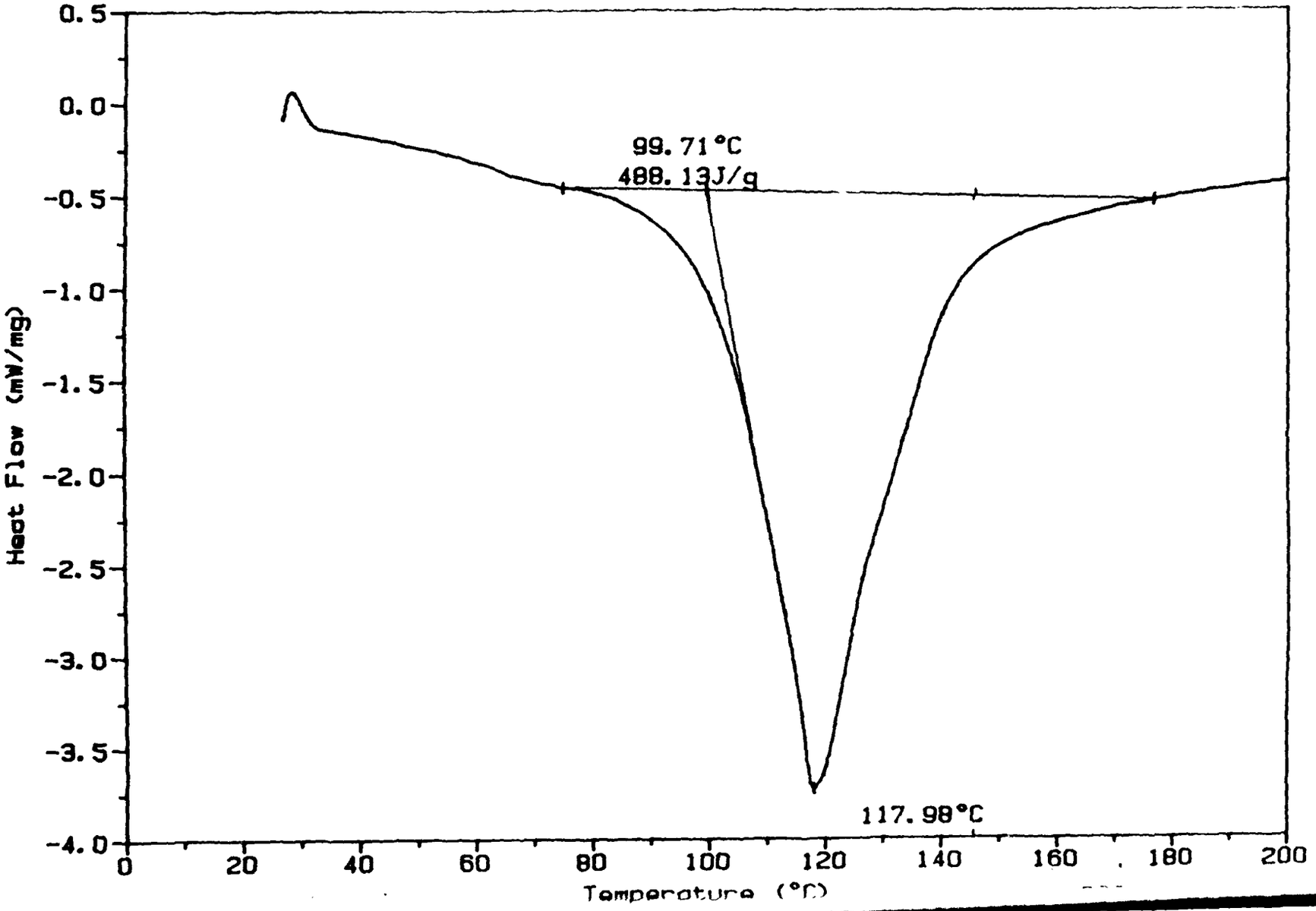

Contract No. N62269-85-C-0245
NADC-89061-60

Sample: COATING 1
Size: 4.40 mg
Method: DSC 10
Comment: PRESSURE DEPENDENCE OF INTUMESCENCE 06-8766-006

DSC

File: A:1-100.10
Operator: VDB
Run date: 07/22/87 08:18

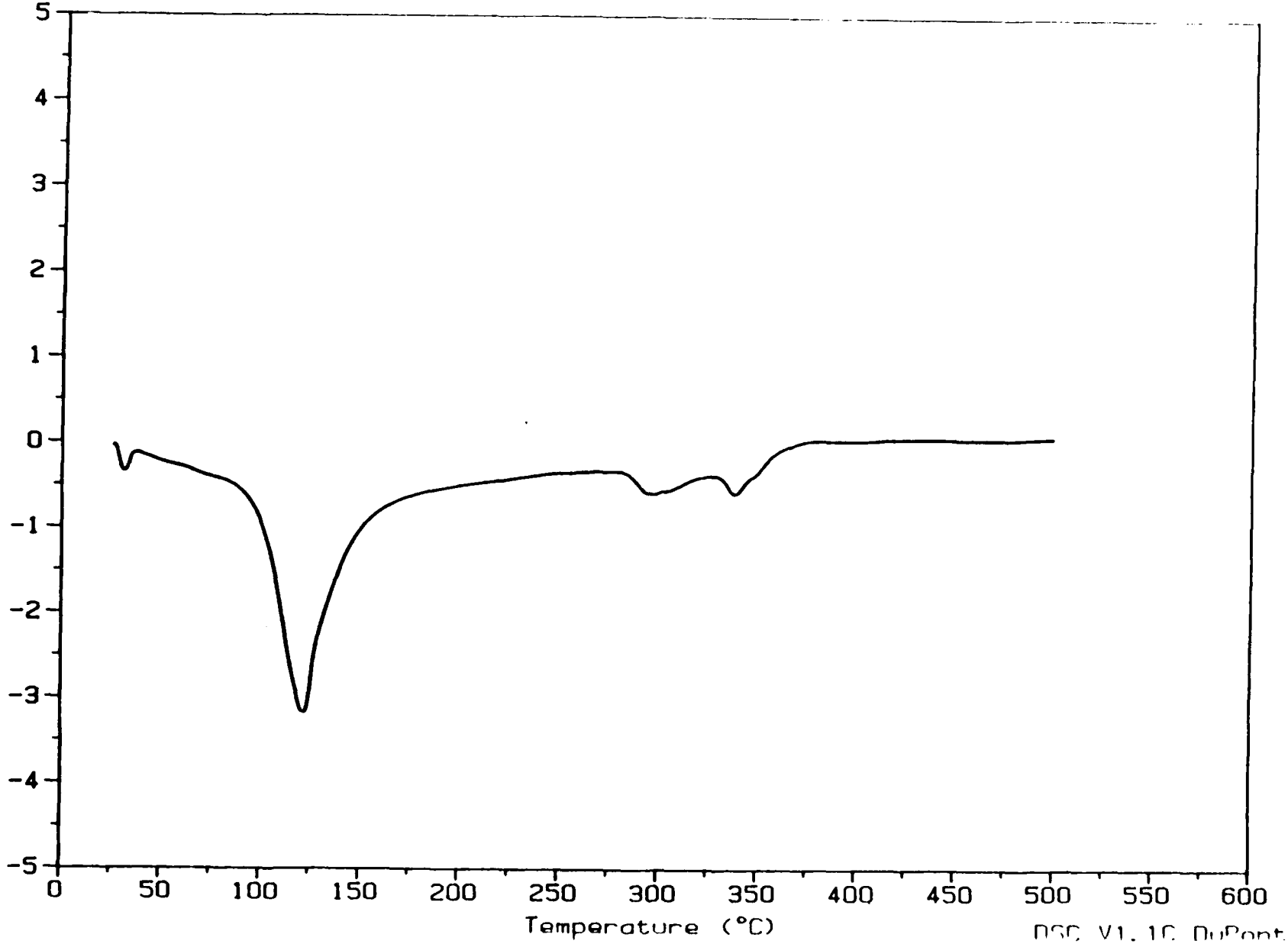

Contract No. N62269-85-C-0245
NADC-89061-60

Sample: COATING 1
Size: 4.40 mg
Method: DSC 10
Comment: PRESSURE DEPENDENCE OF INTUMESCENCE 06-8766-006

DSC

File: A:1-100.10
Operator: VDB
Run date: 07/22/87 08:18

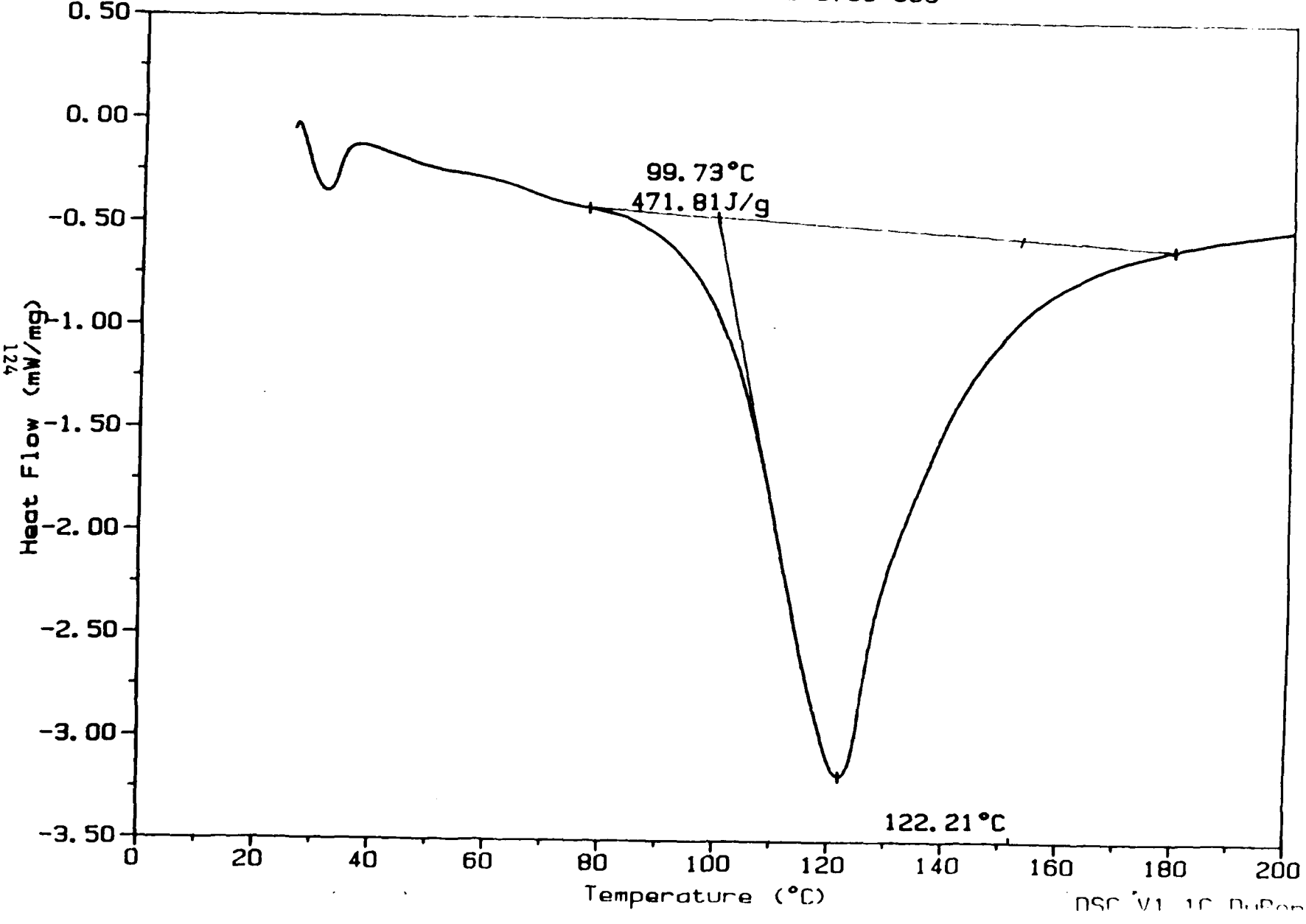

Contract No. N62269-85-C-0245
NADC-89061-60

DSC V1.1C DuPont 9900

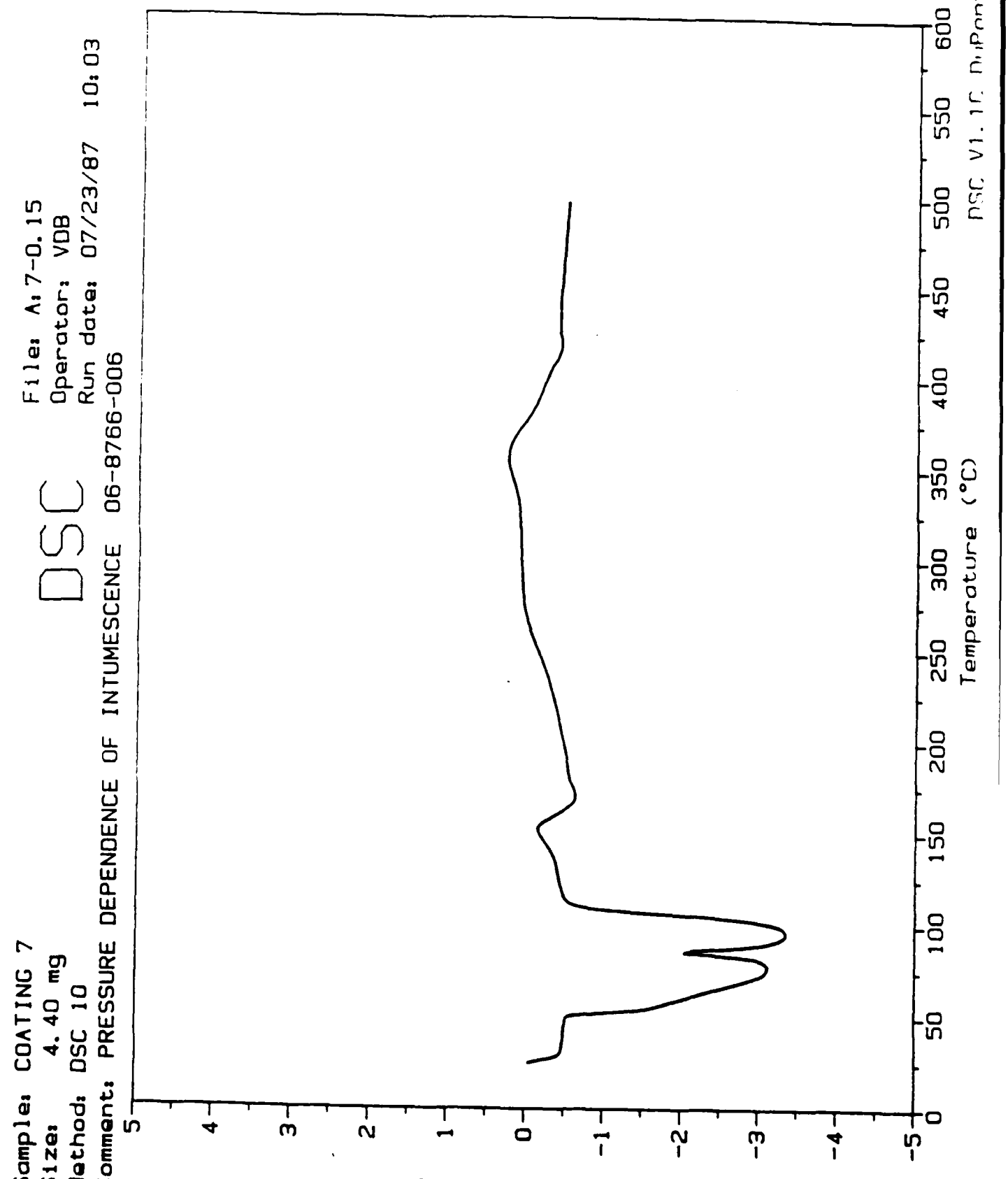
Sample: COATING 7
Size: 4.40 mg
Method: DSC 10
Comment: PRESSURE DEPENDENCE OF INTUMESCENCE 06-8766-006
DSC
File: A:7-0.15
Operator: VDB
Run date: 07/23/87 10:03
Heat Flow (mW/mg)
5
4
3
2
1
0
-1
-2
-3
-4
-5
0
50
100
150
200
250
300
350
400
450
500
550
600
Temperature (°C)
DSC V1.1C DuPont 9000

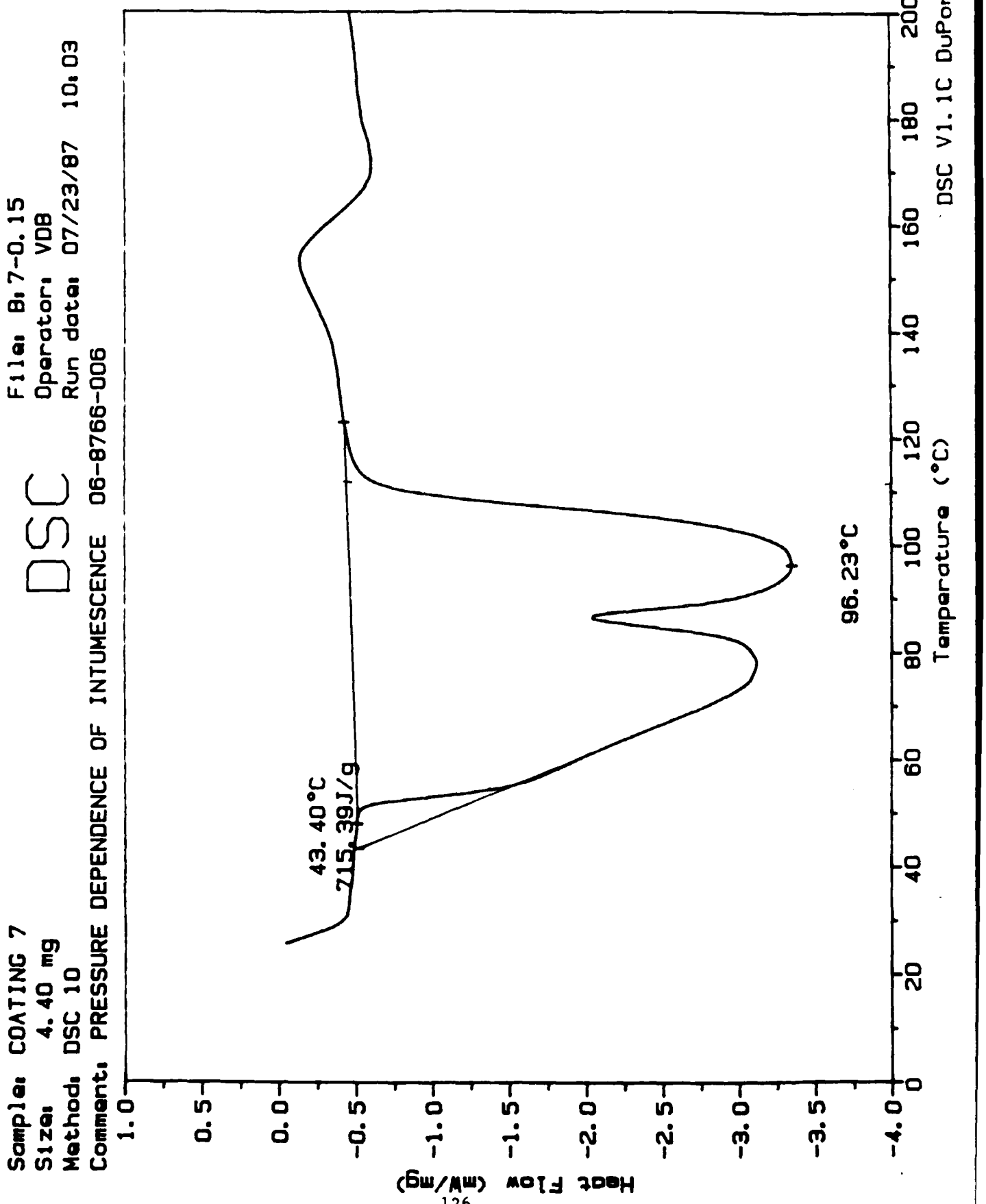
Sample: COATING 7
Size: 4.40 mg
Method: DSC 10
Comment: PRESSURE DEPENDENCE OF INTUMESCENCE 06-8766-006
DSC
File: B:7-0.15
Operator: VDB
Run date: 07/23/87 10:03
DSC V1.1C DuPont 9900
Heat Flow (mW/mg)
Temperature (°C)
43.40°C
215.39J/g
96.23°C
1.0
0.5
0.0
-0.5
-1.0
-1.5
-2.0
-2.5
-3.0
-3.5
-4.0
0
20
40
60
80
100
120
140
160
180
200

Sample: COATING 7
Size: 4.50 mg
Method: DSC 10
Comment: PRESSURE DEPENDENCE OF INTUMESCENCE 06-8766-006

DSC

File: A:7-0.32
Operator: VDB
Run date: 08/13/87 14:27

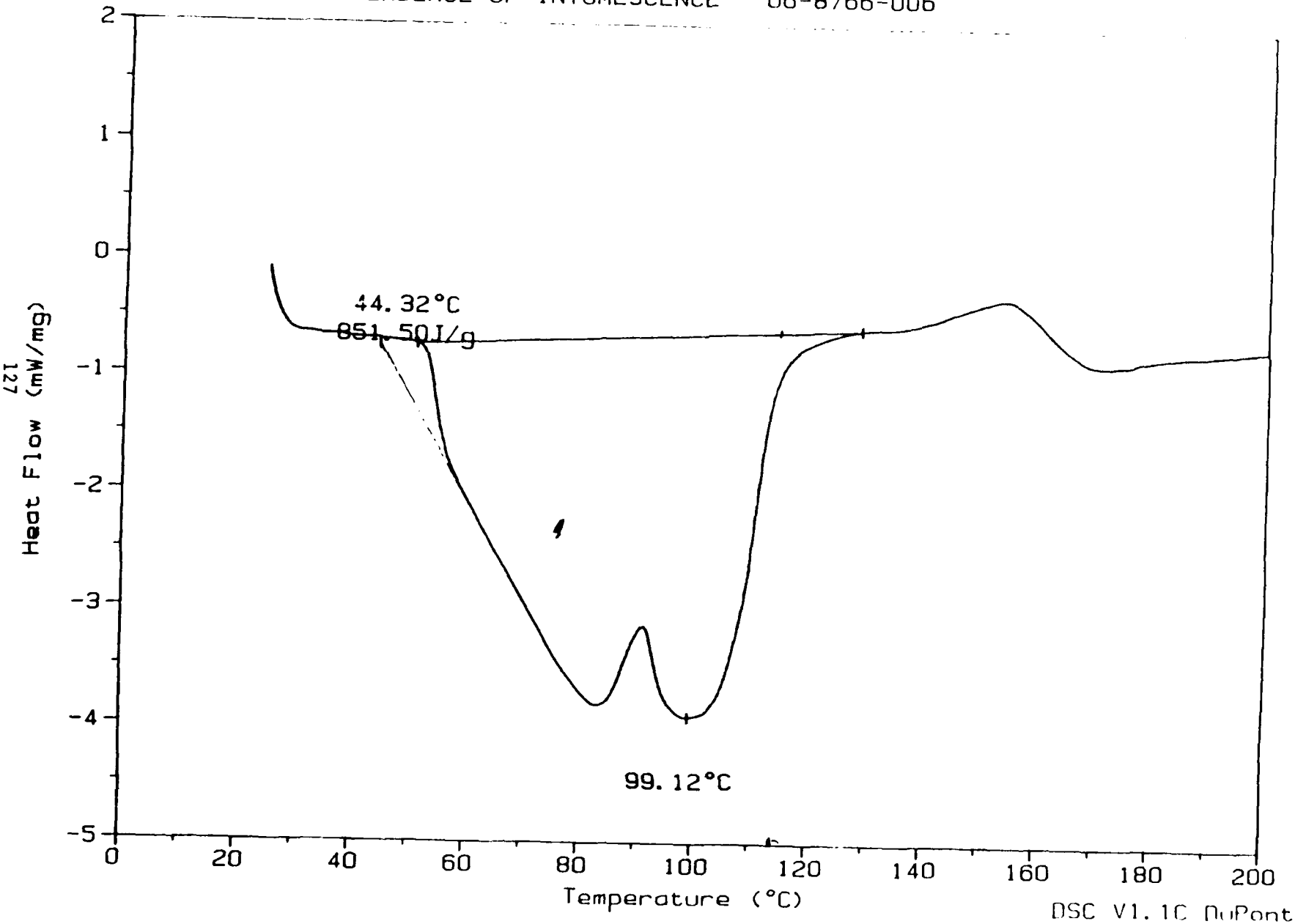

DSC V1.1C DuPont 9900

Contract No. N62269-85-C-0245
NADC-89061-60

Sample: COATING 7
Size: 4.00 mg
Method: DSC 10
Comment: PRESSURE DEPENDENCE OF INTUMESCENCE 06-8766-006

DSC

File: A:7-0.33
Operator: VDB
Run date: 08/14/87 10:16

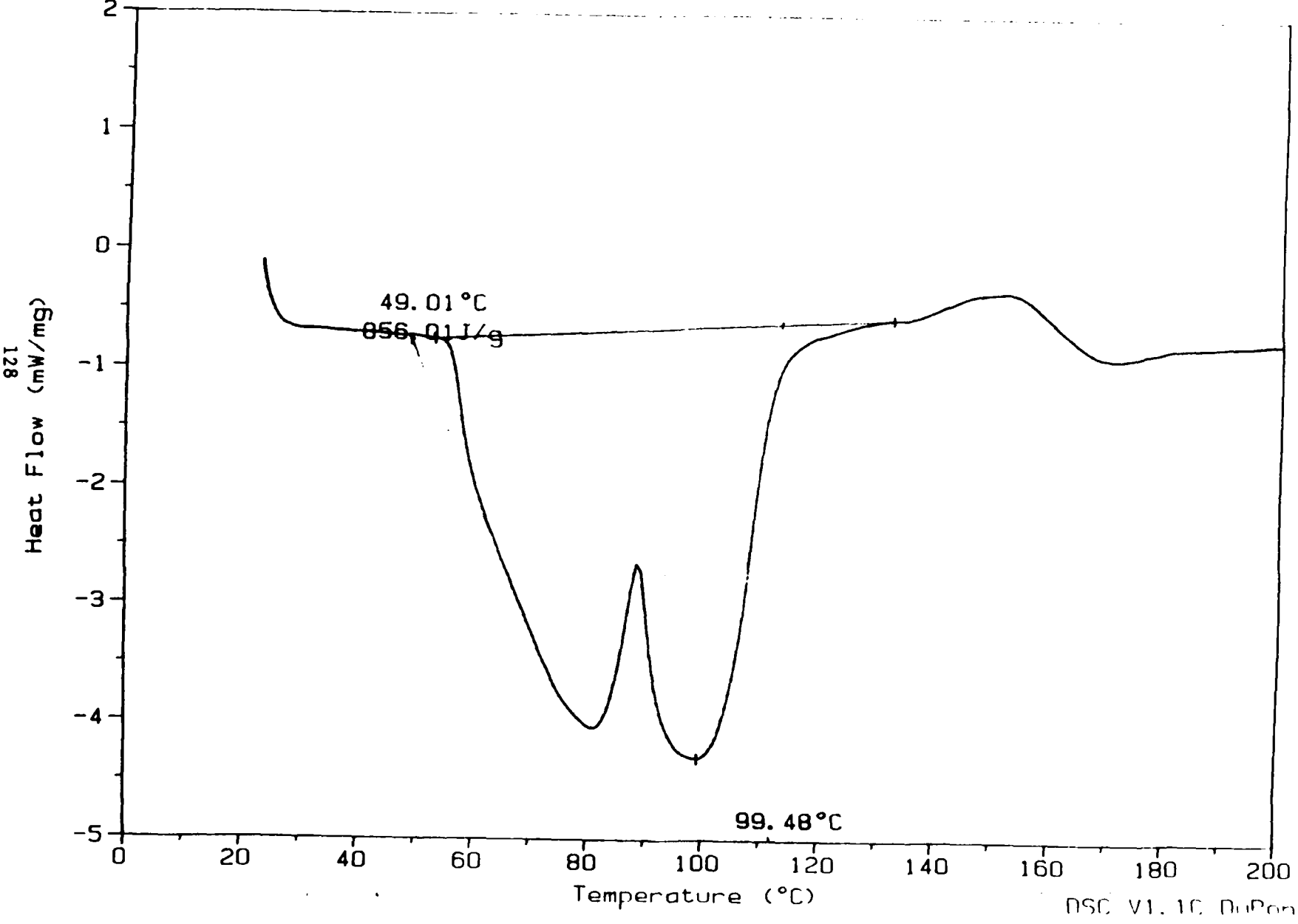

Contract No. N62269-85-C-0245
NADC-89061-60

DSC V1.1C DuPont 9000

Sample: COATING 7
Size: 4.20 mg
Method: DSC 10
Comment: PRESSURE DEPENDENCE OF INTUMESCENCE 68-8786-006

DSC

File: A:7-100.07
Operator: VDB
Run date: 07/21/87 10:50

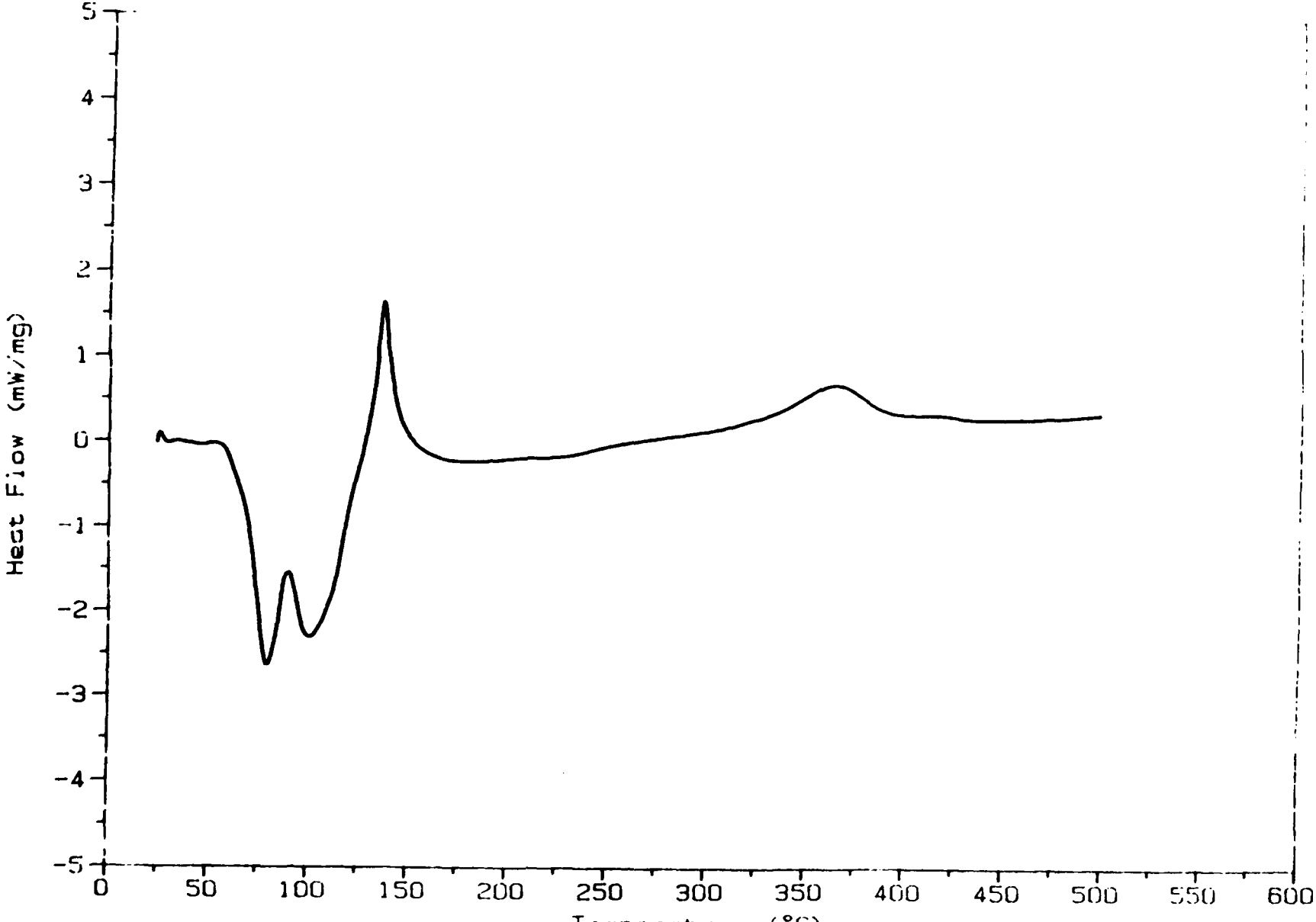

DSC V1.1L DuPont 9900

Contract No. N62269-85-C-0245
NADC-89061-60

Sample: COATING 7
Size: 4.20 mg
Method: DSC 10
Comment: PRESSURE DEPENDENCE OF INTUMESCENCE 06-8766-006

DSC

File: B:7-100.07
Operator: VDB
Run date: 07/21/87 10:50

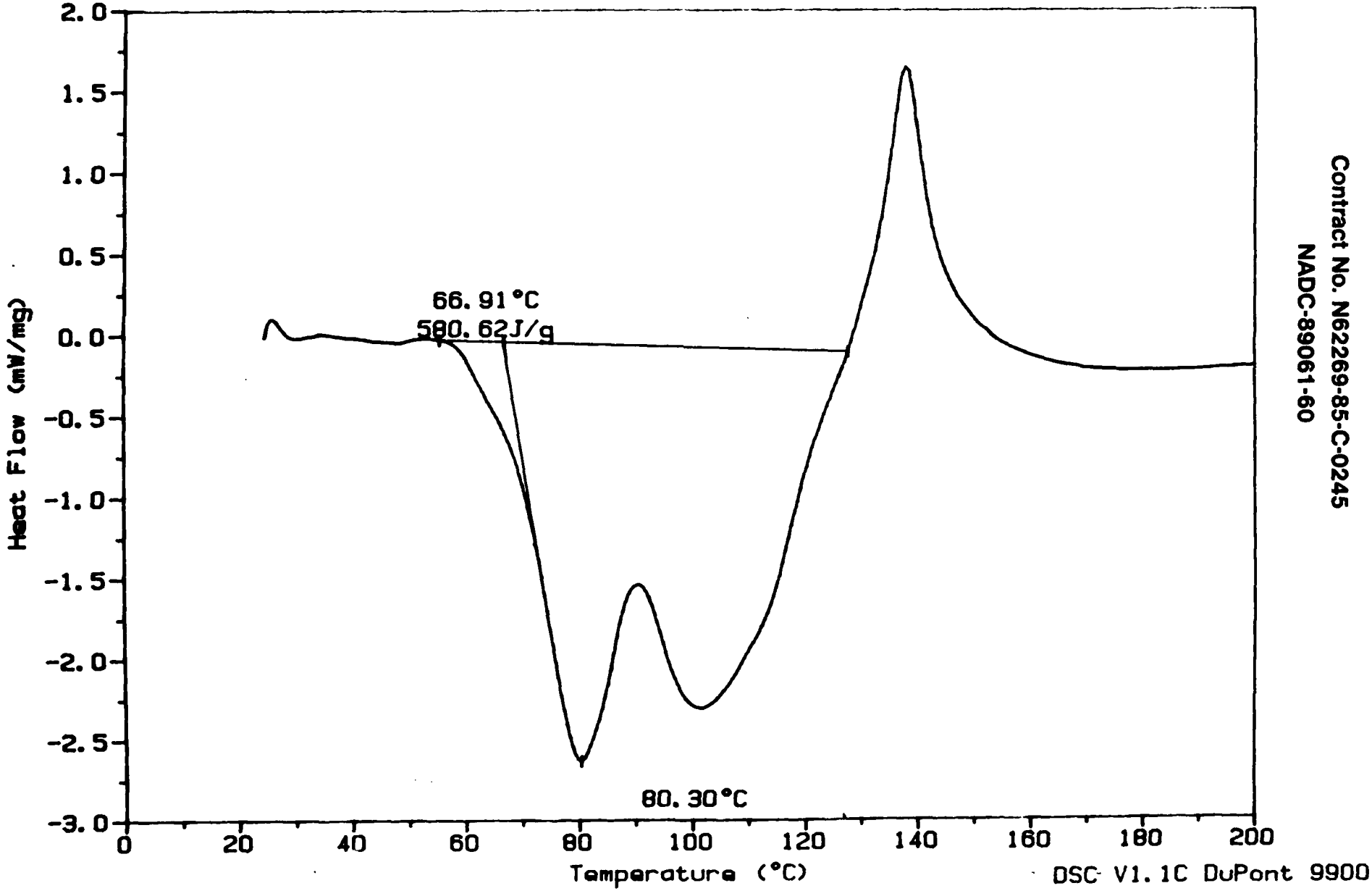

Contract No. N62269-85-C-0245
NADC-89061-60

DSC V1.1C DuPont 9900

Sample: COATING 7
Size: 4.30 mg
Method: DSC 10
Comment: PRESSURE DEPENDENCE OF INTUMESCENCE 06-8766-006

DSC

File: A:7-100.08
Operator: VDB
Run date: 07/21/87 12:51

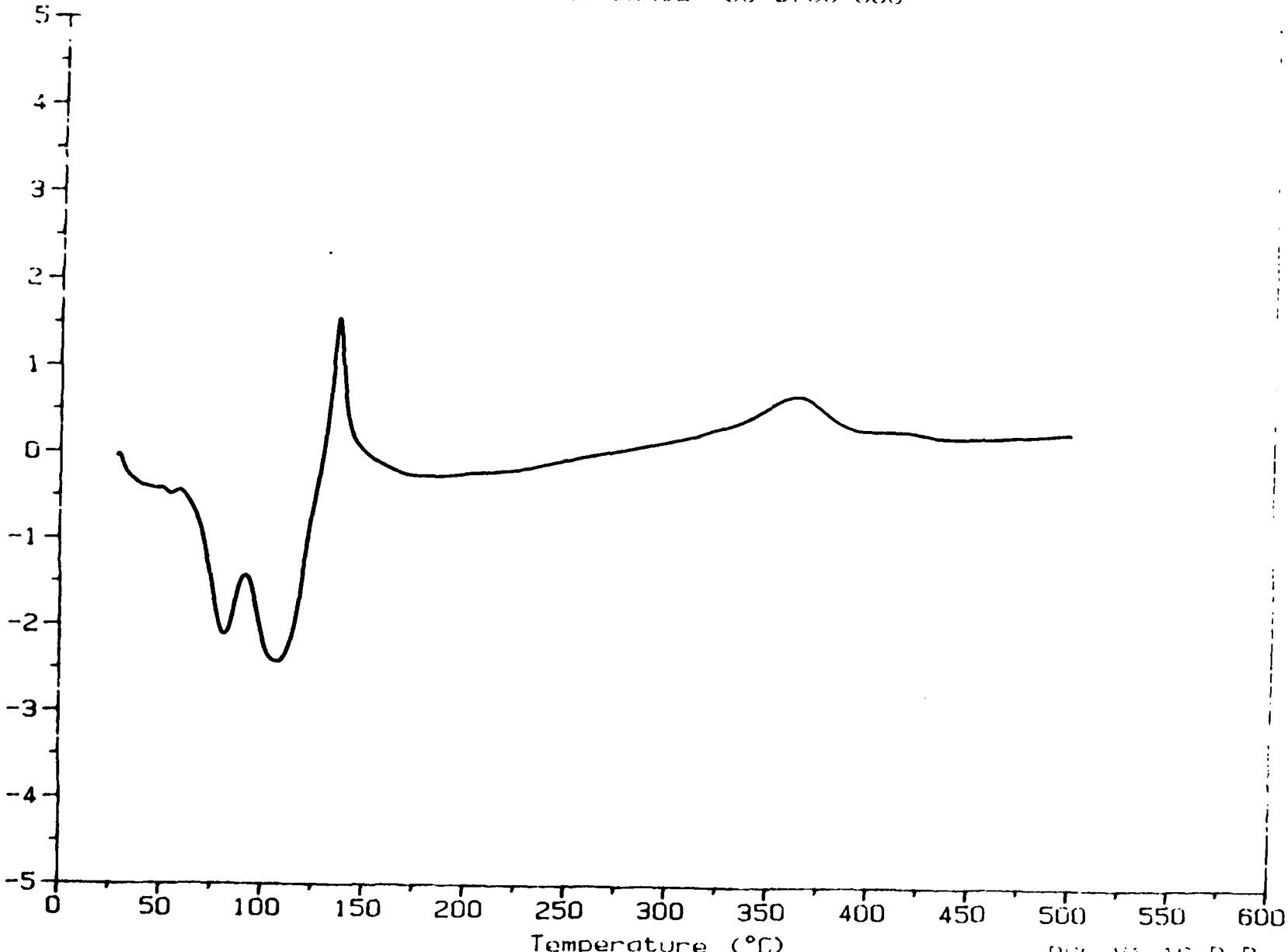

DSC V1.1C DuPont 9900

Contract No. N62269-85-C-0245
NADC-89061-60

Sample: COATING 7
Size: 4.30 mg
Method: DSC 10
Comment: PRESSURE DEPENDENCE OF INTUMESCENCE 06-8766-006

DSC

File: B:7-100.08
Operator: VDB
Run date: 07/21/87 12:51

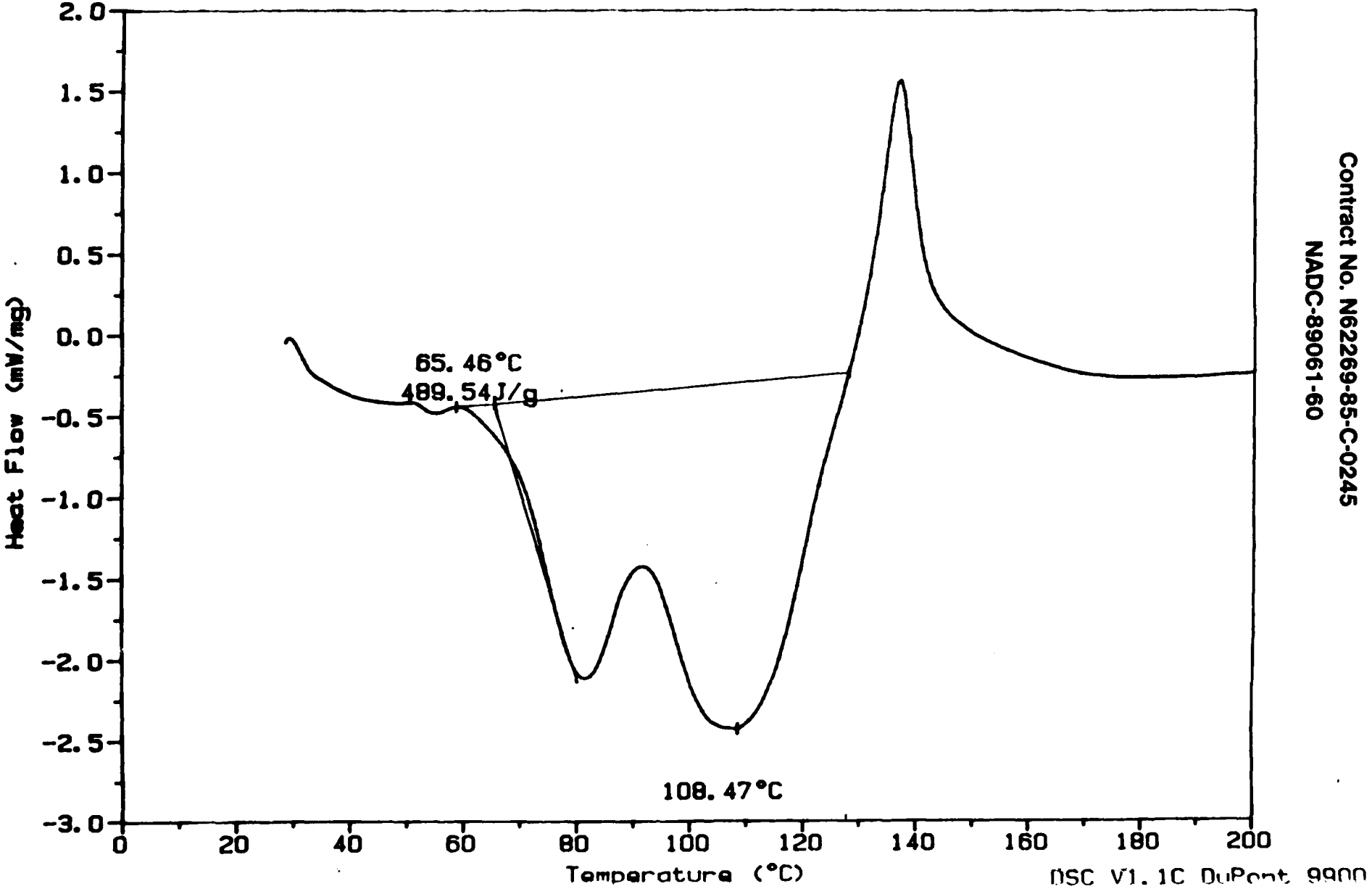

Contract No. N62269-85-C-0245
NADC-89061-60

DISTRIBUTION LIST (Continued)
Report No. NADC-89061-60

Warner-Robbins Air Logistics Command 2
Robbins AFB, GA 31098
(1 for Code MMEMC)
(1 for Code MMTRC)

Wright Research & Development Center 1
Wright-Patterson AFB, OH 45433-6533
(1 for Code MLSA)

Naval Air Development Center 22
Warminster, PA 18974-5000
(2 for Code 8131)
(20 for Code 6062; D. Pulley)

Center for Naval Analysis 1
4401 Fort Avenue
P.O. Box 16268
Alexandria, VA 22302-0268

Contract No. N62269-85-C-0245

NADC-89061-60

DISTRIBUTION LIST (Continued)
Report No. NADC-89061-60

Naval Research Laboratory 3
4555 Overlook Avenue
Washington, DC 20375
(1 for Code 6120)
(1 for Code 6123)
(1 for Code 6124)

Naval Sea Systems Command 1
Washington, DC 20362
(1 for Code SEA-05M1)

Naval Surface Warfare Center 1
Dahlgren, VA 22448-5000
(1 for Code R-15)

Naval Surface Warfare Center, White Oak 1
10901 New Hampshire Avenue
Silver Spring, MD 20903-5000
(1 for Code R-31)

Naval Weapons Center 2
China Lake, CA 93555-6001
(1 for Code 3208)
(1 for Code 3274)

Naval Weapons Station 1
Yorktown, VA 23691-5000
(1 for Code NEDED-505)

Naval Weapons Support Center 1
Army Ammunition Activity
Crane, IN 47522-5050
(1 for Code OED-5044)

Office of Naval Research 2
800 North Quincy Street
Arlington, VA 22217-5000
(1 for Code 12)
(1 for Code 431)

Office of Naval Technology 1
800 North Quincy Street
Arlington, VA 22217-5000
(1 for Code 225)

Pacific Missile Test Center 1
Point Mugu, CA 93042
(1 for Code 2041)

Contract No. N62269-85-C-0245

NADC-89061-60

DISTRIBUTION LIST
Report No. NADC-89061-60

Army Aviation Systems Command 1
4300 Goodfellow Boulevard
St. Louis, MO 63120-1798
(1 for Code DRDAV-DS)

Army Belvoir Research & Development Center 1
Fort Belvoir, VA 22060-5606
(1 for Code STRBE-VO)

Army Materials Technology Laboratory 1
Watertown, MA 02172
(1 for Code DRXMR-MM)

David Taylor Research Center 2
Annapolis, MD 21402-5067
(1 for Code 2813)
(1 for Code 2841)

Defense Technical Information Center 2
Cameron Station
Alexandria, VA 22314

National Institute of Standards & Technology 1
Gaithersburg, MD 20899
(1 for M. McKnight)

Naval Air Engineering Center 1
Lakehurst, NJ 08733-5100
(1 for Code 5321)

Naval Air Systems Command 2
Washington, DC 20361
(1 for Code AIR-310T)
(1 for Code AIR-54111)

Naval Civil Engineering Laboratory 1
Port Hueneme, CA 93043
(1 for Code L52)

Naval Facilities Engineering Command 1
200 Stovall Street
Alexandria, VA 22332-2300
(1 for Code 032)